Durchgeführt am Max-Planck-Institut für Herz- und Lungenforschung,
W.G. Kerckhoff-Institut Bad Nauheim

REGULATION OF CARDIAC PROTEIN QUALITY CONTROL BY DEUBIQUITINATING ENZYMES

INAUGURAL DISSERTATION

Zur Erlangung des Grades Doktor der Naturwissenschaften
- Doctor rerum naturalium –
(Dr. rer. nat.)

Vorgelegt beim Fachbereich 08 – Biologie und Chemie
der Justus-Liebig-Universität Giessen

von

Mareike Susann Poetsch
(Dipl. human. biol.)

aus Altdöbern

Giessen, August 2018

Vom Fachbereich 08 – Biologie und Chemie
der Justus-Liebig-Universität Giessen als Dissertation angenommen.

Dekan: Prof. Dr. Jürgen Janek

Prodekan: Prof. Dr. Thomas Wilke

Erstgutachter: Prof. Dr. Dr. Thomas Braun
Abteilung Entwicklung und Umbau des Herzens
Max-Planck-Institut für Herz- und Lungenforschung
Ludwigstrasse 43
61231 Bad Nauheim

Zweitgutachter: Prof. Dr. Albrecht Bindereif
Institut für Biochemie
Justus-Liebig-Universität Giessen
Heinrich-Buff-Ring 17
35392 Giessen

Datum der Disputation: 05.11.2018

Science is a way of thinking much more
than it is a body of knowledge.

Carl Sagan

Science is not only a disciple of reason but,
also, one of romance and passion.

Stephen Hawking

A scientific truth does not triumph by convincing its opponents
and making them see the light,
but rather because its opponents eventually die,
and a new generation grows up that is familiar with it.

Max Planck

EIDESSTATTLICHE ERKLÄRUNG

Ich erkläre: „Ich habe die vorgelegte Dissertation selbstständig und ohne unerlaubte fremde Hilfe und nur mit den Hilfen angefertigt, die ich in der Dissertation angegeben habe. Alle Textstellen, die wörtlich oder sinngemäß aus veröffentlichten Schriften entnommen sind, und alle Angaben, die auf mündlichen Auskünften beruhen, sind als solche kenntlich gemacht. Ich stimme einer evtl. Überprüfung meiner Dissertation durch eine Antiplagiat-Software zu. Bei den von mir durchgeführten und in der Dissertation erwähnten Untersuchungen habe ich die Grundsätze guter wissenschaftlicher Praxis, wie sie in der „Satzung der Justus-Liebig-Universität Gießen zur Sicherung guter wissenschaftlicher Praxis“ niedergelegt sind, eingehalten.“

Giessen, 28.08 2018

_____

Mareike Susann Poetsch

ACKNOWLEDGEMENTS

This work was carried out in the Department I: Cardiac Development and Remodeling at the Max-Planck-Institute for Heart and Lung Research (MPI HLR) in Bad Nauheim, Germany, where I was supported by an IMRPS and UbiNet fellowship. Working at the MPI HLR provided me an invaluable opportunity to get a first glimpse of life and work in such an excellent scientific research center. First, I would like to thank my supervisor, Prof. Dr. Dr. Thomas Braun, for his support and guidance throughout my time at the MPI HLR and for motivating me to ask, discuss, and develop ideas to open questions in the complex world of cellular and molecular biology. He has taught me how to approach scientific work, express ideas, and try the impossible by developing my own solutions to complex questions, and to overcome many critical situations. Many thanks also to my PI André Schneider for his constant help and advice at various stages of this work, and for thorough and constructive criticism. Thanks also to all the PhD students, postdocs, and technical assistants for scientific guidance and for providing a bedrock of enthusiasm and expertise. Particular thanks to Dr. Kerstin Wilhelm and Silke Kreher for stimulating discussions and all the fun we had in the lab and in our free time within the last years. Thank you for your constant support. It is hard to overemphasize the importance of understanding, encouragement, and constant support from my family and friends. I am blessed to have them around and have never felt alone during my PhD. Although my parents never explicitly expressed what they expected from me, I thank them for allowing me to get the education I wanted. I am very grateful to everything I have and for their trust in my own judgement for the bigger things in life. Many thanks.

SUMMARY

Sustained protein homeostasis – *proteostasis* – is particularly important in the heart as cardiomyocytes are limited to self-renewal. The interaction between molecular chaperones and protein catabolic pathways, above all, the ubiquitin proteasome system (UPS) and (selective) autophagy, plays a critical role for protein turnover in the heart. Malfunctions of these processes due to increased stress caused by gene mutations, translational errors, or reduced efficiency result in accumulation of toxic protein aggregates and the progression of several cardiac diseases, such as dilated cardiomyopathy (DCM). This study identified the ubiquitin-specific peptidase USP5 as a cell-type specific, critical deubiquitinating enzyme for polyubiquitin turnover and proteostasis in mice and human cardiomyocytes.

Loss of USP5 in cardiomyocytes caused effects ranging from profound accumulation of polyubiquitin chains, defective polyubiquitin turnover, and strong suppression of proteolytic activity of the proteasome, irreversibly resulting in the formation of ubiquitin-conjugated protein aggregates. Impaired clearance of such aggregates by selective autophagy augmented the cytotoxic cellular stress response, progressively resulting in cardiac remodeling, severe DCM, and sudden death. Similar to the DCM phenotype observed in the USP5 mouse model, cardiomyocytes from human individuals with end-stage DCM displayed substantially reduced USP5 protein levels and accumulation of ubiquitinated protein aggregates lacking USP5. Interestingly, overexpression of USP5 in cardiomyocytes expressing a mutant form of titin, known to cause cardiomyopathy, abrogated formation of titin aggregates through elevated proteasomal activity. These findings might pave the way for a new innovative

therapeutic strategy by which USP5 may aid in reversing disease-related protein aggregation caused by truncated or missense mutations in structural genes.

In summary, the findings of this study provide the first genetic evidence for the crucial role of USP5 in the regulation of UPS-dependent proteolysis and selective autophagy, two processes that are instrumental for protein quality control in the heart.

ZUSAMMENFASSUNG

Ein konstantes Gleichgewicht an Proteinen – Proteostase – ist besonders im Herzen von Bedeutung, da Herzmuskelzellen aufgrund ihres postmitotischen Charakters nur über eine sehr begrenzte Teilungsfähigsfähigkeit verfügen. Die Interaktion zwischen Chaperonen und Proteinabbauwegen, allen voran das Ubiquitin-Proteasom-System (UPS) und (selektive) Autophagie, spielt eine grundlegende Rolle beim Proteinumsatz im Herzen. Fehlfunktionen dieser Prozesse, die häufig durch erhöhten zellulären Stress etwa infolge von Genmutationen, Translationsfehlern oder verminderter Effizienz der beiden Abbauwege verursacht werden, resultieren oftmals in der Ansammlung von toxischen Proteinaggregaten, die die Entstehung von Herzerkrankungen, wie dilatativer Kardiomyopathie (DCM), zu einem erheblichen Anteil fördern. In der hier vorgelegten Studie wurde USP5 als ein zelltyp-spezifisches deubiquitinierendes Enzym identifiziert, welches essentiell für die Regulierung des zellulären Umsatzes von Ubiquitin ist und bei der Aufrechterhaltung der Proteostase im Herzen von Mäusen und humanen Patienten eine wichtige Rolle einnimmt.

Die Ergebnisse der Studie zeigen, dass der Verlust von USP5 in Herzmuskelzellen von Mäusen mit einer Ansammlung von freien Ubiquitinketten, einem gestörten Umsatz von Ubiquitin, sowie mit einer stark unterdrückten Aktivität des 20S Proteasoms einherging, was die Ansammlung ubiquitinierter Proteinaggregaten zur Folge hatte. Beeinträchtigungen im Abbau dieser Proteinaggregate durch selektive Autophagie führte zu einer verstärkten zytotoxischen Stressantwort, die progressiv zu Umbauprozessen im Herzen und der Entwicklung einer tödlich verlaufenden DCM führte. In Übereinstimmung mit den Daten aus dem USP5-Mausmodell zeigten

Herzmuskelzellen von Patienten mit DCM im Endstadium neben stark reduzierter Expression von USP5 eine verstärkte Ansammlung von Proteinaggregaten auf. Die Überexpression von USP5 in Herzmuskelzellen, die eine veränderte Variante des sarkomeren Proteins Titin exprimierten, trug maßgeblich zur verminderten Bildung von Aggregaten bei, die möglicherweise durch die gesteigerte proteasomale Aktivität zu erklären ist.

Zusammenfassend zeigen die in dieser Studie erhobenen Daten, dass eine erhöhte Expression von USP5 die Bildung pathophysiologisch-relevanter Proteinaggregate eindämmen kann. In diesem Zusammenhang könnte der therapeutische Einsatz von USP5 die außer Kontrolle geratene Ansammlung toxischer Proteinaggregate, die größtenteils durch Mutationen essenzieller Strukturproteine hervorgerufen wird, minimieren. Des Weiteren liefern die Daten den ersten genetischen Beweis für die essentielle Rolle von USP5 bei der Regulierung zwei wichtiger Proteinabbauwege, die für die Proteinqualitätskontrolle im Herzen von überragender Bedeutung sind.

TABLE OF CONTENTS

INTRODUCTION

Proteostasis in Postmitotic Cells

Postmitotic cells, such as neurons and cardiomyocytes, are terminally differentiated cells that exhibit a very limited self-renewal capacity [1]. In this respect, cardiomyocytes are particularly forced in maintaining equilibrated protein homeostasis – *proteostasis* – compared to other cells, which might handle ameliorated proteostasis caused by disturbed protein quality control (PQC) processes by self-division. Even in the absence of pathological conditions, cardiomyocytes are continuously challenged to sustained proteostasis, as they are constantly subjected to diverse cellular challenges, due to several reasons [2]. First, as they are composed of highly specialized proteins, cardiomyocytes must maintain a stable proteome to conduct and contract properly, which is essential for both PQC surveillance and cell stability. Second, as cardiomyocytes are metabolically demanding cells, they have to continuously handle high rates of potentially proteotoxic agents, including reactive oxygen species [3] that arise from oxidative phosphorylation [4]. Third, their status as terminally differentiated, postmitotic cells restricts cardiomyocytes from self-renewal to bypass derailed PQC by cell division. As a result, cardiomyocytes can only neutralize aged- or stress-induced protein aggregates through balanced PQC and not by distribution of aggregates to one daughter cell, while keeping the other daughter cell free from proteotoxic stress [5]. In this respect, maintaining a healthy proteome through persistent PQC is critical for supporting a functional tissue and to keep the contractile property of the cardiac muscle intact and free of potentially toxic protein aggregates [6].

Proteostasis Network

Proteins are complex macromolecules, which are required for most biological processes. In this respect, proper function of the approximately 20,000 to 25,000 proteins encoded in the human genome relies on fine-tuning of cellular processes, collectively referred to as the proteostasis network. The proteostasis network (PN) is composed of a variety of components (Figure 1).

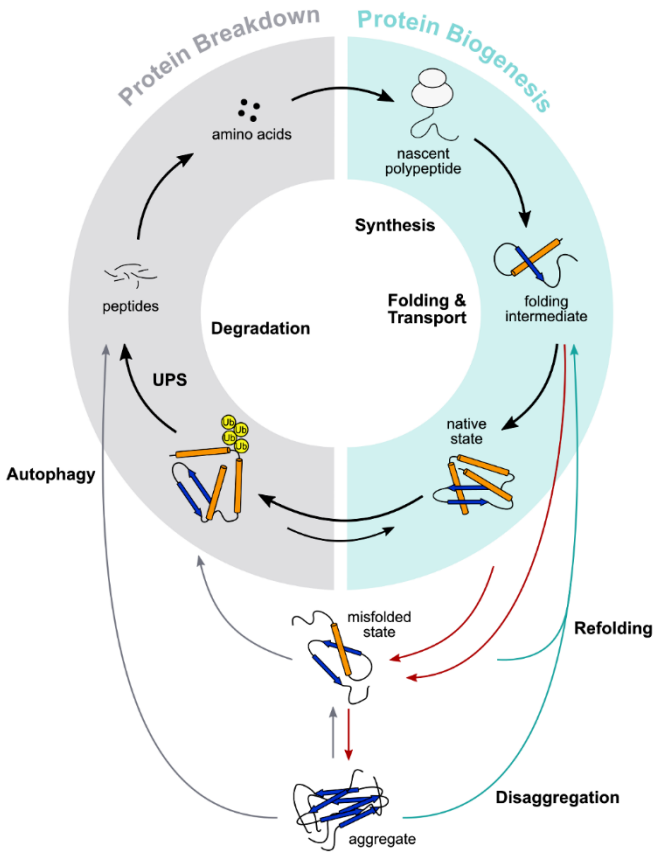

Figure 1 Overview of the cellular proteostasis network.

The proteostasis network (PN) in mammalian cells is composed of the translation machinery, molecular chaperones, the UPS, and (selective) autophagy. All these components are essential to maintain the overall flux of proteostasis (black arrows). Non-native protein conformations (red arrows), resulting from genetic mutations or environmental stress, are recognized by protein quality control processes to prevent accumulation of toxic protein aggregates in the cell. Misfolded, damaged, and aggregated proteins are either redirected to the folding machinery through disaggregation and refolding (blue arrows) or targeted to the two degradative systems if refolding is not an option (grey arrows). The UPS primarily degrades chaperone-presented, soluble misfolded, oxidized, mutant, or otherwise damaged proteins. As the UPS also removes proteins that are no longer needed, it provides temporal regulation of protein activity. Aggregated, insoluble proteins are degraded by lysosomal-dependent (selective) autophagy. Modified from [7].

The mammalian PN comprises approximately 2,000 components that act in concert to maintain cellular homeostasis. Structurally, the PN can be divided into three branches depending on the particular function of individual factors: (a) protein biogenesis (~ 280 components), (b) folding of nascent proteins and conformational maintenance of the respective three-dimensional (3D) protein conformation, frequently coupled to transport, modification, and assembly (~ 330 components), and (c) irreversible proteolytic degradation of unfolded, misfolded, aged, and damaged proteins or protein aggregates to prevent deleterious effects of dysfunctional proteins. Protein degradation is carried out by either the ubiquitin-proteasome system (~ 850 components) or (selective) autophagy (~ 530 components) (Figure 1) [8-10]. All PQC checkpoints dynamically act in concert to meet the requirements of the cell and to maintain organismal health. Thus, a healthy proteome determines the long-term cell viability of cells and organs. Nevertheless, the PN is challenged or rewired in many disorders, including neurodegenerative diseases, inflammation, or cancer, making it an attractive therapeutic target.

Components of the Proteostasis Network in the Heart

Chaperones

Chaperones are the cells' first frontline system to ensure correct folding of newly synthesized, nascent proteins into an active, stabilized, and persistent three-dimensional (3D) conformation [11, 12]. Chaperones assist in this so called '*de-novo*' protein folding process by recognition of generic structures, for instance hydrophobic amino acid residues, on the surface of nascent proteins. Binding to these residues promotes correct folding, implemented by changes in the kinetic partitioning via repetitive ATP- and co-chaperone-dependent binding and release cycles [13]. In addition to assist in correct folding of nascent proteins, chaperones prevent mutual interaction and subsequent formation of toxic protein aggregates, especially under cellular stress conditions, such as oxidative stress [9].

Proteolytic degradation systems

If chaperone activity becomes insufficient to guarantee proper folding of proteins or if the load of terminally un- and misfolded proteins exceeds the folding capacity of chaperones, chaperones keep proteins prone to aggregation in a soluble state to promote their proteolytic degradation by either the ubiquitin-proteasome system (UPS) or (selective) autophagy (Figure 1).

The UPS is the most important cellular protein degradation (proteolytic) system that predominantly directs chaperone-presented, soluble proteins to the 26S proteasome for destruction [14, 15]. For this reason, chaperones and the UPS have to work in concert to degrade chaperone-resistant, potentially harmful proteins [16]. However, the UPS is also involved in the temporal regulation of protein activity by degrading normal proteins that after fulfilling their cellular function are no longer needed. To prevent accumulation of terminally un- or misfolded proteins whenever chaperone or UPS activity becomes compromised, autophagy functions as an extra branch of cellular PQC to guarantee clearance of polyubiquitin-conjugated protein aggregates by lysosome-dependent proteolysis. The autophagic machinery contains a large set of primarily hydrolytic enzymes, hence it also catabolizes proteolytic clearance of many macromolecules [17]. Nevertheless, only a cooperative work of both protein degradation systems assures cellular proteostasis by degrading potentially harmful or toxic protein aggregates. Depending on the physiological state and the respective cell type, the UPS is responsible for the proteolytic degradation of approximately 80-90 % of all cellular proteins, while autophagy accounts for clearance of the remaining 10-20 % of cellular proteins [18].

The significance of the proteolytic degradation pathways has been acknowledged with two Nobel Prizes. In 2004, the Nobel Prize in Chemistry was awarded to Aaron Ciechanover, Avram Hershko, and Irwin Rose for the discovery of ubiquitin-mediated protein degradation. In 2016, Yashinori Ohsumi was awarded with the Nobel Prize in Medicine and Physiology for his studies on the autophagy-lysosome pathway.

Cytoskeleton

The cytoskeleton balances the communication between different constituents of the PQC machinery in contractile cells [19]. In addition to maintain proper proteostasis, the cytoskeleton further provides the fundamental contractile property of the cardiac muscle. The highly specialized network of the cytoskeleton, which comprises of a variety of filaments, including actin and myosin, but also intermediate filaments, and microtubules, interacts with various membrane-associated proteins, sarcomere proteins, or with proteins of the intercalated disc to ensure proper cardiac contraction (Figure 2).

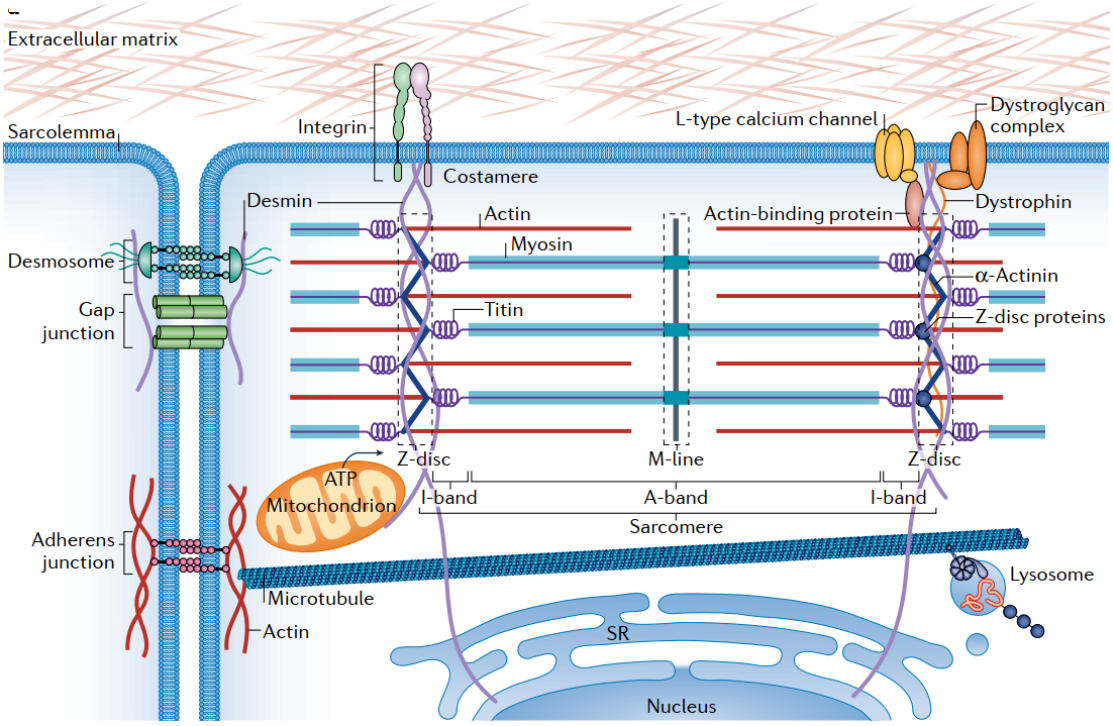

Figure 2 The cardiac cytoskeleton network.

The cardiac cytoskeleton is a complex but rather dynamic network consisting of the filamentous proteins actin and myosin, as well as intermediate filaments, and microtubules. The cytoskeleton substantially contributes to the transmission of mechanical and chemical stimuli within and between cardiomyocytes that is essential for contraction and sustained cardiac function. By anchoring various organelles, such as the nucleus, mitochondria, or the sarcomeric reticulum (SR), the cytoskeleton further acts as a stabilizing force that assists in cell stability. Adapted from [20].

The cytoskeleton also interacts with numerous organelles, including the nucleus, the sarcomeric reticulum (SR), the endoplasmic reticulum (ER), lysosomes, or mitochondria. The synchronized interaction of the cytoskeleton with organelles is critical for the transmission of mechanical and chemical signals within and between cells and the transportation of ubiquitin-conjugated proteins along the PN [21, 22]. In this context, HDAC6-mediated acetylation of microtubules plays a central role for trafficking of proteins within cells. In contrast, acetylation is also fundamental to maintain contractile function as microtubules are in close contact with the SR, the ER and mitochondria to balance calcium homeostasis in various organelles. Impairment of the trafficking and/or contractile function of the cytoskeleton typically results in disturbed communication within the cardiac PN, loss of PQC, and severely impaired cardiac function [23, 24]. Hence, a functional cytoskeletal network protects against cardiac diseases.

The Ubiquitin-Proteasome System

The ubiquitin-proteasome system (UPS) is the key protein degradation system of the eukaryotic PN, taking care of unfolded, misfolded, damaged, oxidized, or mutated proteins, which failed to be properly refolded by chaperones. These mainly soluble proteins are marked by a polyubiquitin chain that is covalently attached to distinct lysine residues on the targeted protein and are subsequently degraded by proteolytic cleavage. In addition, the UPS is also crucial for the regulation of a stable protein pool as it removes short-lived proteins, which have fulfilled their respective function(s) [14].

Ubiquitination

Ubiquitination acts as a broker between cellular function and proteostasis. As free ubiquitin is the precious commodity, ubiquitination intersects and communicates at multiple points to balance homeostasis of diverse organelles and to coordinate cellular proteostasis. Additionally, deubiquitinating enzymes, as well as all four polyubiquitin precursor genes, are necessary to feed into a balanced ubiquitin pool by providing conjugation-competent ubiquitin.

Posttranslational modifications of proteins, with the evolutionary highly conserved 76-amino acid protein tag ubiquitin, are fundamental for eukaryotic cell functions. Ubiquitination helps to facilitate precise communication between and within cells by regulating a variety of cellular processes, including signal transduction, cell division, and cell differentiation, or in developing cells to become complex organisms. Eukaryotic cells encode four distinct ubiquitin precursors, *UBB*, *UBC*, *UBA52*, and *UBA80/RPS27a*, which are translated as polyubiquitin precursor proteins that need to be processed by individual deubiquitinating enzymes (DUBs) to generate active, conjugation-competent ubiquitin [25]. The two polyubiquitin precursor genes *UBB* and *UBC* are composed of 'head-to-tail' linked ubiquitin polymers, with *UBB* comprising 8-10 ubiquitin moieties and *UBC* 3-4 ubiquitin moieties fused in frame one to another. In contrast, the two ubiquitin-ribosomal precursor genes *UBA52* and *UBA80/RPS27a* are translated as a single ubiquitin molecule that is fused at its carboxyl-terminus to a ribosomal protein [26, 27] (Figure 9).

Proteins are labelled with ubiquitin through the cooperated, downwelling action of the following enzymes (Figure 3): E1 ubiquitin-activating, E2 ubiquitin-transferring, and E3 ubiquitin-ligating enzymes, in a cascade requiring ATP [28, 29].

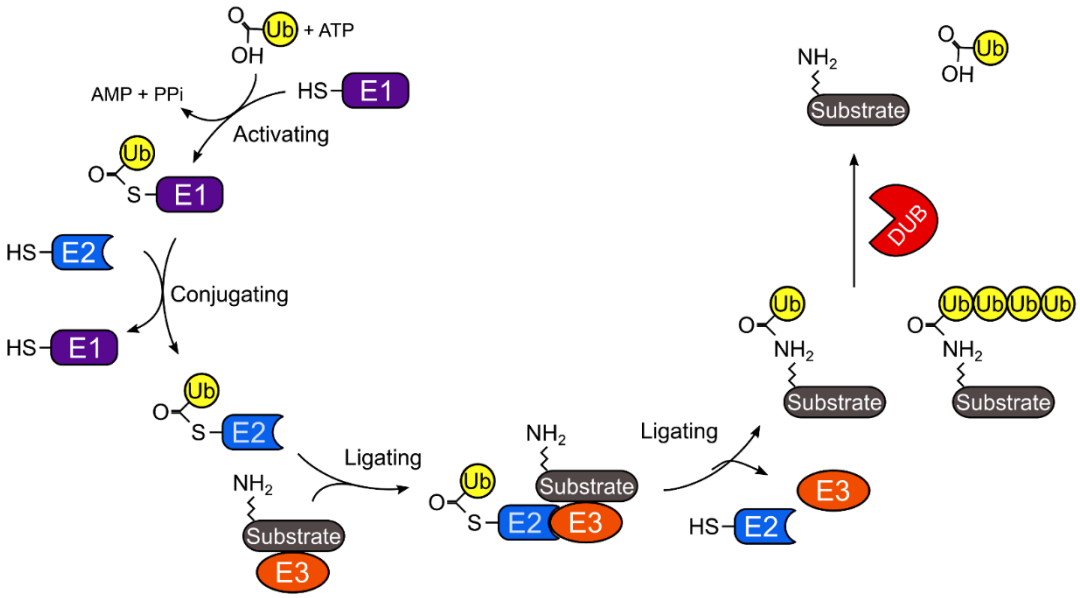

Figure 3 Ubiquitination cascade.

Scheme showing the ubiquitin cascade that is divided into three steps, each of which is catalyzed by a distinct class of enzymes. The first step, mediated by E1 – a ubiquitin-activating enzyme, uses the energy derived from hydrolysis of ATP to AMP and PPi to form a covalent thioester linkage with the carboxyl-terminus of ubiquitin. In a second reaction, ubiquitin is transferred to a cysteine residue within E2 – a ubiquitin-transferring enzyme. In the final step, E2 forms a complex with an E3 – a ubiquitin-ligating enzyme – which coordinates the transfer of ubiquitin, or already formed ubiquitin chains, onto the substrate. Reversal of the ubiquitination cascade is catalyzed by deubiquitinating enzymes (DUBs), which remove ubiquitin molecules or ubiquitin chains from a substrate. Ub, ubiquitin. Modified from [33].

The modification of proteins with ubiquitin can vary from the attachment of a single ubiquitin molecule (monoubiquitination), to the conjugation of several ubiquitin molecules, either attached as a single ubiquitin at multiple lysine residues (multi-monoubiquitination), or of a ubiquitin chain (polyubiquitination) to any of its seven lysine residues (Lys6, Lys11, Lys27, Lys29, Lys33, Lys48, and Lys63), including the first methionine (M1). This so-called ubiquitin code determines the outcome of a ubiquitinated protein with respect to its cellular function (Figure 4, 5) [29-32].

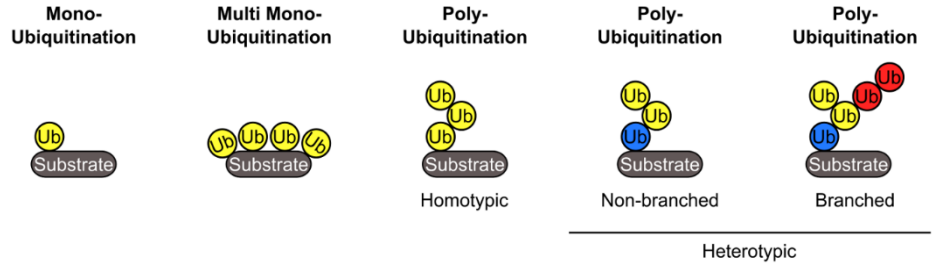

Figure 4 Variety of posttranslational modifications with ubiquitin.

Scheme showing the different types of ubiquitin linkages on a substrate. Ubiquitin can be attached as a single molecule to a specific lysine residue on a substrate (monoubiquitination) or to various lysine residues (multi-monoubiquitination). Conjugation of a ubiquitin chain is nomenclature as polyubiquitination with the ubiquitin chain to be composed of either the same linkage specificity (homotypic polyubiquitination) or two or more different linkages in a single polymerization reaction (heterotypic polyubiquitination), generating a mixed polyubiquitin chain. The latter can be subdivided into non-branched polyubiquitin chains or branched polyubiquitin chains by which a single ubiquitin molecule is modified at two or more lysine residues. Modified from [18].

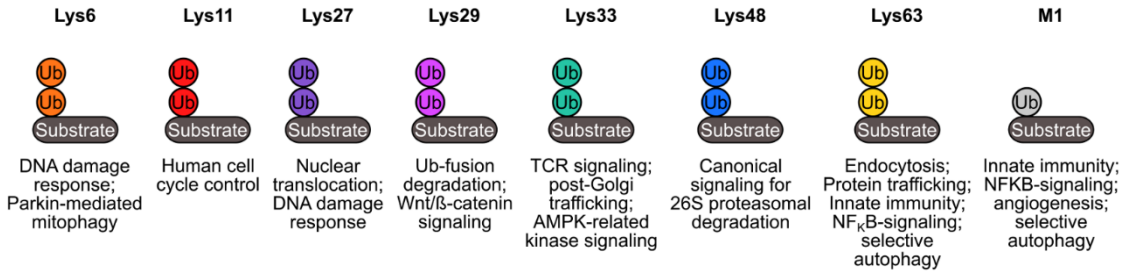

Figure 5 The ubiquitin code and its biological role.

Ubiquitin can be conjugated by another ubiquitin molecule through any of its seven lysine residues (Lys6, Lys11, Lys27, Lys29, Lys33, Lys48, and Lys63), or alternatively the first methionine (M1). The linkage specificity determines the outcome of the protein with respect to its cellular function. Modified from [37].

The 26S Proteasome

The 26S proteasome is a large ~ 2.5-MDa complex, comprised of several subunits forming two major subcomplexes: the proteolytic core particle (20S proteasome) and the regulatory particle (19S proteasome) [33]. Since the proteasome is highly abundant both in the nucleus and cytoplasm, it ensures efficient degradation of short-lived proteins as well as unfolded, misfolded, mutated or otherwise damaged proteins. Therefore, the 26S proteasome governs central signaling processes in the cell.

The proteolytic core particle

The core particle (CP) of the 26S proteasome, often referred to as 20S CP, is composed of 28 subunits. All subunits are uniquely assembled to form a barrel-shaped particle of ~730 kDa, with two outer α-rings and two inner β-rings axially stacked to build a hetero-heptameric ring. Each α-ring and β-ring comprises seven distinct but structurally related α and β subunits, named α1-α7 or β1-β7, respectively (Figure 6) [14]. The center of the α-ring forms a physical barrier, which controls the entrance of proteins into the proteolytically active cavity of the 20S proteasome that is formed by the β1, β2, and β5 subunits. Hereby, each catalytically active β subunit owns distinct peptidase cleavage specificity: the β1 subunit contains the caspase-like peptidase (also referred to as peptidyl–glutamyl–peptide bond hydrolyzing) activity that cleaves after acidic residues. The β2 subunit encodes the trypsin-like peptidase activity that cleaves after basic residues, whereas the β5 subunit, encoding the chymotrypsin-like peptidase activity, cleaves after large hydrophobic residues (Figure 6) [14].

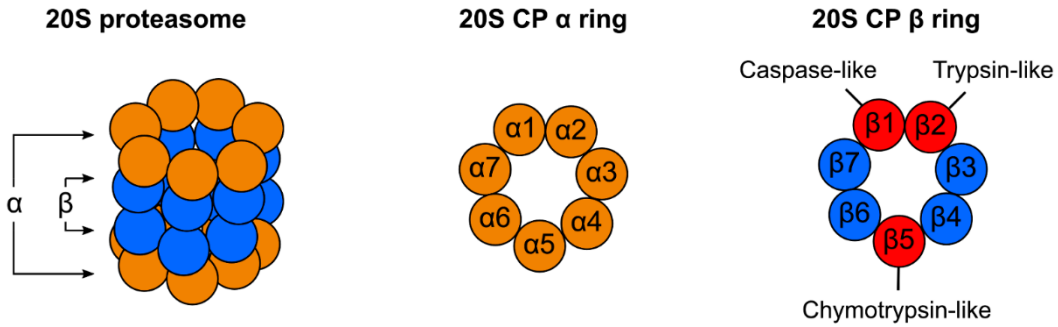

Figure 6 The 20S core particle of the 26S proteasome.

The proteolytically active 20S CP is comprised of two outer α- rings and two inner β-rings, forming the barrel-shaped core particle (CP). Each α- and β-ring is formed by seven distinct but structurally related subunits, with the subunits β1, β2, and β5 to harbor catalytically active peptidase activities.

Enzymatic peptidase activities of the 20S CP can be inhibited, either reversibly by peptidase aldehydes (e.g. MG132) and peptidase boronares (e.g. bortezominb), or irreversibly by β-lactone derivates (e.g. lactacystin) and epoxyketones (e.g. epoxymicin) [34]. It is possible to detect individual peptidase activities of the 20S proteasome via kinetic assays [35].

The regulatory particle

The regulatory particle (RP) of the 26S proteasome, often referred to as 19S RP, is the subunit of the proteasome that first gets in contact with ubiquitinated proteins destined for proteolytic cleavage. The 19S RP harbors 19 integral subunits, which form two subcomplexes: a lid and a base. The lid subcomplex, which sits on top of the base subcomplex, comprises nine non-ATPase subunits (Rpn3, Rpn5-9, Rpn11-12), with Rpn11 exhibiting deubiquitinating enzyme activity that is instrumental for the degradation of ubiquitinated proteasomal substrates [36]. Rpn11 is located next to the substrate entry pore that is formed by the ATPase ring comprising the subunits Rpt1-Rpt6 [37]. By deubiquitinating the ubiquitin chain at a site proximal to the proteasomal substrate, Rnp11 releases the ubiquitin chain *en bloc* from the substrate, which must be further processed by other DUBs, presumably USP5, to generate free conjugation-competent ubiquitin. In contrast, the base subcomplex, which is located next to the 20S CP, comprises six homologous AAA-ATPase subunits (Rpt1-Rpt6), forming a hexameric ring, as well as the non-ATPase subunits Rpn1-Rpn2, Rpn10, and Rpn13 [14]. The ATPase ring essentially unfolds the now deubiquitinated proteasomal substrate, ensures the opening of the channel, and then translocates the substrate into the 20S CP for subsequent destruction by proteolytic cleavage. However, access of the substrate to the proteolytic core is only granted in an ATP bound state (Figure 7).

The predominant role of the 19S RP is recognition, binding, and deubiquitination of polyubiquitinated proteins to recycle ubiquitin moieties. In addition, the ATP-dependent 19S RP unfolds and translocates the now deubiquitinated substrate into the interior of the 20S CP for destruction through regulation of gate opening of the

20 CP α-rings. Collectively, the 19S RP regulates and coordinates all critical steps prior to proteolytic degradation of polyubiquitinated substrates.

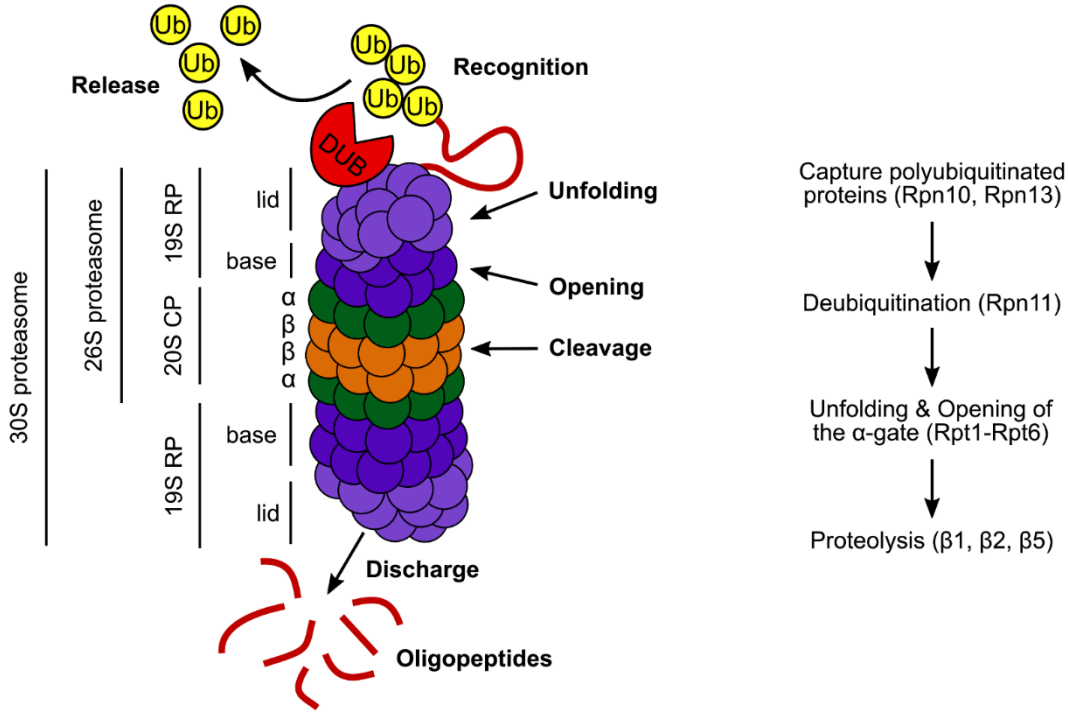

Figure 7 Proteolysis by the proteasome.

The enzymatically active proteasome is capped on either or both ends of the 20S core particle (20S CP) by the 19S regulatory particle (19S RP), forming the 26S- or 30S proteasome, respectively. During proteolysis, the 19S RP captures and removes polyubiquitin chains on proteasomal substrates, unfolds the substrate, and opens the α ring to transfer the unfolded and deubiquitinated substrate into the 20S CP for its destruction.

The 20S CP exists in a free, mainly inactive state, while its default status requires binding via the 19S RP, either as a single-capped 26S proteasome or a double-capped 30S proteasome with two 19S RPs associated with both termini of the 20S CP in opposite directions (Figure 7) [38]. Binding to several proteasome activators, such as PA28 or PA200, opens the gate that is required for entering the catalytic cavity and proteasomal degradation of proteins [39]. However, the 19S RP represents the most potent proteasome activator that promotes ATP- and ubiquitin-dependent substrate turnover.

Impairment of the 26S proteasome

Although proteasome activity is crucial for sustained cell viability, particularly in postmitotic cells such as cardiomyocytes and neurons, the abundance and capacity of proteasomes is rate-limiting. To cope with changing demands under challenging conditions, cells have evolved mechanisms to dynamically modify and adjust the composition and activity of the proteasome when necessary [40, 41]. For instance, increased ubiquitin stress, a condition caused by depletion of free ubiquitin, has been shown to provoke changes in proteasome composition as a result of elevated loading with the proteasomal assembly factor Ubp6 (human orthologue: USP14) [42]. Other studies have shown that the expression of genes encoding several other proteasomal subunits or assembly factors is altered in response to cellular stress. Furthermore, posttranslational modifications of several subunits of the proteasome can alter the composition of the 26S proteasome. Nonetheless, excessive external and internal stressors, e.g. inhibition of proteasome activity, oxidative stress, or aberrantly formed protein aggregates [43-45], results in compromised capacity of the 26S proteasome and extensive accumulation of potentially toxic proteins and protein aggregates, which continuously impede proteostasis [46]. Consequently, diminished proteasome activity and obstructed recycling of free ubiquitin and peptides disturb numerous cellular functions and thus play an important role in the pathology of multiple diseases [47, 48]. Cells respond to reduced proteasome activity, proteasome overload, and shortages of amino acids with efforts to adjust UPS activity via compensatory or regulatory actions of other key components of the PQC network [49]. Hereby, induction of (selective) autophagy eliminates the threat that results from damaged organelles or accumulation of potentially toxic protein aggregates [50, 51].

Deubiquitinating enzymes

Ubiquitination is a reversible process whereby specific proteases, collectively named deubiquitinating enzymes (DUBs), remove ubiquitin moieties of different topology and length from a substrate or within ubiquitin in a polyubiquitin chain [52]. The human genome encodes approximately 100 DUBs, which are classified into six individual families based on sequence and domain similarities (Figure 8): Ubiquitin-specific peptidases (USPs, 56 active members), ovarian tumor proteases (OTUs, 16 active members), JAB1/MPN/Mov34 family (JAMMs, 12 active members), Machado-Joseph disease proteases (MJDs, 4 active members), ubiquitin C-terminal hydrolases (UCHs, 4 active members), and the newly discovered MIU-containing novel DUB family proteases (MINDY, 4 active members) (Figure 8) [53]. JAMMs only comprise zinc metalloproteases, while the other five DUB families are cysteine proteases.

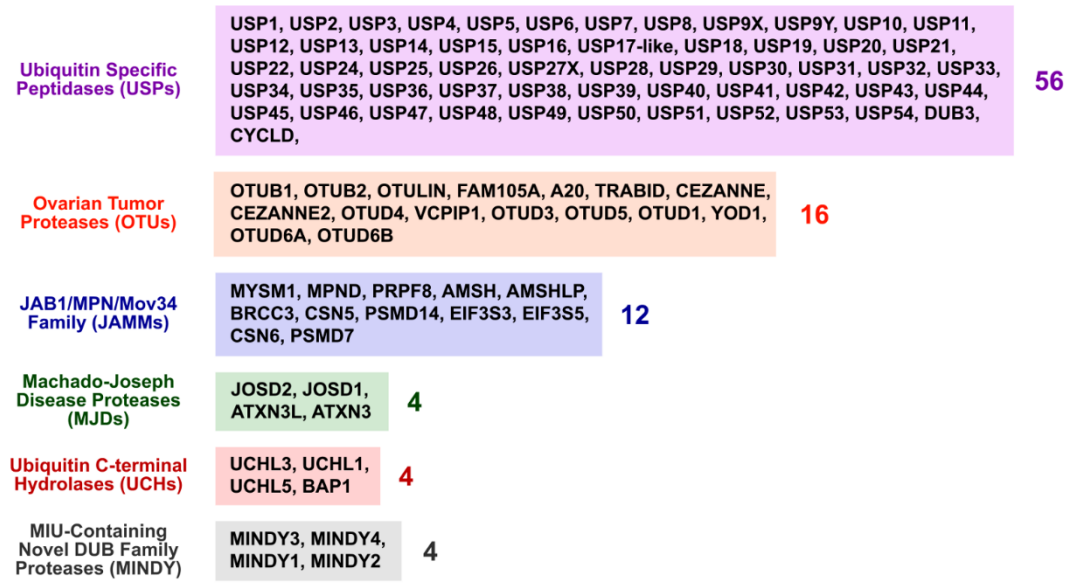

Figure 8 Human deubiquitinating enzymes (DUBs).

Human DUBs are categorized based on their homology in the catalytic domain into six families: ubiquitin specific peptidases (USPs), ovarian tumor proteases (OTUs), JAB1/MPN/Mov34 family (JAMMs), Machado-Joseph disease proteases (MJDs), ubiquitin C-terminal hydrolases (UCHs), and MIU-containing novel DUB family proteases (MINDY). All DUBs are cysteine proteases except for JAMMs, which only comprise zinc-dependent metalloproteases. Modified from [54].

General functions of DUBs

DUBs maintain cellular ubiquitin homeostasis by replenishing the pool of mono-ubiquitin. In addition, many DUBs are important for processing, recycling, and remodeling of polyubiquitin chains on substrates to initiate and sustain ubiquitin-dependent processes, and to release free ubiquitin moieties. In this respect, USP5, a family member of ubiquitin specific peptidases (USPs), maintains the pool of free ubiquitin as it preferentially releases free ubiquitin from unanchored polyubiquitin chains in vitro as well as in flies and yeast [55-58]. However, it remains speculative that USP5 fulfills this function in mammalian cells. Alternatively, there might be other USPs, which catalyze the breakdown of polyubiquitin chain in mammalian cells. In addition to recycling of free ubiquitin, three highly specific DUBs associated with the 19S RP – PSMD14, USP14, and UCHL3 – modulate the fate of a substrate or the rate of substrate degradation by the proteasome by removing ubiquitin moieties, which impede entry of the substrate into the catalytically active 20S CP [59-62]. The 19S RP subunit and metalloprotease PSMD14 (POH1/Rpn11) assists in ubiquitin-dependent proteolysis by removing polyubiquitin chains *en bloc* prior to substrate degradation [63]. Hence, PSMD14 prevents undesired degradation of ubiquitin and releases free ubiquitin chains, which may be further processed by USP5. In contrast, the two transiently proteasome-associated DUBs USP14 and UCHL3 may aid in antagonizing proteolytic cleavage of a substrate by editing the ubiquitin chain, thereby decreasing the affinity of the substrate for the proteasome (Figure 9) [64, 65].

Certain DUBs are further involved in processing of ubiquitin precursor genes to generate active monoubiquitin. Hereby, the two polyubiquitin precursor genes *UBB* and *UBC* are primarily modified by USP5 and Otulin, while UCHL3, USP9X, and USP7 catalyze trimming of the ubiquitin-ribosomal precursor genes *UBA52* and *UBA80* [25]. Moreover, DUBs counteract the ubiquitin cascade by either interfering with the formation of reactive E2- or E3-ubiquitin intermediates or by altering the stability or composition of an E3 complex (Figure 9).

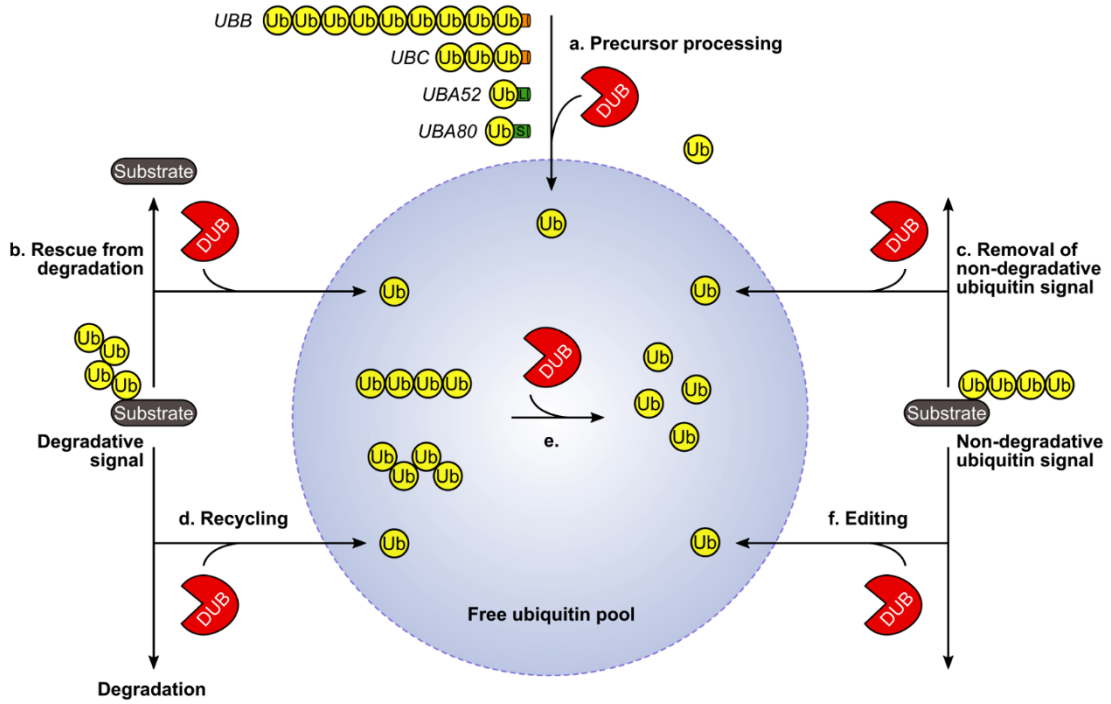

Figure 9 Functions of DUBs.

a. Ubiquitin, encoded by four genes (*UBB, UBC, UBA52,* and *UBA80*), is transcribed and translated as a linear fusion polypeptide consisting of multiple copies of ubiquitin with an extension of one or several amino acids at the carboxyl terminus (shown in orange) or ubiquitin fused to the amino terminus of either the 40S ribosomal protein L40 (L) or 60S ribosomal S27a (S), respectively (shown in green). DUBs assist in processing of these inactive ubiquitin precursors to generate conjugation-competent free ubiquitin. **b.** DUBs can further rescue a substrate from proteasomal degradation **c.** Deubiquitination removes a non-degradative ubiquitin signal from a substrate. **d.** DUBs are central for ubiquitin homeostasis by recycling of ubiquitin prior to degradation of the substrate by the 26S proteasome or autophagy. **e.** DUBs further assist in ubiquitin homeostasis by disassembly of ubiquitin chains generated by *en bloc* removal from a substrate prior to proteolysis. **f.** Some DUBs edit the length and topology of ubiquitin chains with the generated free ubiquitin to re-enter the pool of free ubiquitin. Modified from [60].

As a class of mainly cysteine peptidases that reverse ubiquitination, DUBs play important roles in the regulation of various cellular functions and biological processes, including cell cycle control, DNA damage response [66], gene expression [67], kinase activation [68], microbial pathogenesis [69], UPS-dependent proteolysis, autophagy [70], and many more.

Autophagy

Autophagy, the second major intracellular catabolic system in mammalian cells, acts in lysosomal cleavage of cytosolic fractions, organelles, and macromolecules, to re-supply cells with essential nutrients, which is fundamental for cellular protein homeostasis, cell differentiation, development, cell survival, and cell death. In contrast to UPS-dependent proteolytic processes, autophagy is mainly induced in response to intra- and extracellular stress conditions, including oxidative stress, nutrient deprivation, DNA damage, hypoxia or growth factor depletion. Defects in any step of the autophagic cargo elimination are causative for the development of various diseases, such as cancer, inflammation, neurodegenerative diseases [71, 72], or even cardiovascular disorders [73, 74].

Non-selective autophagy

Non-selective autophagy can be divided into three types: macroautophagy (mainly referred to as autophagy), microautophagy, and chaperone-mediated autophagy (Figure 10). The most common type of non-selective autophagy, macroautophagy, plays a key role for maintaining the energy balance of cells. During macroautophagy, large amounts of cytoplasmic constituents, organelles, and diverse macromolecules (lipids, proteins, carbohydrates, and nuclei acids), are engulfed in a double-membrane vesicle, called an autophagosome, and are transported to the lysosome. Fusion of the autophagosome with lysosomes, which contain diverse hydrolytic enzymes, causes degradation of both the sequestered material and the inner membrane of the autophagosome, and retrograde transport of amino acids across the lysosomal membrane (Figure 10).

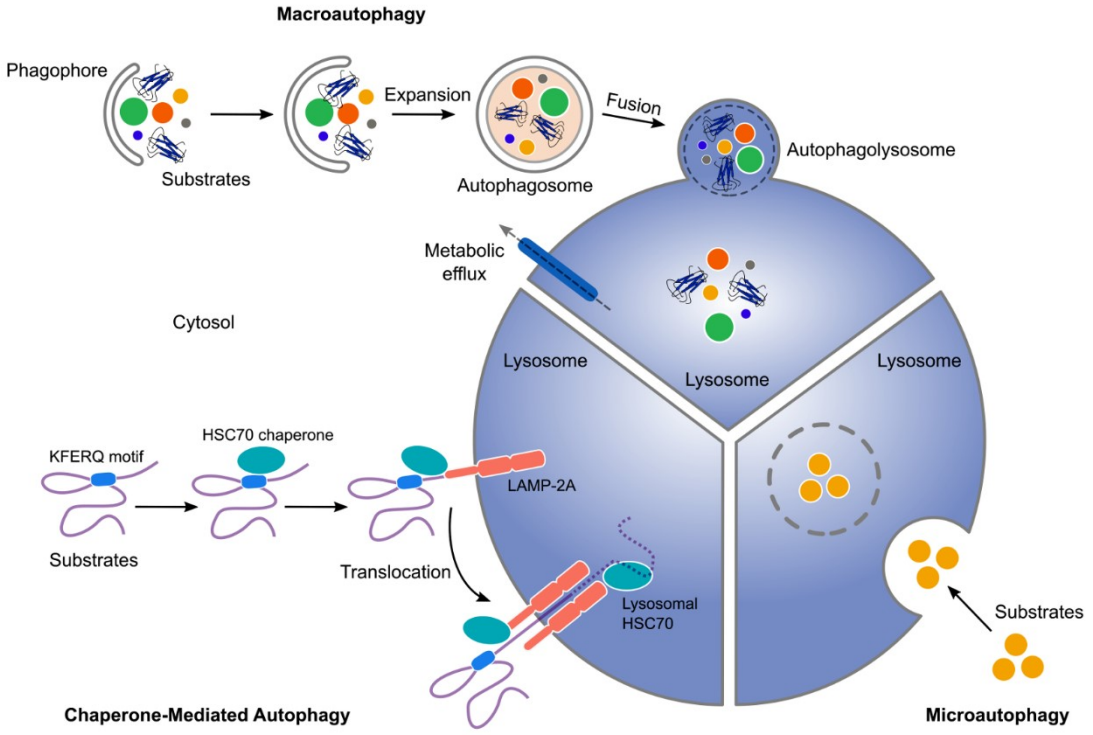

Figure 10 Types of non-selective autophagy.

Autophagy, the intracellular lysosomal-dependent degradation of cellular constituents, macromolecules, and organelles, can be divided into three subtypes according to the cargo delivery to the lysosome lumen: macroautophagy, microautophagy, and chaperone-mediated autophagy. During macroautophagy the cargo is transported inside a double-membrane vesicle, i.e. autophagosome, to fuse with the lysosome. In contrast, microautophagy is characterized by direct delivery of the cargo by local rearrangement of the lysosomal membrane. Chaperone-mediated autophagy requires binding of the cargo carrying a KFERQ motif to the HSC70 chaperone to translocate the cargo across the lysosome, which is mediated by the lysosome-associated membrane protein type 2A (LAMP-2A). Modified from [75].

In contrast, microautophagy and chaperone-mediated autophagy, both equally essential for the energy supply of cells, do not rely on *de novo* synthesis of autophagosomes to sequestrate cytosolic cargos. Microautophagy only requires the formation of lysosomal and endosomal membranes to deliver any cytoplasmic cargos into the lumen of the membranes for subsequent degradation by lysosomal hydrolysis. On the other hand, chaperone-mediated autophagy largely depends on HSC70 and HSC70-associated co-chaperones, which specifically recognize cytosolic cargos carrying the pentapeptide motif KFERQ. Once bound, the Hsc70 complex transports

the cargo with the aid of the lysosomal membrane protein type 2A (LAMP-2A) across the lysosomal membrane for consecutive degradation (Figure 10).

Selective autophagy

Selective autophagy, an alternative type of macroautophagy, evolved as a second major cellular PQC system, which eliminates misfolded and aggregated proteins that – based on their size, structure, and complexity – are excluded from UPS-dependent proteolysis by the 26S proteasome. Selective autophagy further assists in the degradation of specific pathogens and organelles, such as peroxisomes and mitochondria. In contrast to macroautophagy, selective autophagy depends on ubiquitination of the cargo as a common recognition signal. Once ubiquitinated, specific ubiquitin receptors, such as p62, OPTN, or NBR1, recognize and transport the cargo together with its ubiquitin tag, cargo adaptors, and other associated proteins to the autophagic machinery where it is hydrolyzed by lysosomes [76]. Importantly, these adaptors contain two domains: a ubiquitin-binding domain, essential for binding to ubiquitin degrons, and distinct LC3-binding domains, which promote the transport of ubiquitinated protein aggregates to the autophagic membrane (Figure 11) [76].

In parallel, the deacetylase HDAC6 binds via its zinc-finger binding domain to ubiquitin chains on the cargo to induce the retrograde transport of the cargo along microtubule towards the nucleus where it becomes segregated into an aggresome [77]. HDAC6-dependent deacetylation of cortactin is crucial for the final steps of selective autophagy – remodeling of the actinomyosin network, engulfment of the aggresome in autophagosomes, and lysosomal degradation of the aggresome (Figure 11).

In summary, selective clearance by macroautophagy and selective autophagy of potentially harmful cytoplasmic constituents and ubiquitinated proteins, which escaped degradation by the 26S proteasome, is important for PQC to guarantee sustained cellular homeostasis and to avoid cell damage or cell death arising from accumulation of toxic protein aggregates.

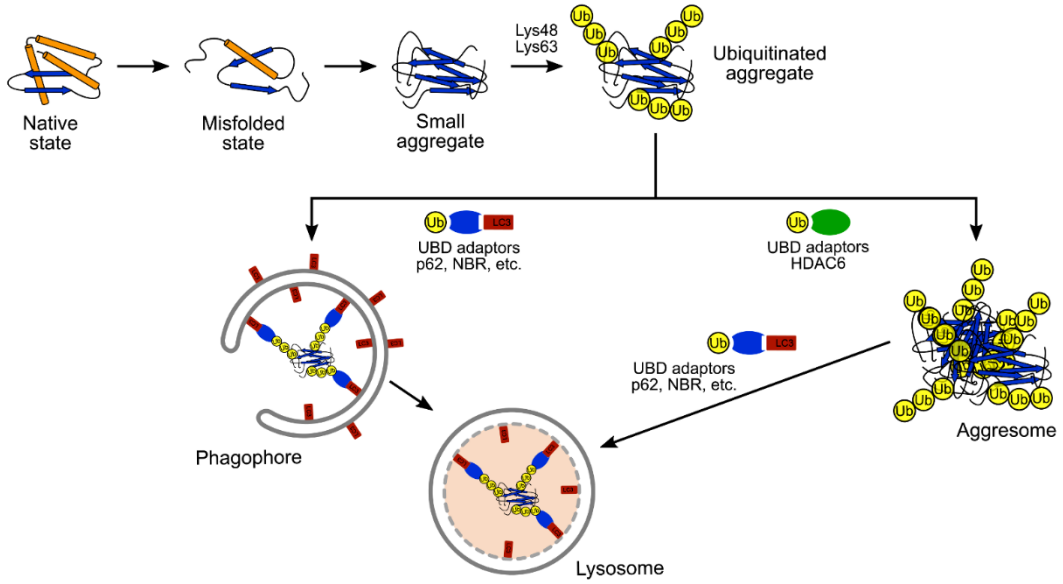

Figure 11 Selective autophagy.

Terminally misfolded proteins, which escaped degradation by the 26S proteasome, tend to form small soluble aggregates, which are tagged with either a Lys48- or Lys63 linkage-specific ubiquitin chain. Binding of these ubiquitin-enriched aggregates by specific adapters of selective autophagy, carrying ubiquitin-binding (UBDs) and LC3-binding domains, e.g. p62, NBR, initiates formation of an autophagosome and autophagic clearance. Alternatively, the deacetylase HDAC6, which carries a zinc-finger binding UBD domain, binds to ubiquitin chains within soluble ubiquitin-conjugated aggregates to support their segregation into aggresomes and subsequent lysosomal degradation. Modified from [18].

Consequences of derailed cardiac protein quality control

Ageing is often accompanied by derailment of proteostasis and concomitant failure of PQC, which not only attenuates protein degradation systems and the cellular stress response [78, 79] but rather favors the formation of protein aggregates. Studies in *C. elegans* have shown that protein synthesis progressively decelerates during aging [80]. While the expression of proteins important for maintaining UPS function, oxidative stress defense, and DNA replication is upregulated, levels of proteins important in mitochondrial and ribosomal PQC continuously decrease. In contrast, ageing in *D. melanogaster* is characterized by enhanced proteotoxicity and protein damage, which is caused by reduced protein synthesis, diminished demand on PQC processes to assist in folding, transport, and clearance of proteins, and failure in proteasome function. In contrast, aged human dermal fibroblasts exhibit reduced levels of chaperones as

well as proteasomal, mitochondrial, and ribosomal proteins. *In-vivo* studies on aged mice yielded similar results, showing mitochondrial proteins and proteins involved in counteracting stress response to be downregulated [81, 82].

As protein functions decline with ageing and as life expectancy continuously increases, successive accumulation of damaged, unfolded, or terminally misfolded proteins along with concomitant failure of PQC processes account for the gradual progression of ageing and age-related diseases, including cancer, immunological and metabolic disorders, and neurodegenerative diseases with most of them still incurable [83, 84]. Numerous studies have shown that derailed proteostasis drives the progression of cardiac disorders, such as atrial fibrillation and cardiomyopathies [3, 85]. Increased proteotoxicity in the heart can result from either loss-of-function or gain-of-function mutations of genes encoding cytoskeletal, sarcolemmal, or nuclear envelope proteins. Loss-of-function mutations impair the contractile and electrophysiological properties of cardiomyocytes due to constant cellular stress and excessive activation of protein catabolic processes [86]. In contrast, gain-of-function mutations favor the formation of amyloid-like protein aggregates causing enhanced proteotoxic stress [87]. Mutations in genes encoding sarcomere and cytoskeleton proteins, including desmin (*Des),* ß-myosin heavy chain *(Myh7),* cardiac troponin (*Tnnt2),* or titin (*Ttn)* are connected to the progression of inherited cardiomyopathies by which chaperone activity and protein catabolic processes are markedly elevated to initially ameliorate accumulation of harmful protein aggregates [88]. Nevertheless, enduring stress drains their capacity and causes degradation of sarcomeric structures, accompanied by cellular dysfunction and loss of functional cardiomyocytes, resulting in cardiac remodeling [89]. During the remodeling process, which mainly affects noncardiomyocytes, such as myofibroblasts, immune cells, and vascular cells, the cardiac muscle is exposed to an increased degree of inflammation and deposition of collagen, intended to maintain cardiac mass. In the end, increased stiffness and disturbed architecture of the myocardium results in cardiac failure [90]. Importantly, inherited cardiomyopathies remain an important cause of cardiac morbidity and

mortality worldwide and are a major cause of cardiac transplantation, since therapeutic strategies still remain limited [88].

Besides cardiac remodeling due to enhanced fibrosis, the derailment of cardiac PQC results in the accumulation of protein aggregates interfering with the 26S proteasome function. Furthermore, protein aggregates impede cellular processes by binding to critical signaling and trafficking molecules, which may induce initiation of the cell death cascade [91, 92]. Protein aggregates have been identified in cardiomyocytes from patients with idiopathic, dilated and hypertrophic cardiomyopathy, but not in cardiomyocytes from healthy aged patients [93].

Cardiomyopathy

Cardiomyopathies are a heterogeneous class of myocardial diseases associated with structural and functional abnormalities, i.e. mechanical or electrical dysfunction, often in combination with inappropriate hypertrophy or dilation of either one or both ventricles. People affected by cardiomyopathies are at high risk for heart failure-related disabilities with most patients dying due to sudden cardiac arrest [15]. The American Heart Association divides cardiomyopathies with regards to the etiology into two major groups: primary (intrinsic) and secondary (extrinsic) cardiomyopathies. Primary cardiomyopathies are myocardial disorders restricted to the cardiac muscle that are caused by either genetic or non-genetic alterations. In contrast, secondary cardiomyopathies are caused by myocardial damage as a result of systemic or multi-organ disorders, such as myocardial ischemia, inflammation, infection, extensive alcohol abuse, or increased drug toxicity.

Alternatively, cardiomyopathies are subdivided into four categories, based on their etiology as well as morphological and functional criteria, which include arrhythmogenic right ventricular cardiomyopathies, restrictive cardiomyopathies, hypertrophic cardiomyopathies, and dilated cardiomyopathies [94].

Arrhythmogenic right ventricular cardiomyopathy

Arrhythmogenic right ventricular cardiomyopathy (ARCV), an inherited type of cardiomyopathy, is characterized by the loss of myocytes and replacement of mainly the right ventricular myocardium with fibrous and white adipose tissue that over time causes ventricular arrhythmias as a result of compromised ventricular inflow, outflow, and apex [94, 95]. The name is misleading, since ARCV is not restricted to the right ventricle. Up to 75 % of all identified patients do also show involvement of the left ventricle [96]. ARV is a very rare type of cardiomyopathy with an estimated prevalence of 1:5000, mainly affecting children, young adults, and athletes.

Restrictive Cardiomyopathy

Restrictive cardiomyopathy (RCM) is the least common form of cardiomyopathies with an unknown prevalence. RMC is mainly characterized by muscle stiffness due to impaired muscle relaxation accompanied by impaired ventricular filling, normal or reduced diastolic volume of the ventricles, and higher diastolic pressure [96]. In most cases, systolic volume remains normal or is slightly reduced while myocardial wall thickness is preserved. In response to restrictive filling with blood and high diastolic pressure, the myocardium is progressively replaced by interstitial fibrotic tissue and calcification, which further promotes muscle stiffness. Patients suffering from RCM often show symptoms of congestive heart failure, including peripheral edema, jugular vein distensions, and gallop rhythm. Other common symptoms of RCM include dyspnea, palpitations, syncope, fatigue, and limited exercise capacity [97].

Hypertrophic cardiomyopathies

Hypertrophic cardiomyopathy (HCM) represents the most common type of cardiomyopathy with a prevalence of 1:500 [98]. HCM is mostly inherited in an autosomal dominant manner and relies often on mutations in genes encoding any of the cardiac sarcomere proteins, although more than 100 genes are linked to the development of HCM with more and more genes being discovered [99]. 70-80 % of

all identified mutations occur in the genes that encode either the ß-myosin heavy chain *(Myh7)*, cardiac myosin binding protein C *(Mybpc)*, or cardiac troponin T *(Tnnt2)*. Mutations in genes that encode cardiac troponin I *(Tnni3)* and α-tropomyosin *(Tpm1)* occur less frequently and account for 10 % of all cases [100].

HCM is characterized by symmetrical or asymmetrical thickening of mainly the left ventricle, increased left ventricular mass, as well as hypertrophied, disorganized cardiomyocytes with enlarged nuclei. In many cases, cardiomyocytes are replaced with fibrotic tissue. Due to the thickness and stiffening of the ventricles, filling of the ventricles with blood becomes limited, which reduces the blood flow to the coronary arteries. Common symptoms of HCM include dyspnea at rest or during exercise, angina pectoris, palpitations, atrial fibrillation, dizziness, and presyncope or syncope. HCM patients, who do not get a heart transplantation in time, most likely die due to arrhythmias and sudden cardiac death [96, 101].

Dilated cardiomyopathies

Dilated cardiomyopathy (DCM) represents the second most common type of cardiomyopathies worldwide with a prevalence of 1:2500. DCM might be primarily caused by genetic and familial non-genetic factors, which account for 20-50 % of all cases, or secondary causes as a result of inflammation and autoimmune diseases. The majority of inherited causes are comprised of genetic mutations, which mainly affect structural proteins, such as the dystrophy-associated glycoprotein complex or components of the sarcomere in addition to cytoskeletal, sarcolemmal, and nuclear envelope proteins. In this regard, mutations in the gene that encodes the sarcomere protein titin *(Ttn)* account for up to 25 % of all identified forms of DCM [102, 103]. Many mutant genes that are linked to the development of DCM encode identical contractile components of the sarcomere, which are already associated with the progression of HCM, such as α-tropomyosin *(TPM1)*, troponin T (*TNNT2*), ß-myosin heavy chain (*MYH7*), or myosin-binding protein C (*MYBPC3*) [96]. Other inherited causes of DCM include mutations in the gene encoding the intermediate filament desmin [104] or in genes encoding heat shock proteins, ion channels, and

mitochondrial proteins [105]. Acquired causes of DCM include infections, e.g., myocarditis, endocrine or metabolic disorders, or progressive alcohol and drug abuse [15].

DCM is characterized by dilation and enlargement of the left ventricle accompanied by persistent weakness, which results in systolic dysfunction in the absence of severe coronary artery disease [106, 107]. Permanent dilation of the left ventricle causes morphological changes and cardiac remodeling, by which the left ventricle becomes increasingly thin and thus acquires a more spherical, less elongated shape. Progressive cardiac remodeling leads to irreversible pathophysiological changes and deposition of interstitial or perivascular fibrotic tissues. Alterations in cardiac function, including decreased stroke volume, cardiac output, and ventricular filling, in combination with elevated end-diastolic pressure and cardiac preload and afterload are clinical characteristics of DCM. Collectively, all these alterations promote increased wall stress and elevated myocardial oxygen demand, which often result in myocyte damage and decline in myocardial performance. Progressive DCM results in congestive heart failure with elevated incidence of thromboembolic events, ventricular arrhythmias, and electromechanical dissociation of cardiomyocytes causing cardiac arrest in approximately 12 % of all DCM patients.

Patients suffering from DCM show signs of tachycardia, excessive sweating, fluid retention, and ankle edema, accompanied by orthopnea and fatigue. Some patients also show symptoms like nausea, anorexia, or cachexia. However, DCM progresses exceptionally slowly until definite symptoms of congestive heart failure become evident. Nevertheless, with a prevalence rate of 25-30 % and a 1-year mortality rate of 50 % survival, DCM remains a most common indication for heart transplantation worldwide [15, 108, 109].

AIM OF THE STUDY

The present study was designed to examine the role of deubiquitinating enzymes (DUBs) in protein quality control (PQC) in the heart and to reveal its physiological function in the myocardium.

To address this aspect, proximity-dependent biotinylation and affinity purification assay (BioID) was used to identify DUBs that interact with defined components of cellular PQC. Cardiac-specific conditional gain- and loss-of-function approaches in combination with diverse molecular and cell biology relevant techniques was applied to determine the function of these DUBs, predominantly with respect to their role in cardiac proteostasis both *in-vitro* and *in-vivo*.

MATERIAL AND METHODS

Material

Animal Nutrition

Table 1 Animal nutrition

Animal nutrition	Company
ssniff M-Z Extrudat	ssniff Spezialdiäten GmbH

Drugs

Table 2 Drugs

Drug	Company	Catalog no.
4-Hydroxytamoxifen	SIGMA-ALDRICH	H7904-5MG
Tamoxifen ≥ 99 %	SIGMA-ALDRICH	T5648-5G

Enzymes

Table 3 Enzymes

Enzyme	Company	Catalog no.
Proteinase K	Carl Roth	7528.2
SuperScript™ II Reverse Transcriptase including 5 x First strand buffer, 0.1 M DTT	ThermoFisher SCIENTIFIC	18064014
Taq Polymerase	Homemade	
Trypsin EDTA	ThermoFisher SCIENTIFIC	R001100
Trypsin	SIGMA-ALDRICH	T0303

Fluorogenic substrates

Table 4 Fluorogenic substrates

Fluorogenic substrate	Company	Catalog no.
Boc-Leu-Arg-Arg-AMC	Enzo	BML-BW8515
Suc-Leu-Leu-Val-Tyr-AMC	Enzo	BML-P802
Z-Leu-Leu-Glu-AMC	Enzo	BML-ZW9345

Inhibitors

Table 5 Inhibitors

Inhibitor	Company	Catalog no.
Aprotinin	SIGMA-ALDRICH	10820
Leupeptin	SIGMA-ALDRICH	L8511-5MG
Sodium fluoride (NaF)	SIGMA-ALDRICH	S7920-100G
Sodium orthovanadate (Na_3Vo_4)	SIGMA-ALDRICH	450243
MG132 In-solution	Calbiochem	474791
Phenylmethylsulfonyl fluoride (PMSF)	SIGMA-ALDRICH	P7626

Chemicals and reagents

Table 6 Chemicals and Reagents

Chemical	Company	Catalog no.
Acetonitrile	Fluka	00687
Agar 100 Resin Kit	Agar Scientific Ltd	AGR1031
Agarose	Carl Roth	2267
Adenosine 5'-triphosphate disodium salt hydrate	SIGMA-ALDRICH	A-3377
Ammonium persulfate	Serva	3375
Anti-V5 agarose conjugated beads	SIGMA-ALDRICH	A7345-1ML
Biotin (≥99 %)	SIGMA-ALDRICH	B4501-100MG
Bis-Tris	AppliChem	A1025,0500
Bovine serum albumin (BSA)	Fisher Scientific	BP 1605
Bovine serum albumin solution (BSA)	SIGMA-ALDRICH	A7284-500ML
2,3-Butanedione monoxime (≥98 %)	SIGMA-ALDRICH	B0753-25G
Calcium chloride x $2H_2O$	Carl Roth	5239.2

Chloroquine	SIGMA-ALDRICH	C6628
Creatinine hydrate	SIGMA-ALDRICH	C3630
DAPI (4', 6-diamidino-2-phenylindole)	ThermoFisher SCIENTIFIC	D1306
Deoxycholic acid	Fluka	30970
Dimethyl sulfoxide (DMSO)	SIGMA-ALDRICH	D-4540
Disodium hydrogen phosphate (Na_2HPO_4)	Merck	6580.0500
Dynabeads® MyOne™ Streptavidin C1	ThermoFisher SCIENTIFIC	65001
1,4-Dithiothreit (DTT)	Carl Roth	6908.2
EDTA	Carl Roth	8040.3
EGTA	SIGMA-ALDRICH	E3889
Entellan	Merck	1079600500
Ethanol (100 %)	Carl Roth	9065.4
Ethidium bromide solution (1 %)	AppliChem	A1152,0100
FSC 22 Frozen Section Compound	Leica	75806-668
Fetal calf serum (FCS)	SIGMA-ALDRICH	F2442
Formic acid	Merck	1.00264.1000
Gelatin from porcine skin	SIGMA-ALDRICH	G1890
Glucose	Carl Roth	X997.2
L-Glutamine-penicillin-streptomycin solution	SIGMA-ALDRICH	G6784-100ML
Glutaraldehyde	SIGMA-ALDRICH	G5882
Glycerin (87 %)	Merck	1.04094.2500
Glycine	SIGMA-ALDRICH	15527
HEPES	Carl Roth	9105.3
Hydrochloric acid (37 %)	Carl Roth	4625.1
InstantBlue Protein Stain	Expedeon	ISB1L
Insulin-Transferrin-Sodium Selenite Media Supplement	SIGMA-ALDRICH	11074547001
Iodoacetamide	SIGMA-ALDRICH	I6125
Isopropanol	Carl Roth	6752.4
L-Carnitine x HCl	SIGMA-ALDRICH	A6706
Leupeptin	ThermoFisher SCIENTIFIC	78435
Liberase™	Roche	05401151001
Lithium chloride	Carl Roth	P007.1
Magnesium chloride x $6H_2O$	Carl Roth	2189.1

Magnesium sulfate heptahydrate ($MgSO_4$ x $7H_2O$)	Merck	5886
Methanol	Carl Roth	4627.5
Miglyol	Caesar + Loretz	3274
Nonidet P40	Fluka	74385
4 x NuPAGE™ LDS Sample Buffer	ThermoFisher SCIENTIFIC	NP0008
Oligo 15 primer	Promega	C110A
Osmium tetroxide	SIGMA-ALDRICH	75632-10ML
Paraformaldehyde	Carl Roth	0335.4
Penicillin-Streptomycin (10,000 U/mL)	ThermoFisher SCIENTIFIC	15140122
Phenylmethylsulfonyl fluoride (PMSF)	SIGMA-ALDRICH	P7626
Polybrene infection reagent	SIGMA-ALDRICH	TR-1003
Potassium chloride (KCl)	Carl Roth	6781.3
Potassium bicarbonate ($KHCO_3$)	Merck	1.04854.0500
Potassium dihydrogen phosphate (KH_2PO_4)	Carl Roth	P018.1
Protein G Sepharose 4 Fast Flow beads	GE Healthcare	17061801
Red Alert™ 10x	Merck	71078-3
RNasin Plus	Promega	
Rotiphorese® Gel 40 (29:1)	Carl Roth	A515.1
Roti® Quant	Carl Roth	K015.2
SDS	Carl Roth	2326.3
Skim milk	Fluka	70166
Sodium azide (NaN_3)	Carl Roth	K305.1
Sodium bicarbonate ($NaHCO_3$)	Merck	1.06329.0500
Sodium chloride (NaCl)	Carl Roth	3957.2
Sodium deoxycholate	Merck	1.06504.0100
Sucrose	Carl Roth	9097.1
Taurine	SIGMA-ALDRICH	T0625
TEMED	Carl Roth	2367.1
Tris	Carl Roth	5429.2
Triton-X 100	Carl Roth	6683.1
TurboFect transfection reagent	ThermoFisher SCIENTIFIC	R0531
Tween-20	Merck	822184.0500
Xylol	Carl Roth	9713.3

Buffers and solutions

Table 7 Buffer Solutions

Buffer	Composition
AbDil-Tx	1 x TBS; 0.1 % Triton X-100; 2 % BSA; 0.1 % NaN_3
10 % APS	Dilute 10 g APS in 100 mL Aqua dest.
BioID lysis buffer	50 mmol L^{-1} TrisCl; pH 7.4; 500 mmol L^{-1} NaCl; 0.2 % SDS; supplemented with protease inhibitors and PMSF
BioID wash buffer 1	2 % SDS
BioID wash buffer 2	0.1 % deoxycholic acid; 1 % Triton X-100; 1 mmol L^{-1} EDTA, pH 8.0; 500 mmol L^{-1} NaCl; 50 mmol L^{-1} HEPES, pH 7.5
BioID wash buffer 3	0.5 % deoxycholic acid; 0.5 % NP-40; 1 mmol L^{-1} EDTA, pH 8.0; 250 mmol L^{-1} LiCl; 10 mmol L^{-1} TrisCl, pH 7.4
5 % BSA	Dilute 5 g APS in 100 mL 1 x TBS-T
Cardiomyocyte isolation calcium-free buffer	113 mmol L^{-1} NaCl; 4.7 mmol L^{-1} KCl; 0.6 mmol L^{-1} KH_2PO_4; 0.6 mmol L^{-1} Na_2HPO_4; 1.2 mmol L^{-1} $MgSO_4$ x $7H_2O$; 12 mmol L^{-1} $NaHCO_3$; 10 mmol L^{-1} $KHCO_5$; 10 mmol L^{-1} HEPES; 30 mmol L^{-1} taurine; 10 mmol L^{-1} 2,3-butanedionemonoxime; 5.5 mmol L^{-1} glucose
Cardiomyocyte isolation enzyme buffer	0.25 mg·mL^{-1} Liberase™ DH; 0.14 mg·mL^{-1} trypsin; 12.5 µmol L^{-1} $CaCl_2$ in calcium-free buffer
Cardiomyocyte isolation stop buffer 1	10% FCS; 12.5 µmol L^{-1} $CaCl_2$ in enzyme buffer
Cardiomyocyte isolation stop buffer 2	5 % FCS; 12.5 µmol L^{-1} $CaCl_2$ in enzyme buffer
Cardiomyocyte cell culture medium	M199 cell culture medium supplemented with 5 mmol L^{-1} creatinine x H_2O; 2 mmol L^{-1} L-carnitine x HCl; 5 mmol L^{-1} taurine; 25 mmol L^{-1} HEPES; 1 % penicillin/streptavidin; 10% fetal calf serum; 1% insulin-transferrin-sodium selenite media supplement, pH 7.3.
Electron Microscopy fixation buffer	1.5 % glutaraldehyde; 1.5 % paraformaldehyde in 0.15 mol L^{-1} HEPES
Extraction buffer	100 mmol L^{-1} Tris-HCl, pH 8.0; 10 mmol L^{-1} EDTA; 10% SDS
Immunofluorescence blocking buffer	2 % FCS; 2 % BSA in 1x PBS
Mass Spec Buffer A	0.1 % formic acid
Mass Spec Buffer B	80 % acetonitrile; 0.1 % formic acid
5 % Immunoblot blocking solution	Dilute 5 g skim milk in 100 mL 1 x TBS-T

10 x PBS, pH 7.4	Dilute 80 g NaCl; 2 g KCl; 14.4 g Na_2HPO_4; 2.4 g KH_2PO_4 in 800 mL Aqua dest.; adjust pH to 7.4; refill to 1000 mL with Aqua dest.
1 x PBS, pH 7.4	100 mL 10x PBS + 900 mL Aqua dest.; adjust pH to 7.4
2 x Proteasome assay buffer	50 mmol L^{-1} Tris, pH 8.0; 0.5 mmol L^{-1} EDTA, pH 8.0; 40 µmol L^{-1} fluorogenic substrate; ± 40 µmol L^{-1} proteasome inhibitor
Proteasome lysis buffer	10 mmol L^{-1} Tris, pH 7.5; 1 mmol L^{-1} EDTA, pH 8.0; 2 mmol L^{-1} ATP; 20% Glycerole; 4 mmol L^{-1} DTT
RIPA lysis buffer, pH 8.0	50 mmol L^{-1} Tris, pH 7,4; 150 mmol L^{-1} NaCl; 1 % NP-40; 0.5 % sodium deoxycholate; 0.1 % SDS; protease inhibitors (2 mg mL^{-1} aprotinin, 2 mg mL^{-1} leupeptin, 1 mol L^{-1} Na_3VO_4, 1 mol L^{-1} NaF, 0.2 mol L^{-1} PSMF)
10 % SDS	Dilute 10 g SDS in 100 mL Aqua dest.
50 x TAE	Dilute 242 g Tris Base; 57.1 mL acetic acid; 100 mL 0.5 mol L^{-1} EDTA, pH 8.0 in 1000 mL Aqua dest.
10 x TBS, pH 7.6	0.2 mol L^{-1} Tris, 1.4 M NaCl
1 x TBS	100 mL 10 x TBS + 900 mL Aqua dest.
1 x TBS/T	100 mL 10 x TBS + 900 mL Aqua dest. + 0.1 % Tween®20
TENS lysis buffer	1 mol L^{-1} Tris/HCl, pH 8.0; 0.5 mol L^{-1} EDAT, pH 8.0; 4 mol L^{-1} NaCl; 20 % SDS
10 x TE	100 mmol L^{-1} Tris-Cl; 10 mmol L^{-1} EDTA, pH 8.0
1 x TE	100 mL 10 x TE + 900 mL Aqua dest.
20 x Transfer buffer	Dilute 163.2 g Bicine; 209.6 g Bis-Tris; 12 g EDTA in 1000 mL Aqua dest.
1 x Transfer buffer	250 mL 20 x transfer buffer; 1000 mL methanol; 3750 mL Aqua dest.
1 M Tris, pH 6.8	Dilute 12.1 g Tris in 80 mL Aqua dest.; adjust pH to 6.8; refill to 100 mL with Aqua dest.
1.5 M Tris, pH8.8	Dilute 18.17 g Tris in 80 mL Aqua dest.; adjust pH to 8.8; refill to 100 mL with Aqua dest.
Ubiquitin immunoblot blocking buffer	0.5 % gelatin from porcine skin + 0.05 % Tween®20 in 1 x PBS

Table 8 Ready-to-use Buffer Solutions

Buffer	Company	Catalog no.
NuPAGE™ MES SDS Running Buffer	ThermoFisher SCIENTIFIC	NP000202
NuPAGE™ MOPS SDS Running Buffer	ThermoFisher SCIENTIFIC	NP000102
TaqMan™ Gene Expression Master Mix	Applied Biosystems™	10525395

Gel electrophoresis

Table 9 Composition of a 9 % separating gel

Reagent	Add	Final concentration
Aqua dest	4.2 mL	
Acrylamide / Bisacrylamide (30 % / 0.8 %)	3.0 mL	9 %
1.5 mM Tris (pH 8.8)	2.6 mL	0.39 mmol L^{-1}
10 % SDS	0.1 mL	0.1 %
10 % APS	0.1 mL	0.1 %
TEMED (> 99 %)	0.01 mL	0.04 %

Table 10 Composition of a 5 % stacking gel

Reagent	Add	Final concentration
Aqua dest	2.975 mL	
Acrylamide / Bisacrylamide (30 % / 0.8 %)	0.67 mL	4 %
0.5 mM Tris (pH 6.8)	1.25 mL	0.125 mmol L^{-1}
10 % SDS	0.05 mL	0.025 %
10 % APS	0.05 mL	0.025 %
TEMED (fertig, 99 %)	0.005 mL	0.00025 %

Marker

Table 11 Marker

Marker	Company / Composition
Protein Marker VI (10 - 245) prestained BC	PanReac AppliChem
PUC Marker	Homemade

Antibodies

Primary antibodies

Table 12 Primary antibodies for immunoblotting

Primary antibody	Dilution	Catalog no.	Company
anti-Caspase-3	1:1000	9662	Cell Signaling Technology
anti-Cleaved Caspase-3 (Asp175) (5A1E)	1:1000	9661	Cell Signaling Technology
anti-GAPDH	1:1000	2118	Cell Signaling Technology
anti-GFP	1:2000	ab6556	Abcam
anti-HDAC6	1:500	PAB18362	Abnova
Anti-HDAC6	1:2000	A301-342A	Bethyl Laboratories
anti-LC3A/B (D3U4C)	1:1000	12741	Cell Signaling Technology
anti-PSMA4	1:1000	ab191403	Abcam
anti-PSMC4	1:1000	TA332530	OriGene
anti-PSMD4	1:1000	12441	Cell Signaling Technology
anti-PSMD11	1:2000	NBP1-46192	Novus Biologicals
anti-PSMD12	1:1000	orb214470	Biorbyt
anti-PSMD14	1:1000	ab109123	Abcam
anti-SQSTM1/p62	1:250	ab56416	abcam
anti-α-tubulin	1:2000	T6074	Sigma-Aldrich
anti-Ubiquitin (P4D1)	1:1000	3936	Cell Signaling Technology
anti-Ubiquitin, Lys48-Specific, clone Apu2	1:1000	05-1307	Millipore
anti-Ubiquitin, Lys63-Specific, clone Apu3	1:1000	05-1308	Millipore
anti-Ubiquitin, Lys63-Specific, clone Apu3	1:1000	ab179434	abcam
anti-USP5	1:1000	A301-542A	Bethyl Laboratories
anti-V5	1:5000	ab9116	Abcam

Table 13 Primary antibodies for immunofluorescence staining

Primary antibody	Dilution	Catalog no.	Company
anti- actin, α-smooth muscle	1:250	A2547	Sigma-Aldrich
anti-ACTN1	1:250	ab68194	Abcam
anti-Cleaved Caspase-3 (Asp175) (5A1E)	1:250	9661	Cell Signaling Technology
anti-HDAC6	1:500	PAB18362	Abnova
anti-Phalloidin-FITC	1:250	P5282	Sigma-Aldrich
anti-Phalloidin-TRITC	1:300	P1951	Sigma-Aldrich
anti-phospho Histone H3 (Ser10)	1:100	9701	Cell Signaling Technology
anti-SQSTM1/p62	1:250	ab56416	Abcam
anti-Ubiquitin (P4D1)	1:250	3936	Cell Signaling Technology
anti-USP5	1:1000	A301-543A	Bethyl Laboratories

Secondary antibodies

Table 14 Secondary antibodies for immunoblot analysis

Secondary antibody	Dilution	Catalog no.	Company
goat-anti-mouse IgG, HRP	1:2000	31430	ThermoFisher SCIENTIFIC
goat-anti-rabbit IgG, HRP	1:2000	31460	ThermoFisher SCIENTIFIC

Table 15 Secondary antibodies for immunofluorescence staining

Secondary antibody	Dilution	Catalog no.	Company
F(ab')2-Goat anti-Rabbit IgG (H+L) Cross-Adsorbed Secondary Antibody, Alexa Fluor 488	1:1000	A-11070	ThermoFisher SCIENTIFIC
Goat anti-Mouse IgG (H+L) Cross-Adsorbed Secondary Antibody, Alexa Fluor 488	1:1000	A-11001	ThermoFisher SCIENTIFIC
Goat anti-Mouse IgG (H+L) Cross-Adsorbed Secondary Antibody, Alexa Fluor 594	1:1000	A-11005	ThermoFisher SCIENTIFIC
Goat anti-Rabbit IgG (H+L) Cross-Adsorbed Secondary Antibody, Alexa Fluor 594	1:1000	A-11012	ThermoFisher SCIENTIFIC

Primers

Table 16 Primers for cloning

Name	Sequence
Flag-HA-BigT-for	5'-GCT AGC AAT CGC CAC ACT ACA GAA CG-3'
Flag-HA-BigT-rev	5'-GCG GCC GCT TAC TAG GCG TAG TCG GG-3'
hsUSP5-isoform-for	5'-gat gac ttc tgg agc acg gcc ctg-3'
hUSP5-isoform-rev	5'-GCG GCC GCt tag ctg gcc act ctc tgg tag aag-3'
Psmd14-GFP-for	5'-aat aTT AAT TAA GCT AGC GCA TCG CCA TGA CCT CAA CCG GCC AGG ATT CC-3'
Psmd14-GFP-rev	5'-ata tGT CGA CGT GTG GGT GGG GCA TAT CCT CC-3'
Psmd14-V5-for	5'-aat aTT AAT TAA GCT AGC GCA TCG CCA TGA CCT CAA CCG GCC AGG ATT CC-3'
Psmd14-V5-rev	5'-atG GCG CGC GGC CGC GGA TCT ATC ACG TAG AAT CGA GAC CGA GGA GAG GGT TAG GGA TAG GCT TAC CTT TAA ATA CAA CAG TAT CCA ACA TTG CGG CC-3'
Hdac6-GFP-for	5'- aat aTT AAT TAA GCT AGC GCA TCG CCA TGG ACA GAC TTC TTA GAC TTG GAG G-3'
Hdac6-GFP-rev	5'- tat CTC GAG TTT AAA TAC AAC AGT ATC CAA CAT TGC GGC C-3'
hsUSP5-C-Fusion-for	5'-atc tcg TTA ATT AAG CAT CGC CAC CAT GGC GGA GCT GAG TGA GGA G-3'
hsUsp5-C-Fusion-rev	5'-ata tCT CGA GGC TGG CCA CTC TCT GGT AG-3'
hsUSP5-N-Fusion-for	5'-ata tCT CGA GAT GGC GGA GCT GAG TGA GGA G-3'
hsUSP5-N-Fusion-rev	5'-ata tGG CGC GCC taT TAG CTG GCC ACT CTC TGG TAG-3'
BirA-HA-for	5'-gcg cTT AAT TAA gat cga tcC TCG Aga agg aca ccg tgc ccc tg-3'
BirA-HA-rev	5'-tat GGC GCG Cct atg cgt aat ccg gta cat cg-3'
Myc-BirA-for	5'-atc tcg TTA ATT AAG CAT CGC CAC Cat gga aca aaa act cat ctc aga gga tct c-3'
Myc-BirA-rev	5'-ata tGG CGC GCC TTA AGC TTG GTA CCG AGC TCG G-3'

qRT-PCR probes

Table 17 TaqMan assay qRT-PCT probes

Name	Assay ID	Species
Acta1	Mm00808218_g1	mouse
Fbxo32	Mm00499523_m1	mouse
Klhl40	Mm01350720_m1	mouse
Myc	Mm00487804_m1	mouse
Myh6	Mm00440359_m1	mouse
Myh7	Mm00600555_m1	mouse
Nppa	Mm01255748_g1	mouse
Psmd4	Mm01263490_m1	mouse
Rps27a	Mm01180369_g1	mouse
Uba52	Mm02601856_g1	mouse
Ubb	Mm01622233_g1	mouse
Ubc	Mm02525934_g1	mouse
Uch-l1	Mm00495900_m1	mouse
Usp5	Mm00496734_g1	mouse
Gapdh	Mm99999915_g1	mouse

Plasmids

Table 18 Plasmids

Plasmid	Catalog no.	Company
Flag-HA-USP5	22590	Addgene (Wade Harper)
Human ORFeome V8.1 Library	OHS7588	Dharmacon™
pcDNA3.1 MCS-BirA*(R118G)-HA	36047	Addgene (Kyle Roux Lab)
pcDNA3.1 mycBirA*	35700	Addgene (Kyle Roux Lab)

Viruses

Table 19 Viruses

Virus	Catalog no.	Company
Ad-Null	1240	VECTOR BIOLABS
Ad-CVM-iCre	1045	VECTOR BIOLABS
eGFP wildtype titin		Gift from Prof. M. Gautel
eGFP p.C31712R titin		Gift from Prof. M. Gautel

Kits

Table 20 Kits

Kit	Catalog no.	Company
Direct-zol™ RNA Kit	R2052	Zymo Research
ProteoStat® Aggresome Detection Kit	ENZ-51035-K100	Enzo
Super Signal® West Pico Chemiluminescent Substrate kit	PI34080	Thermo Fisher SCIENTIFIC

Equipment

Table 21 Equipment

Equipment	Company
2K CCD camera	TRS, Tröndle
Adhesive PCR Plate Seals	ThermoFisher SCIENTIFIC
Agarose gel electrophoresis chamber	Peqlab
Bio Doc analyzer	Bio RAD
Centrifuge	Eppendorf
Centrifuge	Eppendorf
ChemiDoc™ MP Imaging System	BIO RAD
Cold Plate for Tissue Embedding System	Leica
Cryostat	Leica
Eppendorftubes, 0.5 mL, 1.0 mL, 2.0 mL	Eppendorf
Filter tips (10 µL, 20 µL, 100 µL, 1000 µL)	Fisher Scientific
Flattening table	Leica
Fridge/Freezer	Bosch
Gelsystems (Mini, Maxi)	VWR
Greiner 96 well plates, polystyrene	Thermo Fisher SCIENTIFIC
Greiner centrifuge tubes, 15 mL	Sigma-Aldrich
Greiner centrifuge tubes, 50 mL	Sigma-Aldrich
Heating block	IKA Labortechnik
Tissue homogenizer	POLYTRON
Keyence Fluorescence Microscope	Keyence
Micro Centrifuge	Carl Roth
MicroAmp™ Fast Optical 96-Well Reaction Plate	ThermoFisher SCIENTIFIC
Microtome	Leica
Mini centrifuge	Carl Roth

Multimode Microplate Reader	BERTHOLD Technologies
Nitrocellulose membranes	Invitrogen
Orbital platform shaker	Heidolph
PCR Cycler	BIO RAD
pH meter	HANNA instruments
Pipettes	Rainin
Power Supply	Carl Roth, BIO RAD
Scales / Precision Balances	KERN, Sartorius
Sonicator	BANDELIN SONOPLUS
StepOnePlus™ Real-Time PCR System	ThermoFisher SCIENTIFIC
SuperFrost Plus slides	Menzel-Glaeser
Swing mill	Retsch
Thermomixer comfort	Eppendorf
ThermoMixer®	Eppendorf
Tips (10 µL, 20 µL, 100 µL, 1000 µL)	Greiner Bio-One
Tissue cell culture plate	VWR
Transmission electron microscope	Zeiss
Ultra-Turrax mit Netzgerät und Dispersionswerkzeug	IKA Labortechnik
Universal Oven	Memmert
UV Transilluminator	INTAS
Vacufuge™ Concentrator	Eppendorf
Vortex mixer	Scientific Industries, Inc.
Waterbath	Leica
XCell SureLock™ Mini-Cell and XCell II™ Blot Module	ThermoFisher SCIENTIFIC

Software

Table 22 Software

Software	Company
Gimp-2.8	GIMP
Graph Pad Prism 7.0	Graph Pad Software
Image J / Fiji	NIH
Image Lab	Bio RAD
MaxQuant (1.5.3.12)	MPG
Microsoft Office 2016	Microsoft Corporation®

Methods

Animals

Experiments involving animal health care and treatments were performed in agreement with institutional guidelines and the German animal welfare law. Each experiment was approved by the local governmental animal protection committee (Regierungspräsidium Darmstadt, B2/1136). All mice used in this study were housed in individually ventilated cages accompanied with environmental enrichment under specific pathogen-free conditions in the Animal House Facility of the Max Planck Institute for Heart and Lung Research, Bad Nauheim, Germany. Age-matched littermates were used for individual experiments. The number of mice used in each experiment is indicated in the figure legend.

Engineering of genetically modified mice

Conditional USP5 KO mice

Transgenic mice harboring a tissue or cell-type specific deletion of *Usp5* were generated in house. All animals were kept on a C57bl/6 genetic background.

The *Usp5* conditional knockout allele was engineered by electroporating the Targeted Knockout First construct *Usp5*$^{tm1a(EUCOMM)Hmgu}$ (EuMMCR), which contains an antibiotic neomycin resistance selection cassette, a lacZ cassette, and two *loxP* sites flanking exon 3-6, into V6.5 F1 hybrid embryonic stem ES cells (Figure 12). Targeted stem cell clones were selected by G418 treatment and screened by southern blotting with 5' genotyping by SmaI digestion. Positive ES cell clones were injected into C57bl/6 (B6) blastocysts to generate chimeric mice (genotype: *Usp5 flox neo*/+). Chimeras were intercrossed to *Flpe*-recombinase expressing transgenic mice [110] to generate neomycin cassette deleted, heterozygous mice (genotype: *Usp5 flox*/+), which were backcrossed to C57bl/6 mice and bred to homozygosity (genotype: *Usp5 flox*/*flox*).

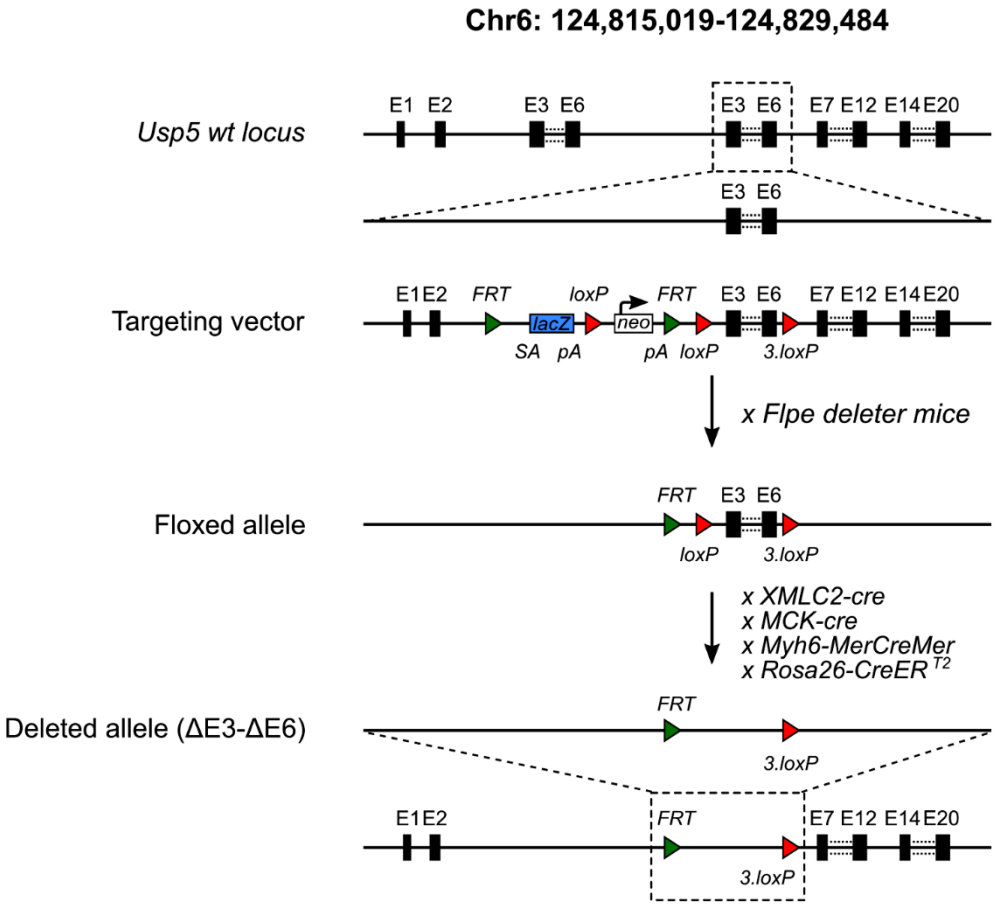

Figure 12 Generation of transgenic mice to conditionally delete USP5 in a cell-type restricted manner.

Schematic illustration of gene targeting strategy to generate a tissue- and cell-type specific *Usp5* mutant allele by which the exons 3 and 6, encoding the zinc-finger binding domain and the catalytic active site of *Usp5*, are flanked by a *loxP* site (red triangles). *Cre* recombinase mediated deletion resulted in a non-functional protein. E, exon; FRT, FLPe recognition target site; lacZ, ß-galactosidase reporter; neo, neomycin resistance cassette; wt, wildtype.

Conditional, *cre*-mediated recombination in the myocardium was implemented by crossbreeding *Usp5 flox/flox* mice with either *XMLC2-cre* [111] or *MCK-cre* [112] transgenic mice to facilitate deletion of *Usp5* at embryonic (genotype: *Usp5 flox/flox//XMLC2-cre*) or juvenile stage (genotype: *Usp5 flox/flox//MCK-cre*). For c*re*-mediated recombination in adult stage, *Usp5 flox/flox* mice were crossbred with transgenic mice by which the *Myh6 (aMHC)* promoter directs expression of a tamoxifen-inducible *MerCreMer* recombinase [113] (Figure 12). Intraperitoneal (i.p.)

injection of 100 mg kg^{-1} tamoxifen to 8 weeks old mice for seven consecutive days resulted in deletion of *Usp5* in mature cardiomyocytes (genotype: *Usp5 flox/flox//Myh6-MerCreMer*). *Cre*-mediated deletion of *Usp5* in mouse embryonic fibroblasts was achieved by crossbreeding *Usp5 flox/flox* mice with tamoxifen-inducible *Rosa26-CreER^{T2}* transgenic mice [114] and subsequent administration of 1 μmol L^{-1} 4-Hydroxytamoxifen (4-OHT) to isolated mouse embryonic fibroblasts (MEFs) for 48 hours. Aged-matched littermates without *cre*-recombinase expression were used as an appropriate control cohort in all experiments.

Conditional overexpression of human USP5

Transgenic mice conditionally overexpressing human (hs) USP5 exon 15 long in the myocardium were generated in house, using a modified ROSA26 targeting locus by which the SA-site of pBigT was replaced by a synthetic CAG promoter [115]. The Flag-HA tagged plasmid of hsUSP5, encoding hsUSP5 exon 15 short, was PCR-amplified (primers used: FlagHA-BigT-for and FlagHA-BigT-rev) to introduce NheI and NotI sites, and cloned into the pBigT-CAG vector. Human heart cDNA was then PCR-amplified (primers used: hsUSP5-isoform-for and hsUSP5-isoform-rev) to replace hsUSP5 exon 15 short with hsUSP5 exon 15 long by using SfiI and NotI cloning sites. The generated pBigT-CAG-Flag-HA-hsUSP5 exon 15 long cassette was subcloned in PacI and AscI site of the pRosa26-PA construct. The final construct was electroporated into V6.5 F1 hybrid ES cells and targeted stem cell clones were selected by G418 treatment and screened by Southern blotting with 5' genotyping by EcoRV. Positive ES cell clones were injected into C57BL/6 (B6) blastocysts. The resultant chimeric mice were backcrossed to C57BL/6 mice to generate transgenic mice harboring a single mutant allele (genotype: *hsUSP5 OE/+*). Conditional *cre*-mediated overexpression of hsUSP5 exon 15 long in the myocardium was achieved by crossbreeding *hsUSP5 OE/+* mice with *XMLC2-cre* transgenic mice (genotype: *hsUSP5 CO/+*) (Figure 13). The *hsUSP5 CO/+* alleles were kept heterozygous in all experimental studies. Aged-matched wildtype littermates with *cre*-recombinase

expression (genotype: *hsUSP5* +/+//*XMLC2-cre* +/-) were used as appropriate control mice in all experiments.

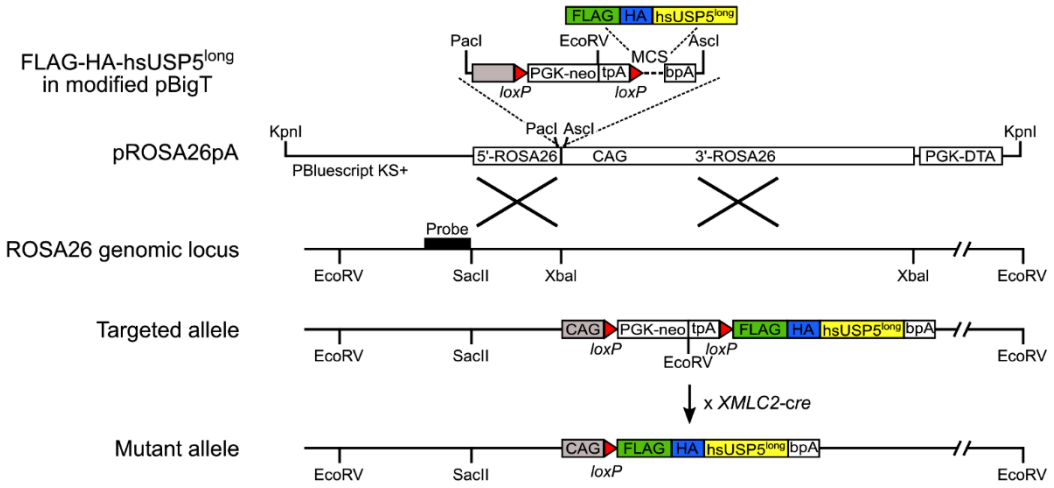

Figure 13 Generation of transgenic mice conditionally overexpressing human USP5 exon 15 long in the myocardium.

Schematic illustration of the gene targeting strategy for conditional overexpression of human (hs) USP5 exon 15 long in cardiomyocytes. The modified pBigT backbone vector, which contains a CAG promotor, a flanked PGK-neo antibiotic selection cassette, and the cDNA encoding for FLAG-HA tagged hsUSP5 exon 15 long, was inserted into the ROSA26 genomic locus by homologous recombination. *XMLC2-Cre* recombinase mediated deletion of the PGK-neo selection cassette resulted in specific overexpression of FLAG-HA tagged hsUSP5 exon 15 long in cardiomyocytes. tpA, transcriptional polyA stop sequence; bpA, bovine growth hormone polyadenylation site; MCS, multiple cloning site; DTA, subunit of the diphtheria toxin gene.

Genotyping

To perform genotyping of mice, tail biopsies were first digested in 500 µL tail lysis buffer, supplemented with 5 µL Proteinase K (20 mg mL^{-1}), at 56 °C overnight. The next day, digested tail pieces were centrifuged at 14,000 rpm for 10 min and decanted into a new tube containing 500 µL isopropanol. Genomic DNA was precipitated by inverting the tubes. After centrifugation at 14,000 rpm for 20 min, supernatants were removed, and the genomic DNA-containing pellets washed in 500 µL 70 % ethanol, followed by centrifugation at 14,000 rpm for 5 min. Genomic DNA was air dried at RT for 1-2 h, resuspended in 300 µL 1x TE buffer, and dissolved by incubation at 56 °C for 2-3 h. Genotyping PCRs were performed with self-designed primers, as indicated in Table 23 using appropriate cycling conditions (Table 24).

The master mix for one PCR reaction was prepared as followed:

10x PCR buffer	2.5 µL
$MgCl_2$ (50 mmol L^{-1})	1.0 µL
dNTPs (10 mmol L^{-1})	0.5 µL
Primer 1 (for)	0.5 µL
Primer 2 (rev)	0.5 µL
Primer 3 (wt)	0.5 µL
Taq polymerase (5 U L^{-1})	0.2 µL
ddH_2O	18.5 µL
Genomic DNA	1.0 µL

PCR products were loaded on a 2 % agarose gel, supplemented with ready-to-use ethidium bromide solution, and ran for 30-45 min at 150-200 V, depending on the size of the gel. Double-stranded DNA was visualized under UV light and gels were imaged using a BioDoc analyzer (Figure 14).

Table 23 Primers used for genotyping

Primer	Sequence
Cre-for	5'-TAA ACT GGT CGA GCG ATG GAT TTC C-3'
Cre-rev	5'-CAT ATC TCG CGC GGC TCC GAC ACG G-3'
$CreER^{T2}$ for	5'-AAG AAC CTG ATG GAC ATG TTC AGG G-3'
$CreER^{T2}$ rev	5'-CCA GAC CAG GCC AGG TAT CTC T-3'
MCM-for	5'-CAA CAT GAA ATG CAA GAA CG-3'
MCM-rev	5'-GGA AAC CAT TTC CGG TTA TTC-3'
Rosa-CAGG-for	5'-CTT GCT CTC CCA AAG TCG CTC TGA G-3'
Rosa-CAGG-rev	5'-ACC GTA AGT TAT GTA ACG CGG AAC TCC-3'
Rosa-WT-rev	5'-CTT TAA GCC TGC CCA GAA GAC TCC C-3'
Usp5-3. loxP-for	5'-AGTCGCCATCTGCTCAGTCACTGTC-3'
Usp5-3. loxP-rev	5'-TGTGGTTGAGGATAGCCTTCACCTCC-3'

Table 24 Genotyping protocols

PCR	Primer	Program	Fragment size
Usp5 3. loxP	*Usp5-for*	95°C 5:00	Wildtype 160 bp
	Usp5-rev	95°C 0:30	Transgene 196 bp
		55°C 0:30	
		72°C 0:30	
		Go to 2, repeat 35x	
		72°C 5:00	
		12°C ∞	
XMLC2-cre	*Cre-for*	94°C 4:00	Transgene 244 bp
MCK-cre	*Cre-rev*	94°C 0:30	
		66°C 0:30	
		72°C 0:45	
		Go to 2, repeat 35x	
		72°C 5:00	
		12°C ∞	
Rosa26-CreER^{T2}	*CreER^{T2} for*	94°C 3:00	Transgene 791 bp
	CreER^{T2} rev	94°C 0:30	
		55°C 0:30	
		72°C 0:40	
		Go to 2, repeat 35x	
		72°C 5:00	
		12°C ∞	
MerCreMer	*MCM-for*	94°C 3:00	Transgene 400 bp
	MCM-rev	94°C 0:30	
		55°C 0:30	
		72°C 0:40	
		Go to 2, repeat 35x	
		72°C 5:00	
		12°C ∞	
ROSA-CAGG	*ROSA-CAGG-for*	94°C 3:00	Wildtype 249 bp
	ROSA-CAGG-rev	94°C 0:30	Transgene 325 bp
	ROSA-wt-rev	57°C 0:30	
		72°C 0:30	
		Go to 2, repeat 35x	
		72°C 5:00	
		12°C ∞	

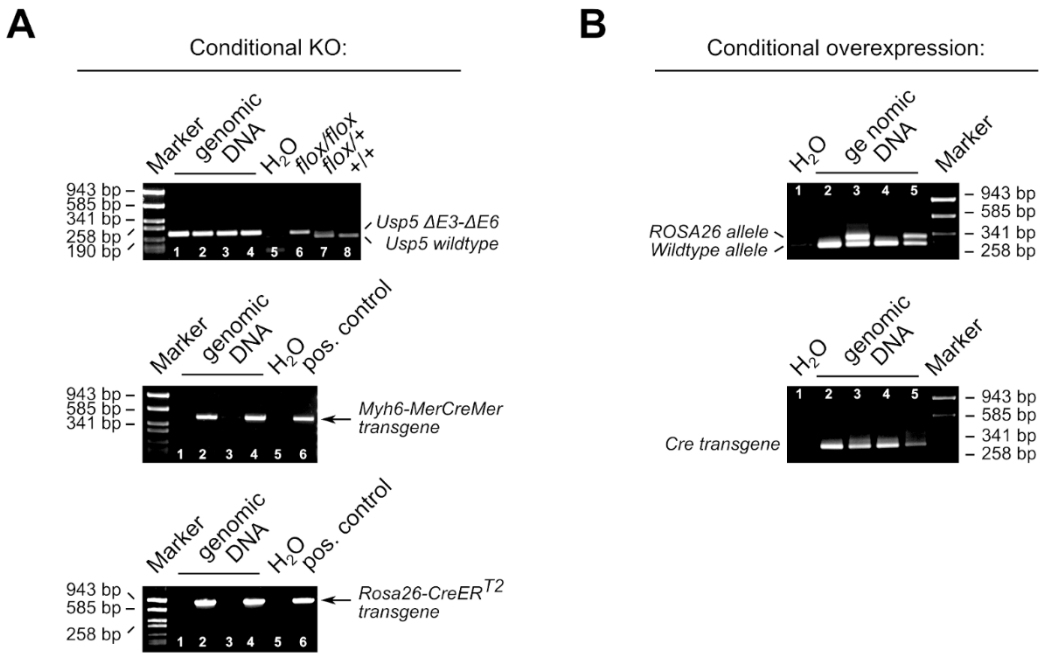

Figure 14 Genotyping PCRs of transgenic mice used in this study.

A. Genotyping of transgenic mice lacking USP5 in cardiomyocytes and MEFs was assessed by PCR analysis of tail-derived genomic DNA. PCRs were performed with primers specific for the 3. loxP site of *Usp5* and the *cre* or *Rosa26-creER^{T2}* transgene. PCR products were separated by agarose gel electrophoresis and visualized using a BioDoc system. Lane 1, 3 show *Usp5 flox/flox* control mice (cre negative); lane 2, 4 show *Usp5cKO* (*Usp5 flox/flox // Myh6-MerCreMer*) or *Usp5iKO* (*Usp5 flox/flox // Rosa26-creER^{T2}*) mice (*cre* or *Rosa26-creER^{T2}* positive). B. Genotyping of transgenic mice overexpressing hsUSP5 exon 15 long in cardiomyocytes was assessed by PCR analysis of tail-derived genomic DNA. PCR was performed with primers specific for the ROSA26 and *cre* recombinase transgene. PCR products were separated by agarose gel electrophoresis and visualized using a BioDoc system. Lane 2, 4 show *hsUSP5* +/+ control mice (*cre* positive); lane 3,5 show *hsUSP5 CO*/+ mice (*cre* positive).

Isolation of adult cardiomyocytes

Isolation of adult cardiomyocytes from 8 weeks old male mice only was performed as previously described by O'Connell *et al* [116]. In brief, dissected hearts were cannulated via the aorta and arrested by retrograde perfusion with calcium-free buffer. Cannulated hearts were enzymatically digested by perfusion with enzyme buffer solution and cut off from the cannula. Atria were separated, and ventricles were minced in stop buffer 1. After gentle pipetting, myocytes were at 500 rpm centrifuged for 1 min and cell pellets, containing the cardiomyocyte fraction, were re-suspended in stop buffer 2. The calcium content of the cell suspension was then stepwise

adjusted to 1 mmol L^{-1} and cardiomyocyte-containing cell pellets were re-suspended in M199 cell culture medium, supplemented with creatinine x H_2O, L-carnitine x HCl, HEPES, penicillin/streptavidin, FCS, and insulin-transferrin-sodium selenite media supplement, and maintained at 37°C and 5 % CO_2.

Isolation of mouse embryonic fibroblasts

Mouse embryonic fibroblasts (MEFs) were isolated from *Usp5iKO* mice *(*genotype: *Usp5 flox/flox //CreER$^{T2+/-}$)* at E13.5 as described by Jozefczuk *et al.* [117]. Briefly, pregnant mice were sacrificed, embryos isolated and placed separately into a fresh petri dish containing ice-cold 1 x PBS. The umbilical cord and the hematopoietic tissue together with the tubular intestine were removed from each embryo and the bulk of the CNS was trimmed off by dissecting away the head above the level of the oral cavity. A small piece of the tail was saved for DNA extraction and genotyping. Each remaining embryo was transferred to a tissue culture hood, placed in a 100 mm dish containing 5 mL of 1 x trypsin, and minced with a sterile scalpel for 2 min. After incubation for 15 min at 37 °C, tissue bits containing MEFs were transferred into a 15 mL canonical tube and pipetted several times to dissociate the tissue bits. After adding 5 mL of DMEM, supplemented with 10 % FCS and 1 % L-glutamine-penicillin-streptomycin, MEFs were spin down at 1,000 rpm for 5 min, and the supernatant was carefully aspirated off. The cell pellets were re-suspended in 10 mL DMEM, supplemented with 10 % FCS and 1 % L-glutamine-penicillin-streptomycin, and plated to a new 100 mm dish. MEFs were maintained at 37°C and 5 % CO_2.

Adenoviral Infection

Adenoviral infection of cardiomyocytes

Isolated cardiomyocytes from *hsUSP5 +/+* and *hsUSP5 CO/+* mice were infected with an adenovirus expressing either an eGFP-tagged wildtype titin or disease-causing eGFP-tagged p.C31712R titin variant [118, 119] overnight. The day after,

cardiomyocytes were washed five times with 1 x PBS to remove remaining virus particles and cultured in fresh M199 medium for additional 48 h.

Adenoviruses were a kind gift from Prof. Mathias Gautel, King's College London, UK.

Adenoviral Infection of MEFs

Subconfluent MEFs were infected with a recombinant adenovirus expressing a codon improved *cre*-recombinase under the CMV promoter (Ad-CMV-iCre; 10^7 PFU mL^{-1}) to induce site-specific recombination of genomic DNA between the two *loxP* sites flanking exon 3-6 of *Usp5*. An empty E1/E3 deletion, type 5 adenovirus (Ad-Null; 10^7 PFU mL^{-1}) was used as an appropriate mock control. Prior to virus infection, adenoviruses were incubated with polybrene to increase transduction efficacy. MEFs were incubated with the adenovirus mixture for 6 h and analyzed six days post-transduction.

Drug Treatment

To study the effects of proteasome impairment *in vitro*, cardiomyocytes and MEFs were treated with the reversible proteasome inhibitor MG132 (10 μmol L^{-1}) for 4 h. DMSO (0.2 %) treated cells served as an appropriate control cohort.

To study the autophagic flux, cardiomyocytes were treated with chloroquine (20 μmol L^{-1}) for 4 h. Chloroquine is a lysosomotropic agent that prevents endosomal acidification as it increases the lysosomal pH, thereby inhibiting the enzymatic activity of lysosomes. This results in impaired fusion of autophagosomes with lysosomes and lysosomal degradation of cell compartments, organelles, or protein aggregates. DMSO (0.2 %) treated cells served as an appropriate control cohort.

Proteasome activity assay

Enzymatic peptidase activities of the 20S proteasome were analyzed as previously described [120] Cardiomyocytes and MEFs were lysed in ice-cold proteasome lysis buffer, sonicated for 20 secs at cycle 9, power 80 % and clarified by centrifugation at 13,000 *x g* for 15 min at 4 °C. Sonication and centrifugation was repeated with the supernatants. 20 – 30 µL of cell lysates were transferred to a black 96 – well plate and mixed with proteasome assay buffer, supplemented with 40 µmol L^{-1} of specific activity-based fluorogenic (AMC-) peptide probes. Fluorescence intensity, which resulted from the release of the AMC, was monitored in 3-min intervals for a total time of 30 min at 37 °C using a multiplate reader with 380-nm excitation and 460-nm emission spectra.

Fluorogenic peptide probes used to determine 20S proteasome activity included: *Z-Leu-Leu-Glu-AMC* to measure peptidylglutamyl-peptide hydrolyzing (referred to as caspase-like) enzymatic activity, which is encoded by the ß1 subunit. *Boc-Leu-Arg-Arg-AMC* was used to determine trypsin-like catalytic activity that is encoded by the ß2 subunit. *Suc-Leu-Leu-Val-Tyr-AMC* was used to measure chymotrypsin-like catalytic activity, encoded by the ß5 subunit (Table 4).

RNA isolation and quantitative RT-PCR

RNA from cardiomyocytes and MEFs was extracted using the Direct-zol™ RNA Kit according to the manufacturer's protocol and stored at – 80 °C until further usage. A total of 1 µg RNA was reverse transcribed to cDNA using the SuperScript™ II Reverse Transcriptase according to a protocol as followed:

RNA sample (1 µg)	1.0 µg
Oligo dT 15 primer	1.0 µL
dNTPs	1.0 µL
add ddH_2O to	12.0 µL

The reaction mix was incubated for 5 minutes at 65 °C and cooled on ice. A synthesis mix, containing

0.1 M DTT	2.0 µg
5 x FS buffer	4.0 µL
RNasin	1.0 µL

was added and the reaction was incubated for 2 min at 42 °C. 1.0 µL of the SuperScript™ II Reverse Transcriptase was added to complete cDNA synthesis by incubation for 50 min at 42 °C followed by incubation for 15 min at 70 °C. Ready-to-use cDNA was stored at – 80°C until further usage.

TaqMan® Gene Expression Assays using specific TaqMan probes (Table 17) were used to perform quantitative RT-PCR (qRT-PCR) on a StepOnePlus Real-Time PCR System.

The master mix for one qRT-PCR reaction was prepared as followed:

TaqMan™ Gene expression master mix	5.0 µL
TaqMan™ gene specific probe (FAM-dye)	0.5 µL
TaqMan™ *gapdh* probe (VIC-dye)	0.5 µL
cDNA (diluted 1:100)	4.0 µL

Each sample was run in technical triplicates and repeated at least two times. Relative mRNA expression was calculated by the $\Delta\Delta C_t$ method and normalized to *gapdh* as an internal housekeeping control.

Microarray analysis and GO term annotation

Quality of extracted RNA of isolated cardiomyocytes was verified with the RNA 6000 Nano Kit on an Agilent 2100 Bioanalyzer. RNA was labeled accordingly to the Affymetrix Whole Transcript Sense Target Labeling protocol and hybridized to Affymetrix Clariom™ D assays. Data were processed and analyzed by RMA algorithm using the Affymetrix Expression Console. Statistics were employed using

DNAStar Arraystar 11 to calculate FC values [121] in combination with students *t*-test of log_2-transformed data to identify significantly differentially expressed transcripts.

Gene ontology annotations of identified gene sets were determined using the Gene Ontology enrichment analysis and visualization tool. GraphPad Prism 7 was used to generate heat maps and graph bars, and Venn diagrams were generated using the Bioinformatics & Evolutionary Genomics tool.

Gorilla – available on http://cbl-gorilla.cs.technion.ac.il/
Bioinformatics & Evolutionary Genomics tool – available on
http://bioinformatics.psb.ugent.be/webtools/Venn/

Protein extraction and immunoblot analysis

Immunoblot analysis was performed accordingly to standard protocols. In brief, cardiomyocytes and MEFs were collected, lysed by homogenization in RIPA buffer, supplemented with protease inhibitor cocktail and PMSF, and sonicated for 20 sec at cycle 3, power 30 %. In contrast, human myocardial samples were homogenized in extraction buffer, supplemented with protease cocktail and PMSF, and sonicated for 20 sec at cycle 3, power 30 %. After incubation on a rotating wheel at 4 °C for a minimum of 30 min, cell and tissue homogenates were clarified by centrifugation at 14,000 rpm for 20 min at 4 °C. Supernatant, representing the cytoplasmic protein fraction, was collected and protein concentration was measured using Roti®Quant universal. 20 – 30 µg of proteins were separated by SDS-PAGE and blotted onto nitrocellulose membranes, followed by RedAlert™ staining to verify loading efficacy. Nitrocellulose membranes were blocked in 5 % skim milk / TBS-T for 30 min at RT and probed with specific primary antibodies overnight at 4 °C, followed by incubation with peroxidase-conjugated secondary antibodies for 2 hours at room temperature. Proteins were visualized by chemiluminescence using the Super Signal® West Pico Chemiluminescent Substrate kit on a ChemiDoc™ MP Imaging System. Densitometric analysis of the chemiluminescence signals in Image J was performed

to quantify the relative protein expression. Absolute protein expressions were calculated by normalization to GAPDH.

The protocol to detect ubiquitin levels in cell extracts of cardiomyocytes and MEFs was marginally modified. After SDS-PAGE and protein transfer, nitrocellulose membranes were boiled in ddH_2O for 30 min and blocked in 0.5 % gelatin from porcine skin + 0.05 % Tween-20 in 1 x PBS. Membranes were probed with pan- and Lys48-linkage specific ubiquitin antibodies overnight at 4 °C or Lys63-linkage specific ubiquitin antibody for 2 hours at room temperature.

All primary antibodies used in this study were diluted as indicated in Table 12 in 5 % BSA/TBS-T apart from ubiquitin antibodies, which were diluted in 5 % skim milk/TBS-T. All secondary antibodies were diluted in 5 % skim milk/TBS-T.

Whole proteome analysis

Whole proteome analysis was performed on cardiomyocytes only. Cells were lysed in ice-cold RIPA buffer, supplemented with protease inhibitors and PMSF, and cytoplasmic proteins were isolated as described in the previous section. 40 µg of protein was separated by SDS-PAGE and the gel was stained with InstantBlue Protein Stain to visualize robustness of protein separation. Thereafter, gel lanes were excised into evenly sized pieces, washed in ddH_2O, and incubated with 50 mmol L^{-1} ABC / 50 % EtOH for 20 min at RT. Gel pieces were dehydrated in absolute EtOH for 10 min, dried in the Vagufuge™ Concentrator for 5 min, and further processed for in-gel digestion [122]. Here, proteins were reduced in 100 mmol L^{-1} DTT, alkylated with 550 mmol L^{-1} iodoacetamide, followed by washing and rehydrating steps with 50 mmol L^{-1} ABC and absolute EtOH, respectively, each for 15 min. Afterwards, gel pieces were again dried in the Vagufuge™ Concentrator for 5 min and digested with 12.5 ng μL^{-1} trypsin at 37 °C overnight. The next day, digested proteins were extracted with 70 % and 100 % acetonitrile, concentrated in in the Vagufuge™ Concentrator to a final volume of ~ 80 µL, mixed with 80 µL buffer C, and finally purified on C-18 stop and go extraction stage tips made in-house [123]. Extracted peptides were separated on a linear 130 min gradient by a binary buffer gradient, consisting of buffer

A (0.1 % formic acid) and buffer B (80 % acetonitrile; 0.1 % formic acid), and analyzed by LC-MS/MS. MS spectra were acquired in the Orbitrap with a resolution of 70,000 at 200 $m \cdot z^{-1}$. Raw data were analyzed by MaxQuant [124] combined with implementation by the Andromeda search engine [125]. Protein assignment was performed by correlating identified spectra with the Uniprot murine database including a list of common contaminants. A minimal peptide length was defined as seven amino acids and the false discovery rate at protein and peptide level was set to 1 %. *P*-values below 0.05 were considered as statistically significant.

Human cardiac samples

Human myocardial tissue samples were obtained from left ventricular biopsies of transplanted hearts from five individuals with late end-stage DCM, not showing any signs of myocardial infarction. Left ventricular myocardial samples, which were not used for heart transplantation, were obtained from two individuals with showing preserved cardiac function (EF > 60 %) and no symptoms of myocardial damage or ventricular dilation. These donor hearts (hereby referred to as non-failing) served as a control cohort. Immediately after tissue procurement, cardiac biopsies were shock frozen in liquid nitrogen and stored at – 80 °C until being processed for molecular analysis and immunohistochemistry. A small fraction of cardiac biopsies was fixed in buffered glutaraldehyde for electron microscopical analysis.

All patients delivered a prospective written informed consent for research use of cardiac tissues to comply with the requirements of the Medical Council in Hesse, Germany, and the institutional ethics guidelines of the Kerckhoff Hospital, Bad Nauheim, Germany. The study was approved by the ethics committee of the Medical Council in Hesse, Germany.

Morphological analysis

To perform cryosections, dissected mouse hearts were fixed in 4 % PFA / 1 x PBS overnight at 4 °C, immersed in 30 % sucrose / 1 x PBS for additional 24 hours at 4 °C, embedded in FSC 22, frozen on dry ice, and stored at – 80 °C. Serial 6-µm thick cross sections were cut using a Leica CM 1950 cryostat, collected on SuperFrost Plus slides, and stored at – 20 °C until being processed for immunohistochemistry.

Heart morphology was assessed by hematoxylin & eosin (H & E) staining following routine procedures. Briefly, frozen cryosections were air-dried and incubated in ddH_2O for 2 min at RT, and stained with hematoxylin for 10 min. Staining solution was washed out in tepid running tap water and sections were counterstained with eosin for 7 min at RT. Afterwards, sections were dipped in increasing ethanol series (70 %, 80 %, 90 % ethanol), incubated in 100 % ethanol and Xylol for 5 min each, and embedded in Entellan.

PROTEOSTAT® aggresome assay

Protein aggregates and aggresomes in isolated cardiomyocytes and MEFs were visualized by the ProteoStat® Aggresome Detection Kit [126]. All components of the kit were prepared according to the manufacturer's instructions.

The kit provides a ready-to-use 488-nm excitable fluorescent molecular rotor dye that binds selectively to the hydrophobic surface of denatured protein cargos within aggresomes and aggresome-like inclusion bodies in fixed and permeabilized cells. Binding to the protein cargos induces a reaction in which protein aggregates become brightly fluorescent.

Immunofluorescence staining of cells and tissues

Cardiomyocytes and MEFs were fixed in 4 % PFA / 1 x PBS for 15 min, washed 3-times in 1 x PBS, permeabilized in 0.1 % Triton X-100 / 1 x PBS for 10 min, and incubated in a blocking solution containing 2 % FCS, 2 % BSA in 1 x PBS for 30 min to reduce non-specific antibody binding. In contrast, cryosectioned tissue samples,

already pre-fixed in 4 % PFA / 1 x PBS, were only permeabilized in 0.1 % Triton X-100 / 1 x PBS for 10 min followed by incubation in blocking buffer solution to reduce non-specific binding affinity towards antibodies. Afterwards, cells or tissue sections were incubated with primary antibodies, diluted in the blocking solution as indicated in Table 13, overnight at 4 °C. The day after, cells or tissue sections were washed 3-times in 1x PBS and incubated with secondary antibodies conjugated with either Alexa Fluor™ 488 or Alexa Fluor™ 594, again diluted in the blocking solution, for 2 hours at RT. After three washing steps in 1 x PBS, nuclei were counterstained with 4',6-diamidino-2-phenylindole (DAPI), 1:1000 diluted in the blocking solution, for 15 min. Cells or tissue sections were again washed 3-times with 1 x PBS, mounted in Mowiol, and analyzed using a fluorescence microscope.

Staining protocol to detect autophagosomes was solidly modified. Cardiomyocytes were first treated with 20 μmol L^{-1} chloroquine for 4 h to permit fusion of autophagosomes with lysosome. Afterwards, cardiomyocytes were fixed in ice-cold methanol for 5 min at RT, washed with 1 x PBS, incubated in an AbDil-Tx blocking buffer for 30 – 60 min at RT, followed by incubation with anti-LC3B (1:200 diluted in AbDil-Tx blocking buffer) overnight at 4 °C. The next day, cardiomyocytes were washed 3-times with 1 x PBS and incubated with appropriate secondary antibody conjugated with either Alexa Fluor™ 488 or Alexa Fluor™ 594 for 2 hours at RT.

Electron microscopy

Electron microscopy was used to analyze cardiomyocyte-restricted effects of loss of *Usp5* on heart morphology. Animals were anesthetized, hearts were perfused with a fixative solution containing 1.5 % glutaraldehyde *(v/v)*, 1.5 % paraformaldehyde *(v/w)* in 0.15 M HEPES *(v/w)*, pH 8.0 and kept in fixative solution for at least 24 h until being processed for post-fixation in 1 % osmium tetroxide. Thereafter, samples were stained *en bloc* in 50 % saturated watery uranyl acetate, dehydrated by an ascending ethanol series, and embedded in Agar 100. Ultrathin sections were cut using an ultramicrotome at the Institute for Anatomy and Cell Biology, Justus-Liebig-University Giessen, Germany, and image acquisition was performed with a

transmission electron microscope. All images were captured with a slow-scan 2K CCD camera.

Plasmids

All V5-tagged plasmids encoding human ubiquitin-specific peptidases (USPs) as well as the V5-tagged human HDAC6 plasmid were provided by the CCSB Human ORFeome V8.1 Library. In contrast, GFP- and V5-tagged plasmids encoding mouse PSMD14, human HDAC6, and human USP5, and the BioID fusion plasmids encoding human USP5 exon 15 long were generated by PCR amplification in house.

Generation of PSMD14-GFP

PCR amplification of the mouse *Psmd14*-GFP ORF was performed with the *Psmd14-GFP-for* and *Psmd14-GFP-rev* primers. The final PSMD14-GFP vector was generated by 3-piece ligation of the *Psmd14* amplicon (restriction sites: PacI and XhoI) and PCR amplified eGFP (restriction sites: XhoI and AscI) inserts into the modified pPyCAG-IP backbone vector (restriction sites: PacI and AscI).

Generation of PSMD14-V5

V5-tagged PSMD14 was generated by PCR amplification of the mouse *Psmd14-V5* ORF with the *Psmd14-V5-for* and *Psmd14-V5-rev* primer. PCR amplified *Psmd14-V5* (restriction sites: PacI and XhoI) was inserted into the modified pPyCAG-IP backbone vector (restriction sites: PacI and AscI).

Generation of HDAC6-GFP

PCR amplification of the human *Hdac6* ORF was performed using the *Hdac6-GFP-for* and *Hdac6-GFP-rev* primers. The final HDAC6-GFP vector was generated by 3-piece ligation of the PCR amplified *Hdac6* (restriction sites: PacI and SalI) and eGFP (restrictions sites: XhoI and AscI) inserts into the modified pPyCAG-IP backbone vector (restriction sites: PacI and AscI).

Generation of USP5-GFP

GFP-tagged USP5 was generated by PCR amplification of human *USP5* ORF using the with *USP5-N-fusion-for* and *USP5-N-Fusion-rev* primer, followed by 3-piece ligation of the *hsUSP5* amplicon (restriction sites: XhoI and AscI) together with eGFP (restriction sites: PacI and XhoI) into the modified pPyCAG-IP (restriction sites: PacI and AscI) backbone vector.

Generation of USP5-BirA*(R118G)-HA

The final hsUSP5-BirA(R118G)*-HA-tagged BioID fusion plasmid was generated by PCR amplification of the human *USP5* ORF, encoding hsUSP5 exon 15 long, using the following primer combination *hsUSP5-C-Fusion-for* and *hsUSP5-C-Fusion-rev*. The BirA*(R118G)-HA fusion plasmid was PCR amplified by *BirA-HA-for* and *BirA-HA-rev* using the pcDNA3.1 MCS-BirA*(R118G)-HA plasmid, which was provided by Addgene. A 3-piece ligation of the PCR amplified BirA*(R118G)-HA (restriction site: PacI and XhoI) and hsUSP5 (restriction site: XhoI and AscI) into the modified pPyCAG-IP backbone vector (restriction sites: PacI and AscI) resulted in generation of the final hsUSP5-BirA*(R118G)-HA vector.

Generation of Myc-BirA(R118G)*-USP5

The corresponding Myc-BirA*(R118G) tagged fusion plasmid was generated in a similar manner. First, human USP5 ORF was PCR amplified using *hsUSP5-N-Fusion-for* and *hsUSP5-N-Fusion-rev*. The Myc-BirA*(R118G) fusion plasmid was PCR amplified by *Myc-BirA-for* and *Myc-BirA-rev* using pcDNA3.1 mycBirA* plasmid, which was provided by Addgene. The final Myc-BirA*(R118G)-hsUSP5 vector was generated by 3-piece ligation of PCR amplified Myc-BirA*(R118G) (restriction site: XhoI and AscI) and hsUSP5 (restriction site: PacI and XhoI) inserts into the modified pPyCAG-IP backbone vector (restriction sites: PacI and AscI).

Transfection and immunoprecipitation

Subconfluent HEK293 cells, cultured in 100-mm cell culture dishes under humified atmosphere at 37 °C and 5 % CO_2, were transiently transfected with 6 μg of individual plasmid DNA using TurboFect transfection reagent, as implemented by the manufacturer's instructions. 24 h post-transfection, HEK293 cells were lysed in ice-cold RIPA buffer, supplemented with protease inhibitors and PMSF, sonicated for 20 secs at cycle 3, power 80 % and incubated on a rotating wheel for a minimum of 30 min at 4 °C. Thereafter, homogenates were centrifuged at 14,000 rpm for 20 min at 4 °C, protein concentration was measured, and clarified cell lysates were further processed for immunoprecipitation.

To precipitate V5-tagged USPs, a total amount of 1 mg mL^{-1} of the clarified cell lysates were incubated with 40 μg of anti-V5 agarose conjugated beads on a rotating wheel for 90 min at 4 °C. Beads were washed 4-times in 1 x PBS and immunoprecipitated V5-tagged USP protein complexes were eluted by boiling agarose beads in 2 x NuPAGE® LDS sample buffer for 5 min at 100 °C. In contrast, precipitation of GFP-tagged hsUSP5 variants was assessed by incubating 1 mg mL^{-1} of the clarified cell lysates with 5 μg of either anti-GFP or anti-IgG on a rotating wheel for 75 min at 4 °C. Afterwards, cell lysates were supplemented with 40 μg protein g sepharose 4 fast flow beads and allowed to rotate for additional for 60 min 4 °C. Beads were washed 3-times in ice-cold RIPA buffer, supplemented with protease inhibitors and PMSF, and immunoprecipitated GFP-tagged hUSP5 protein complexes were eluted by boiling beads in 2 x NuPAGE® LDS sample buffer for 3 min at 95 °C. Precipitated protein complexes were subjected to SDS-PAGE and analyzed by immunoblotting.

Bio-ID analysis

HEK293 cells were transiently transfected with BioID fusion proteins using TurboFect transfection reagent according to manufacturer's instruction. 24 h post-transfection, HEK293 cells were supplemented with 50 μmol L^{-1} biotin for a maximum of 18 h and subjected to stringent lysis in BioID lysis buffer as described

[127]. Cell lysates were triturated with 20 % Triton X-100, twice sonicated for 30 secs at cycle 5, power 30 %, and mixed with pre-chilled TriCl. After another sonication step, cell lysates were cleared by centrifugation at 16,500 *x g* for 10 min at 4 °C. Proximity dependent biotin affinity capture was performed by incubating 1 mg·mL^{-1} of clarified cell lysates with 40 µL of magnetic beads coated with streptavidin on a rotating wheel overnight at 4 °C. Streptavidin coated beads were twice washed in wash buffer 1, twice washed in wash buffer 2, and once washed in wash buffer 3. Biotinylated proteins were eluted by boiling streptavidin coated beads in 1 x NuPAGE® LDS sample buffer for 10 min at 98 °C, followed by SDS-PAGE, and in-gel digestion coupled to LC-MS/MS to identify protein interaction partners in close proximity to hsUSP5. BioID analysis was performed using technical triplicates for each condition.

Image acquisition and processing

Stained cardiomyocytes, MEFs, and cardiac cryosections were analyzed using the Keyence BZ-9000 fluorescence microscope. All settings for laser excitation were kept constant between the different groups to ensure robust comparison of the immunofluorescence signal. Images were processed using software as BZ-II Analyzer, ImageJ/Fiji [128], and GIMP (Version 2.8).

Statistical analysis

Statistical analysis was performed by using the following two-tailed tests: (a) for two groups, we used unpaired t-test with Welch's correlation, or Wilcoxon-rank sum test (Mann-Whitney U-test) for nonparametric datasets or heterogeneous variance of the data; (b) for three or more groups, we used one-way ANOVA and subsequent Holm-Sidak's multiple comparison test, or Kruskal-Wallis test and subsequent Dunn's or Tukey's multiple comparisons in case of missing normal distribution or heterogeneous variance of the dataset. Survival curve analysis was performed using Kaplan-Meier log-rank (Mentel-Cox) test.

All data are expressed as mean ± standard error (s.e.m.) and *P*-values less than 0.05 were considered statistically significant. No statistical method was used to predetermine samples size. All analyses were based on neither randomization or blinding. No animals were excluded from statistical analysis. GraphPad Prism Software, Version 7 was used for all statistical analyses.

RESULTS

USP5 interacts with components of the cellular PQC machinery

Efficient function of PQC processes, especially ubiquitin-dependent proteolysis and (selective) autophagy, relies on disassembly of ubiquitin conjugates from targeted proteins for reutilization of ubiquitin moieties. Previous studies highlighted the importance of a PSMD14-driven release of free ubiquitin chains to be essential for sustained proteostasis by stimulating HDAC6-dependent autophagic clearance of ubiquitinated protein aggregates and aggresomes in conditions of insufficient or impaired proteasome activity [129]. Initial binding of ubiquitin conjugates is catalyzed by three DUBs: PSMD14, USP14/Ubp6, and UCH37/UCHL5. PSDM14, as an integral subunit of 19S RP of the 26S proteasome, is essential for the release of ubiquitin chains *en bloc* from targeted proteins prior to proteasomal degradation. In contrast, the two DUBs USP14/Ubp6 and UCH37/UCHL5 reversibly associate with the 19S RP of the 26S proteasome to assist in deubiquitination of ubiquitinated proteins. To investigate the principal role of DUBs in PQC and to explore whether additional DUBs are involved in the regulation of PQC processes, an unbiased screen was utilized to identify newly, yet not described ubiquitin-specific peptidases (USPs) collaborating with PSMD14 to regulate turnover and reutilization of ubiquitin molecules (Figure 15 A). The screen revealed that 11 of 40 tested USPs were present in complexes containing PSMD14 (Figure 15 B-D), among them USP5 (Figure 15 B-D).

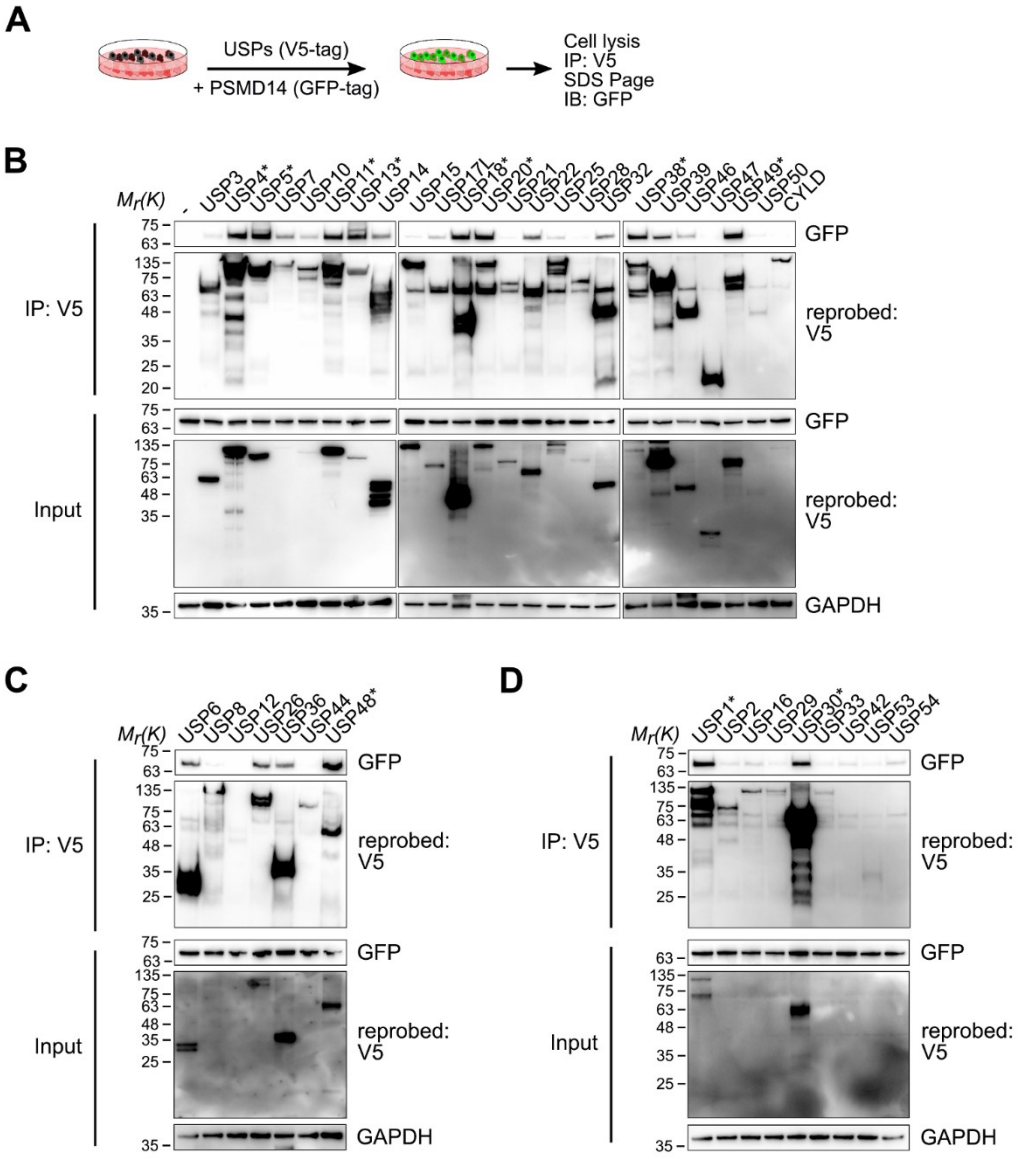

Figure 15 Screen for complex formation of ubiquitin-specific peptidases (USPs) with PSMD14.

A. Workflow for co-immunoprecipitation (co-IP) of GFP-tagged mouse PSMD14 with a V5-tagged library of ubiquitin-specific peptidases (USPs) in HEK293 cells. B-D. Immunoblot analysis of anti-V5 precipitated cell lysates probed with anti-GFP and anti-V5 antibody. Input and IP fractions are shown. * USPs interacting with PSMD14.

The interaction of USP5 with PSMD14 was a surprise, since USP5 has yet not been described as a stable interaction partner of PSMD14 nor of the 19S RP of the 26S proteasome. In fact, USP5 is predominantly linked to assist in disassembly of free, unattached ubiquitin chains *in vitro* [130]. In this context, complex formation of PSMD14 with USP5 makes sense as USP5 can disassemble unanchored ubiquitin chains, released by PSMD14-mediated deubiquitination, to assist in maintaining of a stable ubiquitin pool.

To further characterize the function of USP5 in PQC processes, proximity-dependent biotinylation and affinity purification (BioID) was utilized, which complements and extends co-immunoprecipitation techniques [127]. For this purpose, HEK293 cells were transiently transfected with Bio-ID fusion plasmids encoding human (hs) USP5 fused in frame to an amino-terminal Myc- or carboxyl-terminal HA-tagged mutated biotin ligase BirA*(R118G). 24 h post-transfection, cells were supplemented with 50 μmol L^{-1} biotin for additional 18 h and biotinylated proteins in close vicinity to the hsUSP5 BioID fusion proteins were affinity purified and subsequently identified by liquid chromatography-mass spectroscopy (LC-MS/MS) (Figure 16 A). Immunoblot analysis confirmed robustness of the BioID approach as the hsUSP5 BioID protein was affinity purified along with biotinylated proteins (Figure 16 B). In all conditions, HEK293 cells transiently transfected with either Myc- or HA-tagged BirA*(R118G) served as an appropriate control to minimize identification of false-positive hsUSP5 interaction partners, which may arise from unspecific complex formation (Figure 16 C). Immunoblot analysis confirmed robustness of the BioID approach as the hsUSP5 BioID protein was affinity purified along with biotinylated proteins (Figure 16 B). In all conditions, HEK293 cells transiently transfected with either Myc- or HA-tagged BirA*(R118G) served as an appropriate control to minimize identification of false-positive hsUSP5 interaction partners, which may arise from unspecific complex formation (Figure 16 C).

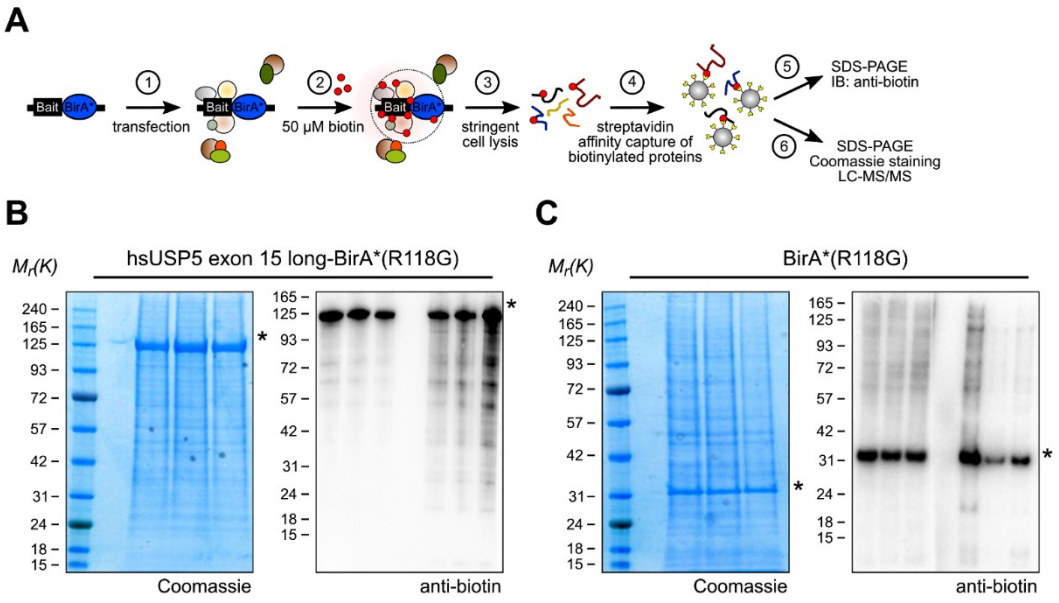

Figure 16 Proximity dependent biotinylation and affinity purification approach (BioID) to identify the interactome of hsUSP5 exon 15 long.

A. Workflow for BioID analysis in HEK293 cells transfected with either Myc- or HA-tagged BioID-USP5 fusion plasmid. Biotinylated endogenous proteins in close proximity to the fusion protein were isolated by affinity capture on streptavidin coated beads and identified by LC-MS/MS. B, C. Coomassie stained SDS gels after streptavidin pulldown (left) and immunoblot of biotinylated proteins (right). Input and biotin-IP fraction are shown. *, expressed fusion proteins.

Dependent on the position of the tag, mass spectroscopy detected 4-times more biotinylated endogenous proteins in cells transfected with hsUSP5-BirA*(R118G)-HA in comparison to Myc-BirA*(R118G)-hsUSP5 transfected cells (Figure 17 A-E). The list of putative interaction partners of hsUSP5 identified by mass spectroscopy comprises numerous ubiquitin-related proteins, including ubiquitin ligases (E3s), DUBs, and subunits of the 26S proteasome, in addition to components of the (selective) autophagy pathway (Figure 17 F). Importantly, all detected proteins differed by a log_2 ratio > 1.0 and a $-log_{10}$ *P-value* > 1.3 to control experiments using BirA*(R118G) transfected cells, demonstrating the specificity of the BioID approach.

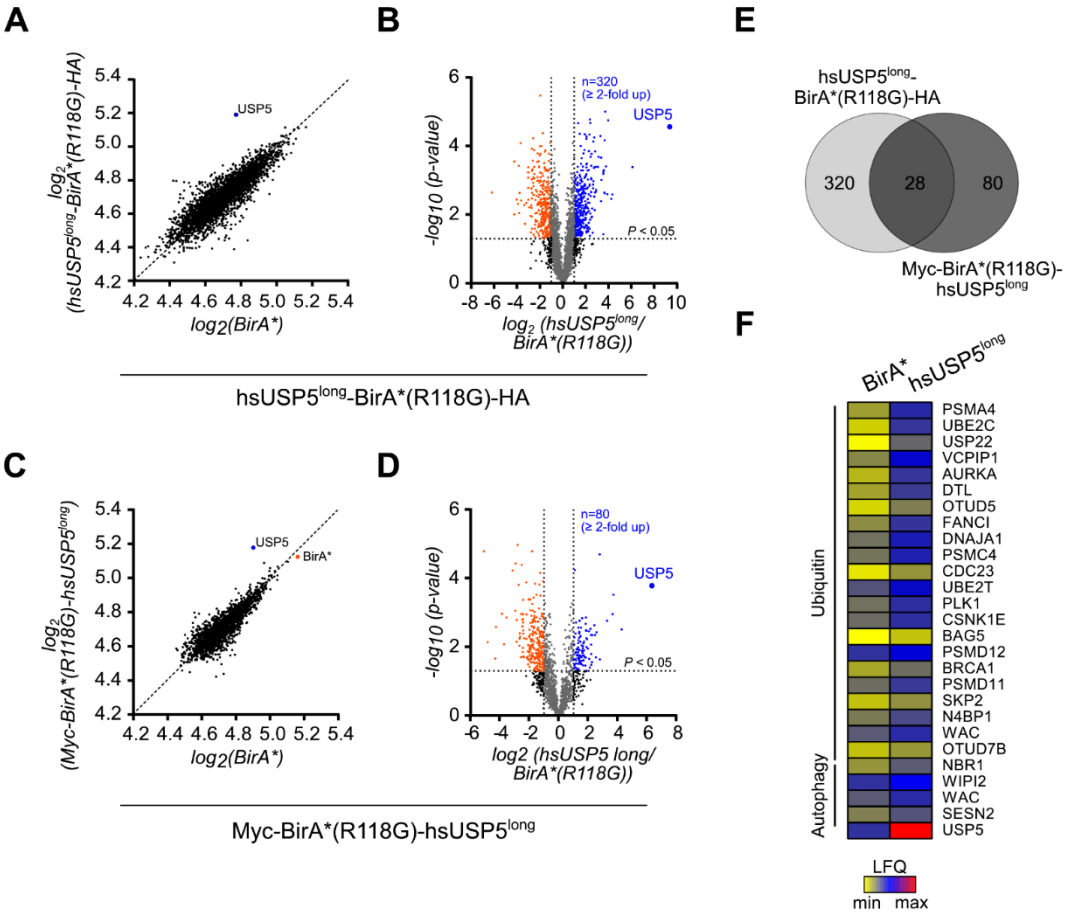

Figure 17 BioID analysis of amino- and carboxyl-terminal tagged hsUSP5 exon 15 long.

A, C. Scatter plots showing biotinylated proteins identified in triplicate experiments using either HA (A)- or Myc-tagged (C) hsUSP5 fusion proteins. B, D. Volcano plots showing hsUSP5 interaction partners. Proteins biotinylated by hsUSP5-BirA*(R118G) are depicted in blue, proteins labelled by BirA*(R118G) are shown in orange. Adjusted *P*-values based on the *-log10* ratio (y-axis) are plotted against chances based on the *log2* ratio (x-axis). E. Venn diagram showing the overlap between proteins identified by different hsUSP5 fusion proteins. F. Heat map depicting proteins biotinylated by hsUSP5-BirA*(R118G).

Next, all identified proteins were categorized based on cellular processes and their localization within the cell, whereas statistical significance was given by the $-log_{10}$ *P-value*. The majority of detected proteins was involved in the regulation of cellular protein catabolic processes, including proteolysis, protein polyubiquitination, and protein deubiquitination (Figure 18 A), in addition to an enrichment in proteins connected to either the ubiquitin ligase complex or the proteasome complex (Figure 18 B).

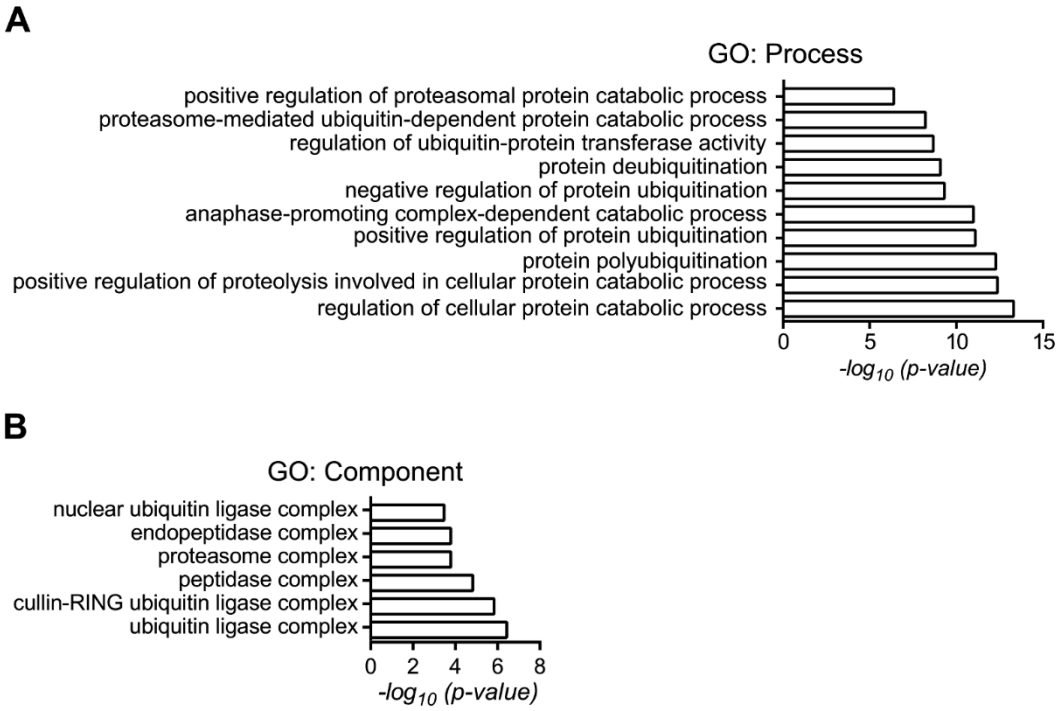

Figure 18 Enrichment analysis of hsUSP5 exon 15 long interactome.

A, B. Box plots showing enriched GO terms of proteins biotinylated by hsUSP5^{long}-BirA*(R118G). GO terms referring to molecular function (A) and cellular component (B) are shown. Significance was calculated based on the *-log10 P*-value.

Although the BioID approach validated the association of hsUSP5 with components of UPS-dependent protein catabolic processes and (selective) autophagy, PSMD14 was not detected as a putative interaction partner, which might be due to technical reasons. Alternatively, it might indicate that complexes containing PSMD14 and USP5 only form transiently. Nevertheless, the data clearly demonstrate the overall importance of USP5 in the regulation of processes of the UPS, which is instrumental for cellular protein homeostasis.

Cardiomyocytes express a non-spliced variant of USP5 that is recruited to protein aggregates in response to proteasomal stress

Izaguirre *et al.* showed USP5 to undergo a PTBP1-dependent differential splicing event at the genomic locus of exon 15 [131]. Splicing results in the formation of an exon 15 short isoform lacking 23 amino acids due to an alternative splice acceptor at the carboxyl-terminus of exon 15 (Figure 19 A, B). Exon 15 short isoform was reported to enhance cell growth and migration, while the exon 15 long isoform is associated with arrest of cell proliferation and migration in glioblastoma cells. As differential spliced variants of USP5 have solely been described in glioblastoma cells, the questions arose whether the two USP5 isoforms may also exist in other tissues and cells.

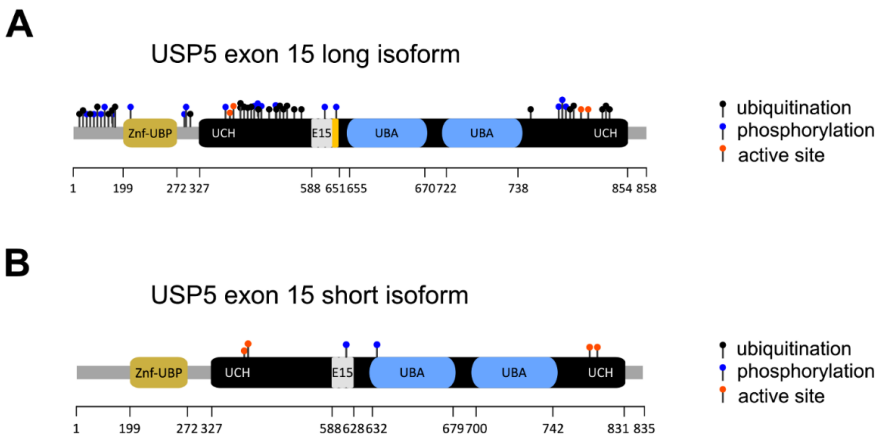

Figure 19 *Usp5* undergoes differential splicing at exon 15.

A, B. Scheme depicting alternative spliced transcripts of mouse *Usp5,* encoding for an 858 amino acid long isoform (A), or an 835 amino acid short isoform (B), respectively. Alternative spliced part of exon 15 is depicted in a yellow box. ZnF-UBP, zinc-finger ubiquitin binding domain; UCH, ubiquitin carboxyl-terminal hydrolase domain; UBA, ubiquitin-binding associated domain; E15, exon 15; UBA, ubiquitin-associated domain.

To explore which USP5 isoform is present in a variety of mouse organs, semi-quantitative reverse transcription PCR (sqRT-PCR) was performed with primers specifically detecting *Usp5* exon 15 (Figure 20 A, B). sqRT-PCR detected the exon 15 long isoform in organs containing large amounts of postmitotic cells prone to protein aggregation, such as the brain, heart, and skeletal muscles (e.g. Soleus, EDL), while the corresponding exon 15 short isoform was broadly expressed (Figure 20 C).

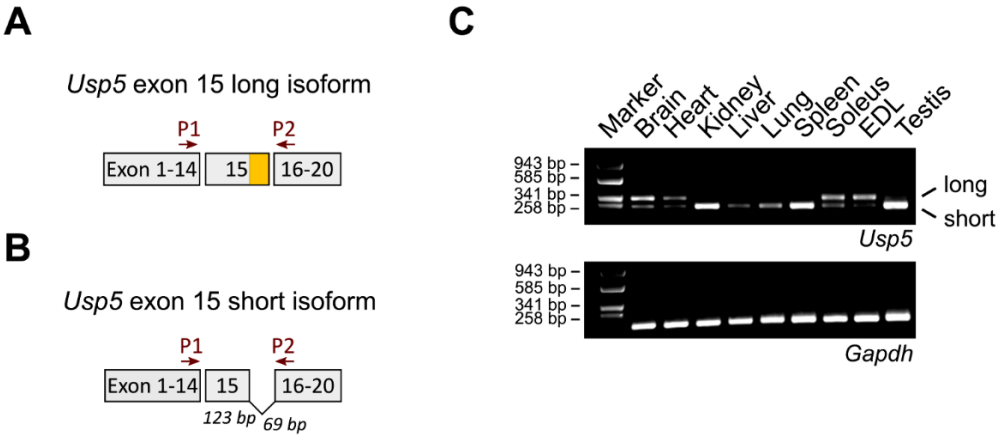

Figure 20 *Usp5* undergoes tissue-specific differential splicing.

A, B. Scheme depicting alternative spliced transcripts of mouse *Usp5* exon 15. Arrows indicate the location of primers used for semi-quantitative RT-PCR. *Usp5* spliced transcripts differ by 69 bp (23 aa) at the C-terminus of exon 15. **(C)** Splice variants of mouse *Usp5* in different tissues assessed by semi-quantitative RT-PCR.

To evaluate the splicing event in a more cell-type specific manner and with regards to postmitotic - versus proliferative cells, sqRT-PCR was performed with primary cardiomyocytes isolated at different developmental stages and mouse embryonic fibroblasts (MEFs) (Figure 21 A-D). Interestingly, adult cardiomyocytes, which lack self-renewal capacity, solely expressed the exon 15 long isoform, while primary cardiomyocytes isolated at E13.5 showed similar expression of both isoforms. Fetal cardiomyocytes isolated at juvenile stage generated both isoform with a shift towards expression of the exon 15 long isoform (Figure 21 A).

On the other hand, non-cardiomyocytes isolated from adult hearts and MEFs generated only the short isoform (Figure 21 B). Taken together, these findings indicate that alternative splicing of USP5 is restricted to proliferative cells as postmitotic cells lack the splicing event.

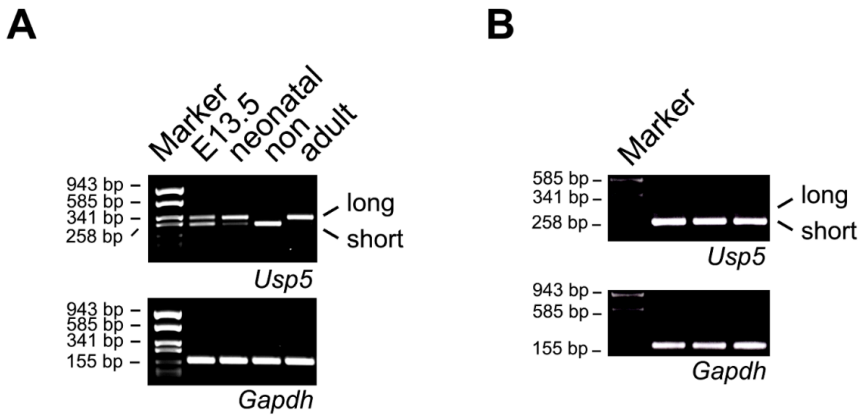

Figure 21 *Usp5* undergoes cell-type specific differential splicing.

A. Splice variants of mouse *Usp5* in isolated cardiomyocytes at different developmental stages and adult non-cardiomyocytes. B. Splice variants of mouse *Usp5* in mouse embryonic fibroblasts (MEFs).

Reciprocal co-immunoprecipitations (co-IPs) were performed to investigate exon 15 isoform-specific differences of USP5 regarding protein complex formation with PSMD14 (Figure 22 A). I found that alternative splicing of USP5 had no impact on binding affinity towards PSMD14 (Figure 22 B, C). These results corroborate the previous results that USP5 and PSMD14 are part of the same protein complex. In addition, both exon 15 isoforms were able to interact with the deacetylase HDAC6 (Figure 23 A-C), which is another crucial component of PQC, especially under stress conditions. HDAC6-restricted binding to free ubiquitin chains that are released *en bloc* by PSMD14-mediated deubiquitination promotes concentration and selective autophagy-dependent clearance of protein aggregates in cells with compromised proteasome activity [71, 129, 132].

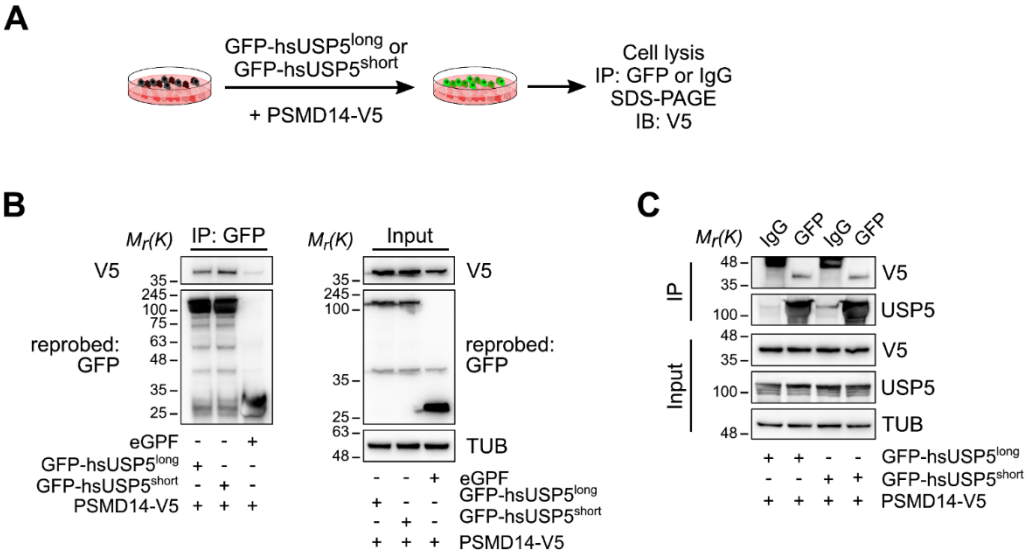

Figure 22 USP5 co-immunoprecipitates with components of cellular PQC – PSMD14.

A. Workflow for co-immunoprecipitation (co-IP) of GFP-tagged human isoforms of USP5 with V5-tagged mouse PSMD14 in HEK293 cells. B. Immunoblot analysis of anti-GFP precipitated cell lysates probed with anti-V5 and anti-GFP antibody. Input and IP fractions are shown. C. Immunoblot analysis of anti-GFP and IgG precipitated cell lysates probed with anti-V5 and anti-USP5 antibody. Input and IP fractions are shown.

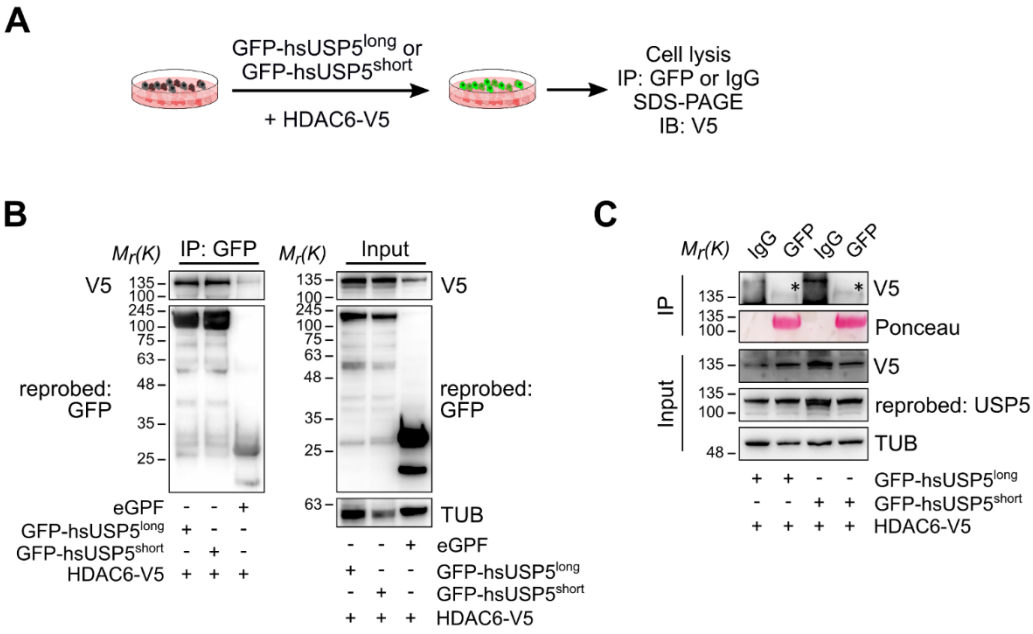

Figure 23 USP5 co-immunoprecipitates with components of cellular PQC – HDAC6.

A. Workflow for co-immunoprecipitation of GFP-tagged human isoforms of USP5 with V5-tagged human HDAC6 in HEK293 cells. B. Immunoblot analysis of anti-GFP precipitated cell lysates probed with anti-V5 and anti-GFP antibody. Input and IP fractions are shown. C. Immunoblot analysis of anti-GFP and IgG precipitated cell lysates probed with anti-V5 and anti-USP5 antibody. Input and IP fractions are shown.

As the previous results suggested that USP5 plays a role in the regulation of PQC processes, the cellular localization of USP5 in conditions of elevated proteostatic stress, causing formation of potentially toxic protein aggregates, was analyzed. Accumulation of misfolded proteins, resulting from genetic mutations, ineffective refolding by molecular chaperones, defective protein maturation, failure in protein catabolic processes, or environmental stress, is known to cause formation of large protein aggregates [133]. Once formed, these large protein aggregates often become toxic, since they are not removed by proteolytic degradation via the 26S proteasome and thus interfere with cellular homeostasis and proteostasis. To induce proteostatic stress in mature cardiomyocytes and MEFs, proteasome activity was inhibited by administration of MG132 for 4 h, which caused accumulation of protein aggregates and formation of large aggresomes that were visualized by the immunofluorescence-based PROTEOSTAT® aggregation assay (Figure 24 A, B). The PROTEOSTAT® aggregation assay is based on a fluorophore coupled dye that binds covalently and irreversibly to hydrophobic surfaces of misfolded proteins, causing emission of a red fluorescent signal that can be detected by immunofluorescence-based microscopy [126].

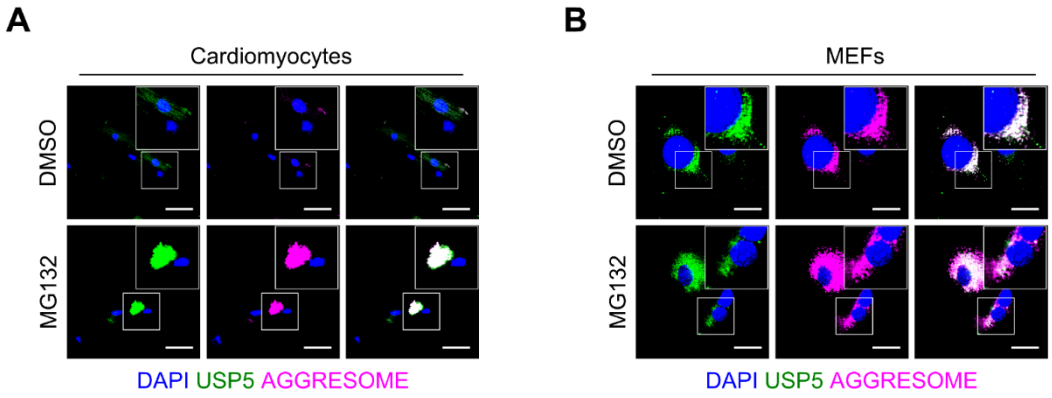

Figure 24 USP5 co-localizes with aggresomes in response to proteostatic stress.

A, B. Immunofluorescence staining of USP5 (green), aggresomes (magenta), and nuclei (DAPI, blue) in isolated mature cardiomyocytes (A) and MEFs (B). Cells were treated with 0.2 % DMSO or 10 µmol L^{-1} MG132 for 4 h to induce aberrant protein aggregation and aggresome formation.

Remarkably, USP5 co-localized with protein aggregates and aggresomes in mature cardiomyocytes and MEFs, concomitant with enhanced USP5 staining intensity in response to proteostatic stress (Figure 24 A, B). Collectively, these data emphasize an important role of USP5 in the regulation of cellular PQC processes to maintain proteostasis, probably by handling of free, unanchored polyubiquitin chains provided by PSMD14-mediated deubiquitination.

Isoform- and cell-type specific role of USP5 in the maintenance of ubiquitin pools

As the physiological role of USP5, especially in the cardiovascular system, had not been studied, the aim of the study was to recapitulate possible consequences arising from loss of USP5 in a cell-type and isoform specific manner. For this purpose, *Usp5 flox/flox* mice, carrying a conditionally inactive allele of *Usp5*, were generated. Infection of MEFs derived from homozygous *Usp5 flox/flox* mice with an adenovirus expressing a codon improved *cre*-recombinase (hereafter called: Ad-Cre) for 6 h resulted in efficient recombination reducing USP5 protein levels by approximately 90 % six days after virus transduction. Homozygous *Usp5 flox/flox* infected with an empty adenovirus (hereafter called: Ad-Null) served as controls (Figure 25 A-D). Immunoblot analysis of Ad-Cre infected MEFs did not show dramatic changes in the ubiquitin levels compared to MEFs transfected with Ad-Null (Figure 26 A, B), despite a moderate accumulation of polyubiquitin chains and polyubiquitinated proteins (Figure 26 C).

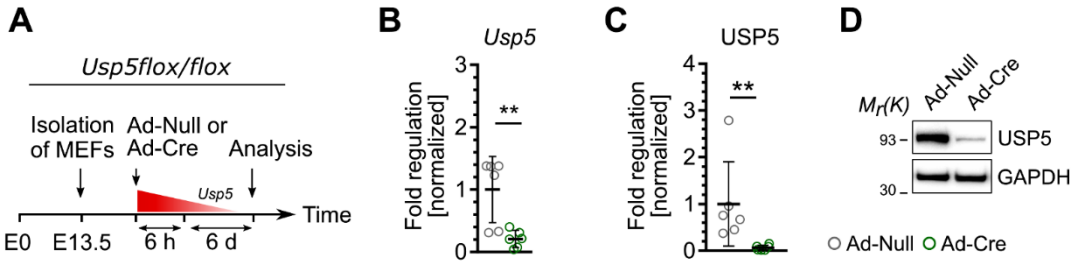

Figure 25 Inactivation of *Usp5* in MEFs via adenoviral transduction.

A. Strategy for *Usp5* gene inactivation in MEFs via adenoviral transduction. MEFs were isolated from pregnant *Usp 5flox/flox* mice at E13.5 and after several passages; MEFs were infected with a recombinant adenovirus expressing an empty adenovirus (Ad-Null) or a codon improved cre-recombinase (Ad-Cre) for 6h. Analysis was performed six days after virus transduction. B. Quantification of *Usp5* mRNA levels in *Usp5 flox/flox* MEFs six days after virus transduction. Values were normalized to *gapdh* mRNA levels. n = 6 for each group. Two-tailed unpaired Wilcoxon-rank sum test. ** $P < 0.0021$. C, D. USP5 protein levels (D) and quantification (C) in Ad-Null- or Ad-Cre transduced MEFs. Values were normalized to GAPDH protein levels. n = 6 for each group. Two-tailed unpaired Wilcoxon-rank sum test. ** $P < 0.0021$.

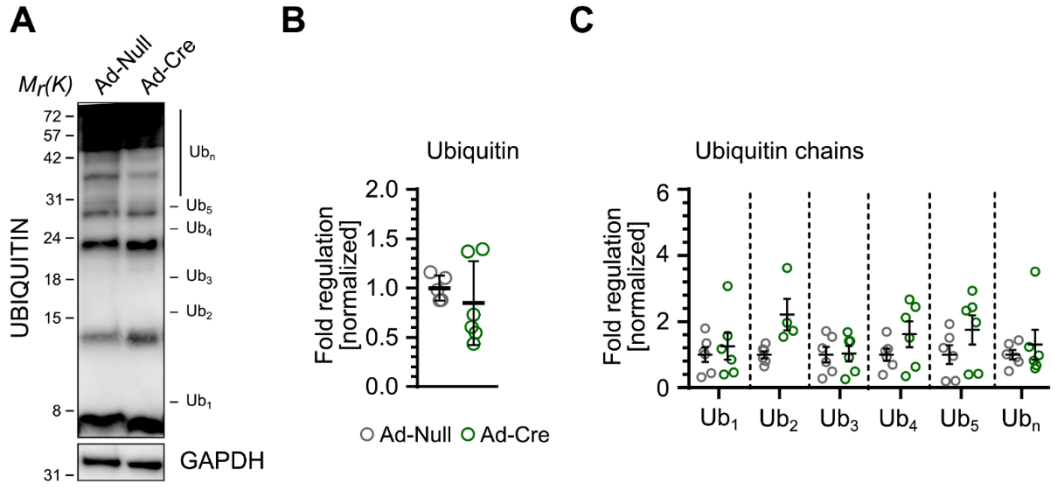

Figure 26 Depletion of USP5 in MEFs via adenoviral transduction does not affect the ubiquitin pool.

A. Immunoblot analysis of ubiquitin in MEFs six days after adenoviral transduction with a recombinant adenovirus expressing a codon improved cre-recombinase (Ad-Cre) or an empty adenovirus (Ad-Null) for 6h. B, C. Quantification of ubiquitin levels (B) and ubiquitin chains (C) in Ad-Cre and Ad-Null infected MEFs. Values were normalized to GAPDH protein expression. n = 6 per group.

I also generated homozygous *Rosa26-CreER^{T2}//Usp5 flox/flox* mice to delete *Usp5* in MEFs after treatment with 4-hydroxytamoxifen (hereafter called *Usp5iKO*) (Figure 27 A). 48 h after treatment with 10 µmol L^{-1} 4-hydroxytamoxifen (4-OHT), USP5 protein levels in *Usp5iKO* MEFs were reduced by approximately 50-65 % in comparison to 4-OHT-treated *Usp5 flox/flox* MEFs (Figure 27 B-D).

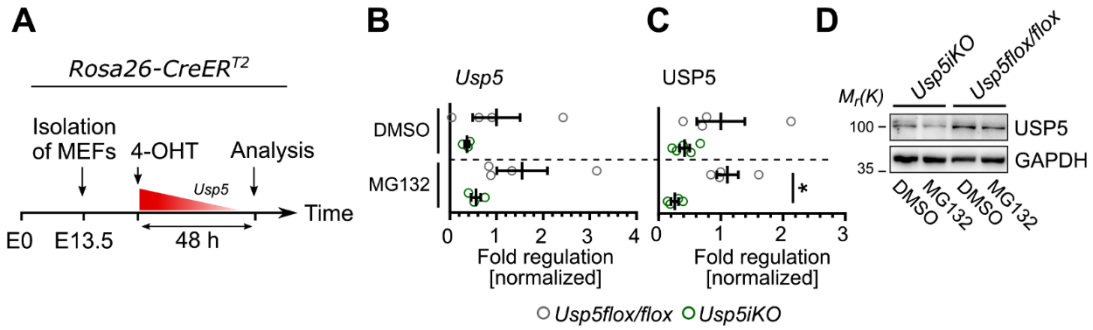

Figure 27 4-Hydroxytamoxifen (4-OHT) induced inactivation of *Usp5* in MEFs.

A. Strategy for depletion of *Usp5* in MEFs. *Usp5flox/flox* mice were crossbred with mice harboring a conditional *Rosa26-CreER^{T2}* (Cre recombinase – estrogen receptor T2) transgene, by which the ER^{T2} moiety retains the *cre* recombinase until 4-hydroxytamoxifen (4-OHT) administration releases this inhibiting effect. MEFs were isolated from pregnant mice at E13.5 and after several passages, cells were treated with 4-OHT for 48 h to induce recombination and depletion of *Usp5*. B. Quantification of *Usp5* mRNA levels in MEFs from *Usp5iKO (CreER$^{T2+/-}$//Usp5flox/flox)* and *Usp5 flox/flox* control littermates 48 h after 4-OHT administration. In addition, MEFs were treated with 0.2 % DMSO or 10 µmol L^{-1} MG132 for 6 h before RNA was extracted. Values were normalized to *gapdh* mRNA levels. n = 4 for each genotype. C, D. USP5 protein levels (D) and quantification (C) in MEFs with or without MG132 treatment after 4-OHT-induced depletion of *Usp5*. Values were normalized to GAPDH protein levels. n = 4 for each genotype. One-way ANOVA followed by Dunn's post-test. * $P < 0.05$.

Although recombination efficacy was lower compared to Ad-Cre infected *Usp5 flox/flox* MEFs, I detected the same moderate increase in polyubiquitin levels and levels of polyubiquitinated proteins, even in MG132-treated *Usp5 flox/flox* MEFs after 4-OHT administration (Figure 28 A-C). USP5 protein levels were not affected by MG132-mediated inactivation of the 20S proteasome activity (Figure 28 C, D). These data show that already a moderate reduction of USP5 in MEFs impacts ubiquitin levels, particularly in the high molecular weight range.

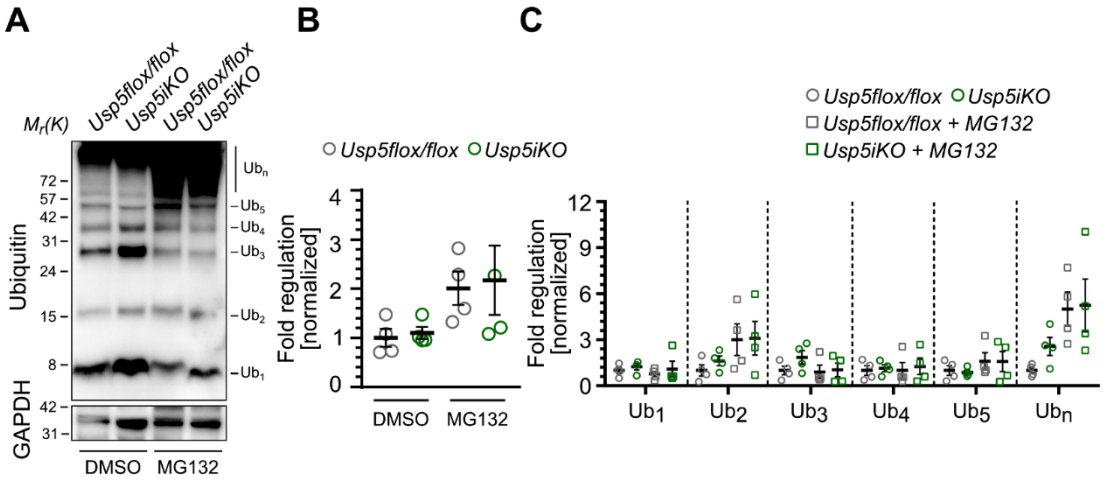

Figure 28 4-OHT-induced inactivation of *Usp5* in MEFs does not change the ubiquitin pool.
A. Immunoblot analysis of ubiquitin levels in *Usp5iKO* and *Usp5iKO* MEFs with or without MG132 treatment after 4-OHT-induced depletion of *Usp5*. B, C. Quantification of ubiquitin levels (B) and ubiquitin chains (C) relative to GAPDH expression. n = 4 for each group.

In a second approach, *Usp5 flox/flox* mice were crossbred with the *Myh6-MerCreMer* transgenic mouse strain to generate homozygous *Myh6-MerCreMer//Usp5 flox/flox* mice (hereafter called *Usp5cKO*), which enabled conditional inactivation of *Usp5* in postmitotic, protein aggregation prone mature cardiomyocytes by administration of tamoxifen. Administration of 100 mg kg^{-1} tamoxifen intraperitoneal (i.p.) to P56 old male mice for seven consecutive days and subsequent isolation of cardiomyocytes 15 days after the last tamoxifen doses at P78 resulted in reduction of USP5 protein levels by approximately 95 % (Figure 29 A-D).

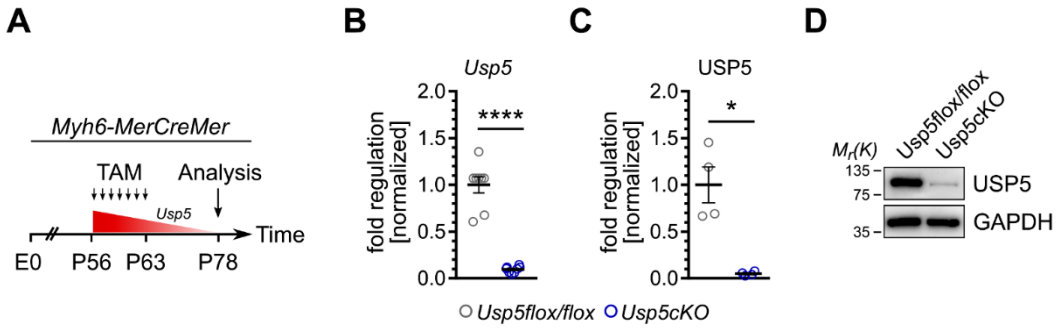

Figure 29 Tamoxifen-induced inactivation of *Usp5* in mature cardiomyocytes.

A. Strategy for ablation of *Usp5* in postmitotic, mature cardiomyocytes. *Usp5 flox/flox* mice were crossbred with mice expressing a tamoxifen-inducible *Myh6-MerCreMer* transgene. P56 old male mice were injected with 100 mg kg^{-1} tamoxifen for seven consecutive days and cardiomyocytes were isolated 15 days post-infection (= P78). B. Quantification of *Usp5* mRNA levels in isolated cardiomyocytes from *Usp5cKO (Myh6-MerCreMer//Usp5 flox/flox)* mice and *Usp5 flox/flox* control littermates at P78. Values were normalized to *gapdh* mRNA levels. n = 8 for each genotype. Unpaired t-test with Welch's correlation. **** $P < 0.0001$. C, D. USP5 protein levels (D) and quantification (C) in isolated cardiomyocytes from *Usp5cKO* mice and *Usp5flox/flox* control littermates at P78. Values were normalized to GAPDH protein levels. n = 4 for each genotype. Unpaired t-test with Welch's correlation. * $P < 0.05$.

In contrast to MEFs, inactivation of *Usp5* in mature cardiomyocytes resulted in increased ubiquitin levels (Figure 30 A, B), primarily resulting from elevated poly- but also monoubiquitin (Figure 30 C). Treatment of cardiomyocytes from *Usp5 flox/flox* control littermates with MG132 yielded results similar to those observed in MG132-treated *Usp5 flox/flox* MEFs, including elevated levels of ubiquitin particularly in the high molecular weight range, while the levels of monoubiquitin remained unchanged (Figure 30 D-F). Treatment of USP5-deficient cardiomyocytes (*Usp5cKO*) with MG132 did not further increase (poly-) ubiquitin levels in comparison to untreated USP5-deficient cardiomyocytes (Figure 30 F). Importantly, effects on ubiquitin levels were stronger in *Usp5cKO* cardiomyocytes compared to ubiquitin levels *Usp5iKO* MEFs. Collectively, these data point towards an instrumental role for USP5 in maintaining robust polyubiquitin levels in mature cardiomyocytes, since its inactivation affects both mono- and polyubiquitin levels substantially. These findings further indicate that inactivation of *Usp5* in mature cardiomyocytes may be sufficient to completely disrupt proteasome activity.

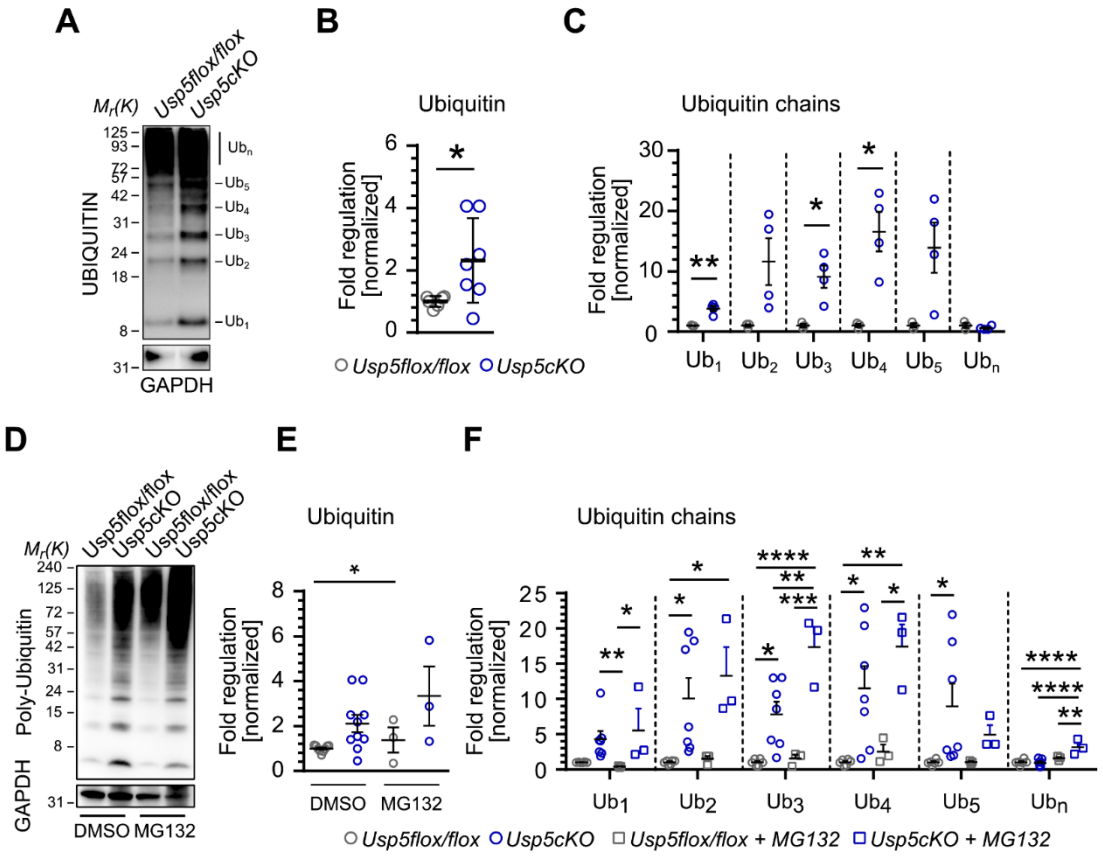

Figure 30 Inactivation of USP5 in mature cardiomyocytes causes accumulation of ubiquitin.

A. Immunoblot analysis of ubiquitin levels in isolated mature cardiomyocytes from *Usp5 flox/flox* and *Usp5cKO* mice 15 days after the last tamoxifen administration. B. Quantification of ubiquitin levels relative to GAPDH protein expression. n = 6 in *Usp5 flox/flox*, n = 7 in *Usp5cKO*. Two-tailed unpaired t-test with Welch's correlation. * $P < 0.05$. C. Quantification of ubiquitin chains relative to GAPDH protein expression. n = 4 for each group. Two-tailed unpaired t-test with Welch's correlation. * $P < 0.05$, ** $P < 0.0021$. D. Immunoblot analysis of ubiquitin levels in cardiomyocytes from *Usp5 flox/flox* and *Usp5cKO* mice 15 days after the last tamoxifen administration and with (n = 3 for each group) or without (n = 9 for each group) MG132 treatment. E. Quantification of ubiquitin levels relative to GAPDH between the groups. One-way ANOVA followed by Tukey's post-test. * $P < 0.05$. F. Quantification of ubiquitin chains relative to GAPDH between the groups. One-way ANOVA followed by Dunn's and Tukey's post-test. * $P < 0.05$; ** $P < 0.0021$; *** $P < 0.002$; **** $P < 0.0001$.

Consistent with an active recruitment of USP5 to sites of atypical protein aggregation and increased USP5 staining intensity in MG132-treated cardiomyocytes (Figure 24 A, B), USP5 protein levels were drastically elevated in MG132-treated *Usp5 flox/flox* cardiomyocytes, while USP5 protein levels remained constantly reduced by 95 % in cardiomyocytes isolated from *Usp5cKO* mice (Figure 31 A, B).

These data further support a crucial role of USP5 in the cellular PQC response to proteotoxic stress, in addition to its already reported role to maintain the ubiquitin pool. In this regard, mature cardiomyocytes seem to specifically rely on sufficient USP5 levels and USP5-dependent ubiquitin homeostasis.

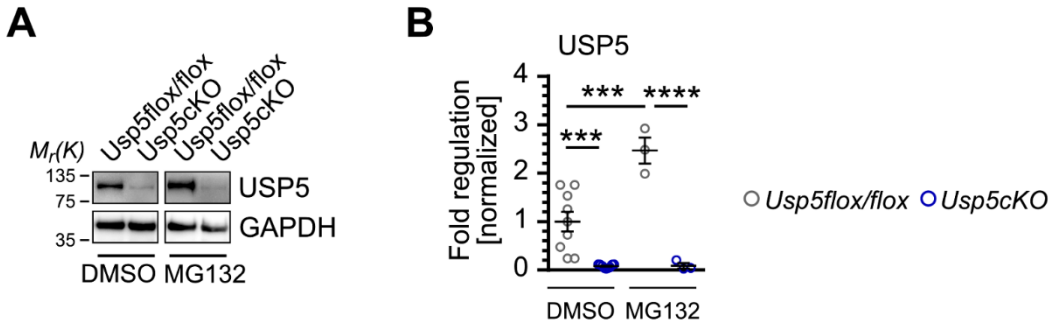

Figure 31 USP5 protein levels increases in response to proteostatic stress.

A. USP5 protein levels in isolated cardiomyocytes 15 days after the last tamoxifen administration and with (n = 3 for each group) or without (n = 9 for each group) MG132 treatment. B. Quantification of USP5 protein levels relative to GAPDH protein expression. One-way ANOVA followed by Turkey's post-test. *** $P < 0.0002$; **** $P < 0.0001$.

USP5-deficient cardiomyocytes display reduced 20S proteasome activity

Inactivation of *Usp5* in mature cardiomyocytes resulted in elevated ubiquitin levels, predominantly in the high molecular weight range, reflecting either polyubiquitin chains or polyubiquitinated proteins. Aberrant accumulation of ubiquitin-enriched protein aggregates is known to impair proteasome activity both *in vitro* and *in vivo*. Since accumulation of free, protein unattached ubiquitin chains competitively inhibit proteasome activity *in vitro* in response to loss of USP5 [56, 130, 134], the evident question was whether inactivation of *Usp5* alone was sufficient to disrupt activity of the 20S proteasome. A fluorescence-based kinetic assay [35] was used to specifically assess the proteolytic capability of the 20S proteasome in cell extracts of MEFs and isolated mature cardiomyocytes. To guarantee robustness of the results and to increase the sensibility of the assay, MG132-treated control groups were included.

Consistent with the only moderate increase in ubiquitin levels, inactivation of *Usp5* in MEFs by 4-OHT administration did not impair any of the three peptidase activities of the 20S proteasome (Figure 32 A-C). In fact, *Usp5iKO* MEFs showed slightly enhanced caspase- and chymotrypsin-like peptidase activities, while administration of MG132 almost completely blocked these two peptidase activities both in MEFs from *Usp5 flox/flox* and *Usp5iKO* mice (Figure 32 A, C). On the other hand, inactivation of *Usp5* in *Usp5 flox/flox* MEFs by adenoviral infection (Ad-Cre) slightly decreased caspase- and chymotrypsin-like peptidase activities, while MG132 administration resulted in almost complete inhibition (Figure 32 D, F).

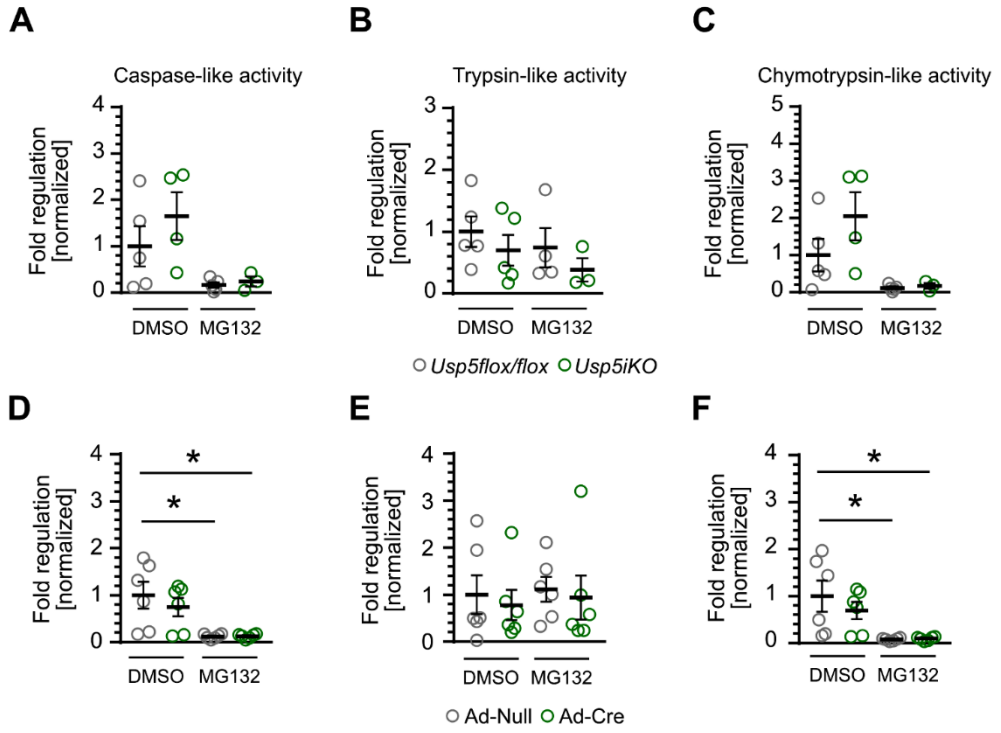

Figure 32 Inactivation of *Usp5* in MEFs does not affect 20S proteasome activities.

A-C. Quantification of proteasomal caspase-like activity by Z-Leu-Leu-Glu-AMC digestion (A), proteasomal trypsin-like activity by Boc-Leu-Arg-Arg-AMC digestion (B), and chymotrypsin-like activity by Suc-Leu-Leu-Val-Tyr-AMC digestion (C) in *Usp5 flox/flox* and *Usp5iKO* MEFs treated with (n = 4 for *Usp5flox/flox*, n = 3 *Usp5iKO*) and without (n = 5 for each group) MG132 after 4-OHT administration. D-F. Quantification of proteasomal caspase-like activity by Z-Leu-Leu-Glu-AMC digestion (D), proteasomal trypsin-like activity by Boc-Leu-Arg-Arg-AMC digestion (E), and chymotrypsin-like activity by Suc-Leu-Leu-Val-Tyr-AMC digestion (F) in MEFs treated with (n = 6 for each group) and without (n = 6 for each group) MG132 after infection with Ad-Null or Ad-Cre. One-way ANOVA followed by Sidak's post-test. * $P < 0.005$.

In stark contrast, inactivation of *Usp5* in cardiomyocytes strongly suppressed all three peptidase activities of the 20S proteasome, comparable to inactivation of the 20S proteasome by MG132 treatment (Figure 33 A-C). These data not only support the high sensitivity of the assay, but also argue for defective proteolysis in USP5-deficient cardiomyocytes, possibly in response to inappropriate ubiquitin levels.

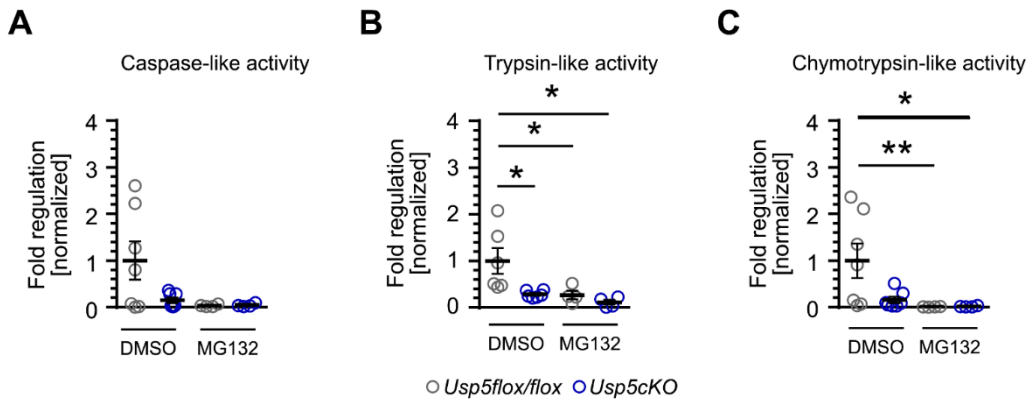

Figure 33 Impaired proteasome peptidase activities in USP5-deficient cardiomyocytes.
A-C. Quantification of proteasomal caspase-like activity by Z-Leu-Leu-Glu-AMC digestion (A), proteasomal trypsin-like activity by Boc-Leu-Arg-Arg-AMC digestion (B), and chymotrypsin-like activity by Suc-Leu-Leu-Val-Tyr-AMC digestion (C) in isolated cardiomyocytes from *Usp5 flox/flox* and *Usp5cKO* mice 15 days after the last tamoxifen administration. Cardiomyocytes were treated with (n = 4 for each group) and without (n = 6 for each group) MG132. One-way ANOVA followed by Dunn's post-test (B) or Tukey's post-text (C). * $P < 0.005$; ** $P < 0.0021$.

In addition to the total increase in ubiquitin levels in USP5-deficient cardiomyocytes, immunoblot analysis revealed elevated levels of Lys48- and Lys63-linkage specific ubiquitin, again predominantly in the high molecular weight range (Figure 34 A-D). These findings suggest that diminished proteasome activity and consequently impaired ubiquitin-dependent proteolysis potentially in combination with failure in (selective) autophagy disturbs proteostasis in cardiomyocytes in response to inactivation of *Usp5*. Moreover, the data strengthens the importance of USP5 in maintaining normal ubiquitin levels, which are essential for sustained ubiquitin-dependent proteolysis in cardiomyocytes.

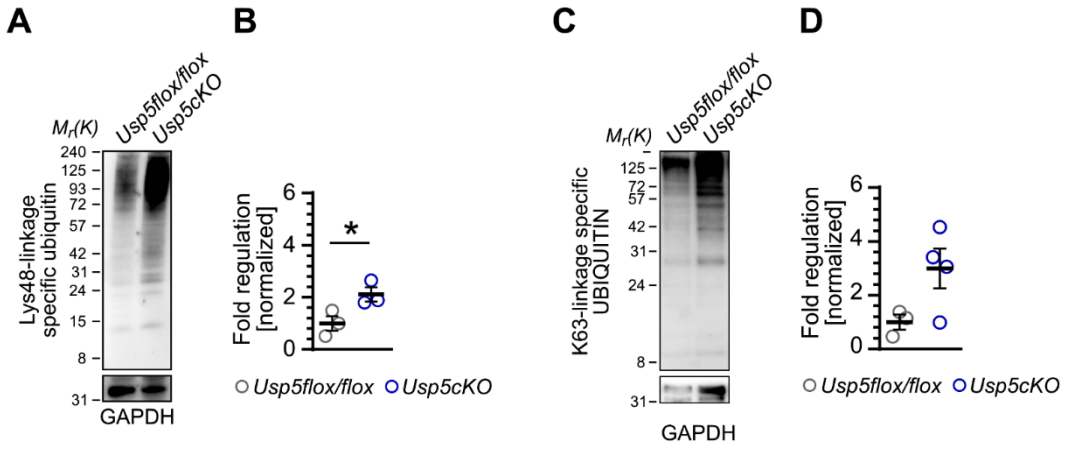

Figure 34 Elevated levels of Lys48- and Lys63-linkage specific ubiquitin in cardiomyocytes lacking USP5.

A. Immunoblot analysis of Lys48-linkage specific ubiquitin in isolated cardiomyocytes from *Usp5 flox/flox* and *Usp5cKO* mice and B. quantification relative to GAPDH expression. n = 3 for each group. Two-tailed unpaired t-test with Welch's correlation. * $P < 0.05$. C. Immunoblot analysis of Lys63-linkage specific ubiquitin in isolated cardiomyocytes from *Usp5flox/flox* and *Usp5cKO* mice and D. quantification relative to GAPDH expression. n = 3 for *Usp5flox/flox*, n = 4 for *Usp5cKO*

USP5-deficient cardiomyocytes accumulate ubiquitin-enriched protein aggregates

Since forced inactivation of proteasome activity by MG132 resulted in accumulation of USP5-containing misfolded proteins to mainly perinuclear aggresomes (Figure 24 A, B), one might argue that the observed suppression of all three peptidase activities of the 20S proteasome in combination with elevated levels of Lys48-linkage specific ubiquitin might be sufficient to evoke aberrant protein aggregation in USP5-deficient cardiomyocytes but not in USP5-deficient MEFs. To verify this hypothesis, the PROTEOSTAT® aggregation assay in combination with immunofluorescence staining was used to visualize any ubiquitin-enriched protein aggregates and aggresomes. Unexpectedly, *Usp5iKO* MEFs accumulated large perinuclear aggresomes, comparable to *Usp5 flox/flox* MEFs treated with MG132 (Figure 35 A, B). The majority of detected aggresomes in *Usp5iKO* MEFs contained ubiquitin, which argues for accumulation of ubiquitin-conjugated protein aggregates.

In contrast, aggresomes in *Usp5 flox/flox* MEFs were rarely conjugated with ubiquitin (Figure 35 C). However, forced inhibition of 20S proteasome activity in *Usp5 flox/flox* MEFs by MG132 treatment also resulted in accumulation of ubiquitin-conjugated aggresomes (Figure 35 D).

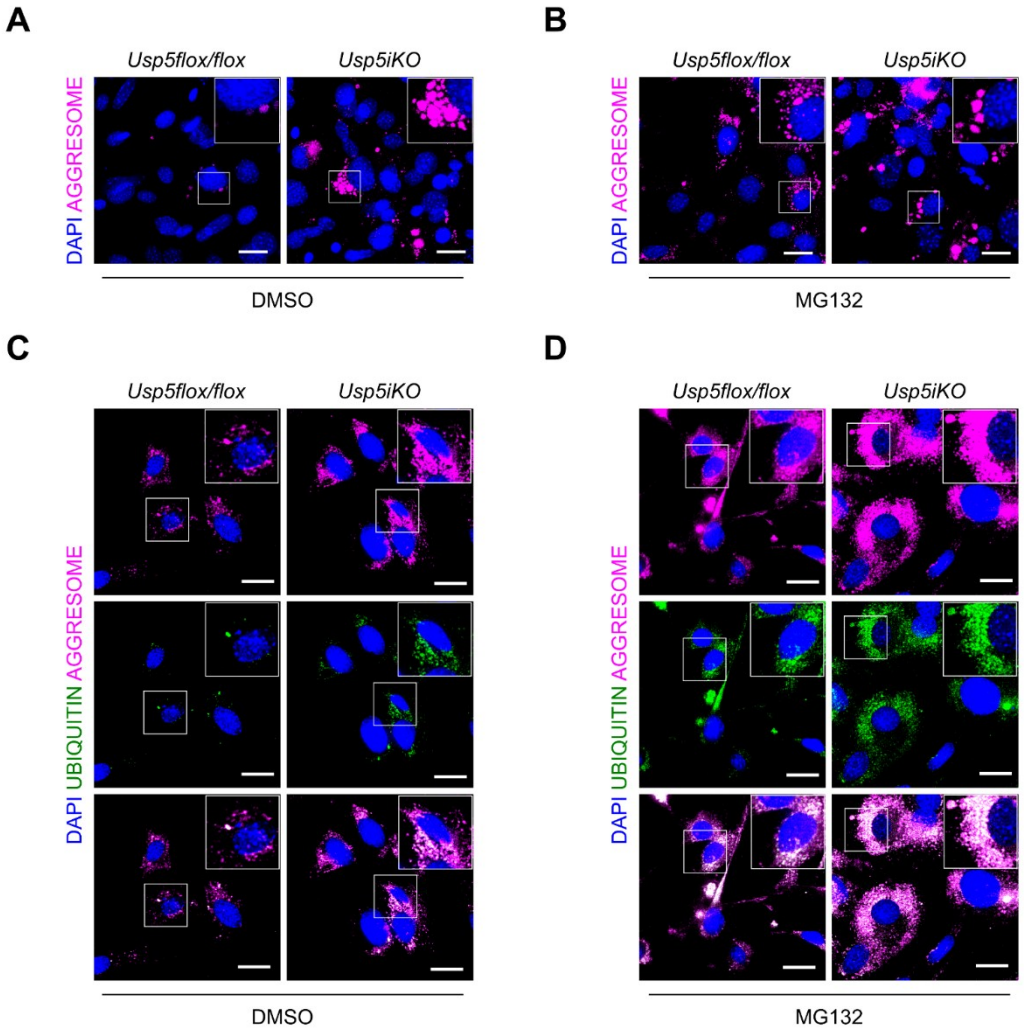

Figure 35 Accumulation of ubiquitin-conjugated aggresomes in USP5-deficient MEFs.

A, B. Immunofluorescence staining of aggresomes (magenta) and nuclei (DAPI, blue) in *Usp5 flox/flox* and *Usp5iKO* MEFs following administration of 4-OHT and treatment with DMSO or MG132 for 6 h. n = 3 for each group. Scale bars, 50 µm. C, D. Immunofluorescence staining of ubiquitin (green), aggresomes (magenta), and nuclei (DAPI, blue) in *Usp5 flox/flox* and *Usp5iKO* MEFs following administration of 4-OHT and treatment with DMSO (n = 2 for each group) or MG132 (n = 3 for each group) for 6 h. Scale bars, 50 µm.

Consistent with the hypothesis, inactivation of *Usp5* in mature cardiomyocytes resulted in enhanced load of mainly perinuclear aggresomes (Figure 36 A), which co-localized with large ubiquitin deposits (Figure 36 B). In summary, these findings suggest that accumulation of ubiquitin-conjugated protein aggregates and aggresomes in *Usp5iKO* MEFs might be caused by failure of selective autophagy rather than impaired proteasome activity, whereas both branches of cellular PQC – UPS-dependent proteolysis and clearance of protein aggregates by selective autophagy – are impaired in cardiomyocytes in response to inactivation of *Usp5*.

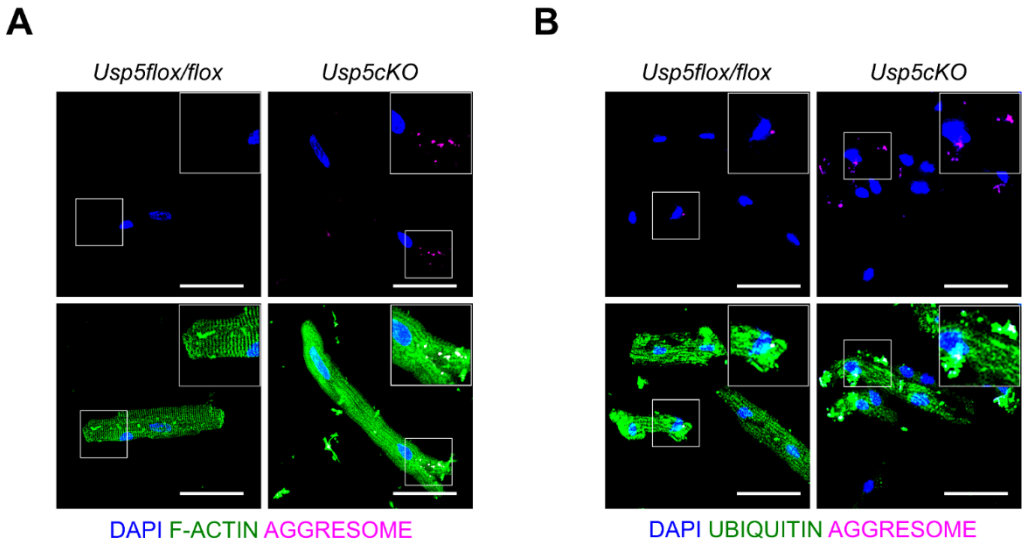

Figure 36 Accumulation of ubiquitin-containing aggresomes in USP5-deficient cardiomyocytes.

A. Immunofluorescence staining for F-actin (green), aggresomes (magenta), and nuclei (DAPI, blue) in isolated cardiomyocytes from *Usp5 flox/flox* and *Usp5cKO* mice 15 days after the last tamoxifen administration. n = 4 for each group. Scale bars, 50 µm. B. Immunofluorescence staining of ubiquitin (green), aggresomes (magenta), and nuclei (DAPI, blue) in isolated cardiomyocytes from *Usp5 flox/flox* and *Usp5cKO* mice 15 days after the last tamoxifen administration. n = 4 for each group. Scale bars, 50 µm.

Profiling of USP5-deficient cardiomyocytes

To gain deeper insights into the underlying mechanisms, we employed both RNA microarray-based transcriptional profiling and whole proteome analysis of USP5-deficient cardiomyocytes compared to isolated cardiomyocytes from *Usp5 flox/flox* control littermates (Figure 37-41).

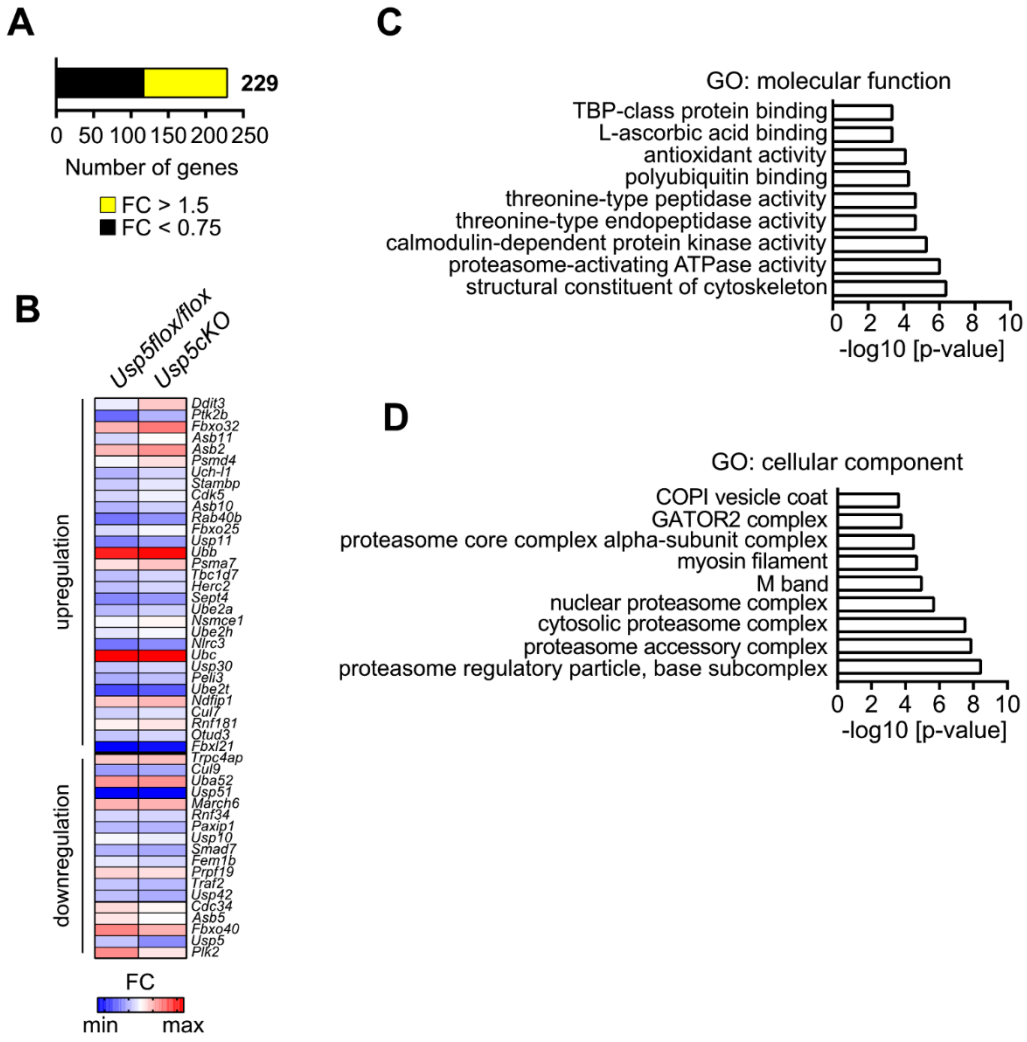

Figure 37 Transcriptional profiling of USP5-deficient cardiomyocytes.

A. Graph bar showing total the total number of up- (yellow, $log_2 > 1.0$, $P < 0.05$) and down-regulated (black, $log_2 > -1.0$, $P < 0.05$) genes in cardiomyocytes from *Usp5 flox/flox* and *Usp5cKO* mice 15 days after the last tamoxifen administration. B. Heat map showing differences in expression of ubiquitin-related genes based on fold chances (FC). C, D. Box plots showing significantly enriched GO terms of differentially expressed genes based on *-log10 P*-values. GO terms refer to molecular function (C) and cellular components (D).

Microarray analysis revealed substantial changes in the expression of 229 genes. Half of the deregulated genes were either up- or down-regulated in response to *Usp5* inactivation in cardiomyocytes (Figure 37 A). The majority of differentially expressed genes encode ubiquitin-related proteins, including various ubiquitin ligases, DUBs, or components of the 26S proteasome (Figure 37 B). GO term analysis showed that strongest differentially expressed genes are structural components of the cytoskeleton or the 19S proteasome. In line with the enrichment analysis, most dysregulated genes play important roles in polyubiquitin binding and regulation of the ATPase activity, which is crucial for activation of proteasome-dependent catabolic processes (Figure 37 C, D). Interestingly, microarray analysis also revealed strong changes in the expression of the mouse polyUbs *Ubb* and *Ubc* (Figure 37 C). RT-qPCR analysis using gene-specific TaqMan probes confirmed a 2- to 2.5-fold increase in the mRNA levels of *Ubb* and *Ubc* in cardiomyocytes of *Usp5cKO* mice (Figure 38 A). Inhibition of 20S proteasome activity by MG132 treatment of isolated cardiomyocytes from *Usp5 flox/flox* mice resulted in increased transcription of *Ubb* and *Ubc* similar to inactivation of *Usp5* in cardiomyocytes (Figure 38 A).

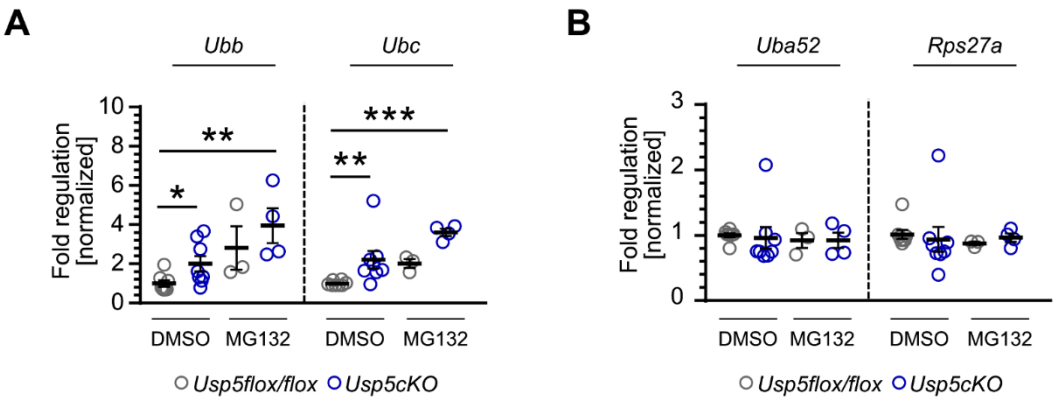

Figure 38 Upregulation of polyUbs in USP5-deficient cardiomyocytes.

A, B. RT-qPCR analysis of polyUbs (A) and Ub-RPs (B) expression in cardiomyocytes from *Usp5 flox/flox* and *Usp5cKO* mice 15 days after the last tamoxifen administration. Cardiomyocytes were treated with 0.2 % DMSO (n = 8) or 10 µmol L^{-1} MG132 (n = 3 for *Usp5 flox/flox*, n = 4 for *Usp5cKO*) for 4 h. Values were normalized to *gapdh* expression. One-way ANOVA followed by Dunn's post-test. * $P < 0.05$; ** $P < 0.0021$; *** $P < 0.0002$.

MG132 treatment did not further enhance transcription of *Ubb* and *Ubc* in USP5-deficient cardiomyocytes, suggesting that derailed proteasome activity in response to inactivation of *Usp5* in cardiomyocytes correlates with transcriptional changes in the expression of polyUbs, which argues for an enhanced ubiquitin stress response. In contrast, no changes in the mRNA levels of the two Ub-RPs *Uba52a* or *Rps27a* in USP5-deficient cardiomyocytes were detected, even after treatment with MG132 (Figure 38 B). In addition to the observed transcriptional changes in polyUbs and ubiquitin-associated genes, mRNA levels of several cardiac stress-response genes, such as *Nppa, Myh7, Acta1, Fbxo32, and Uchl1* were substantially upregulated in cardiomyocytes from *Usp5cKO* mice (Figure 39 A). RT-qPCR analysis confirmed increased expression of the indicated genes in addition to decreased mRNA levels of *Myc* (Figure 39 B).

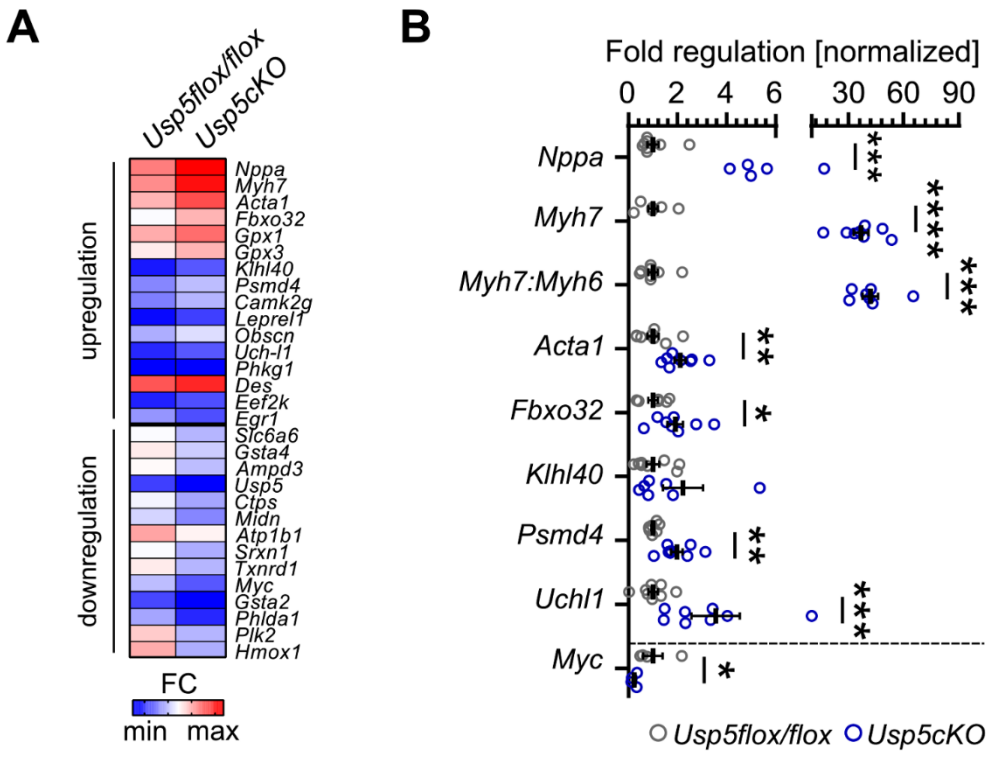

Figure 39 Upregulation of cardiac stress response genes in USP5-deficient cardiomyocytes.

A. Heat map showing most significantly changed transcripts in USP5-deficient cardiomyocytes versus cardiomyocytes isolated from *Usp5 flox/flox* control littermates based on fold chances (FC). B. RT-qPCR analysis of differentially expressed genes. Values were normalized to *gapdh* mRNA expression. n = 8 for each group. Two-tailed unpaired t-test with Welch's correlation or Wilcoxon-rank sum test. * $P < 0.05$; ** $P < 0.0021$; *** $P < 0.0002$; **** $P < 0.0001$.

Comprehensive whole proteome analysis by LFQ mass spectroscopy of USP5-deficient cardiomyocytes identified 186 dysregulated proteins with mostly ubiquitin-associated proteins (Figure 40 A, B). Enrichment analysis of the altered proteome revealed USP5-dependent changes of proteins forming the proteasome or ubiquitin ligase complexes (Figure 40 C). The majority of identified proteins with significantly different LFQ intensities are important for the regulation of protein catabolic processes, including proteolysis (Figure 40 D).

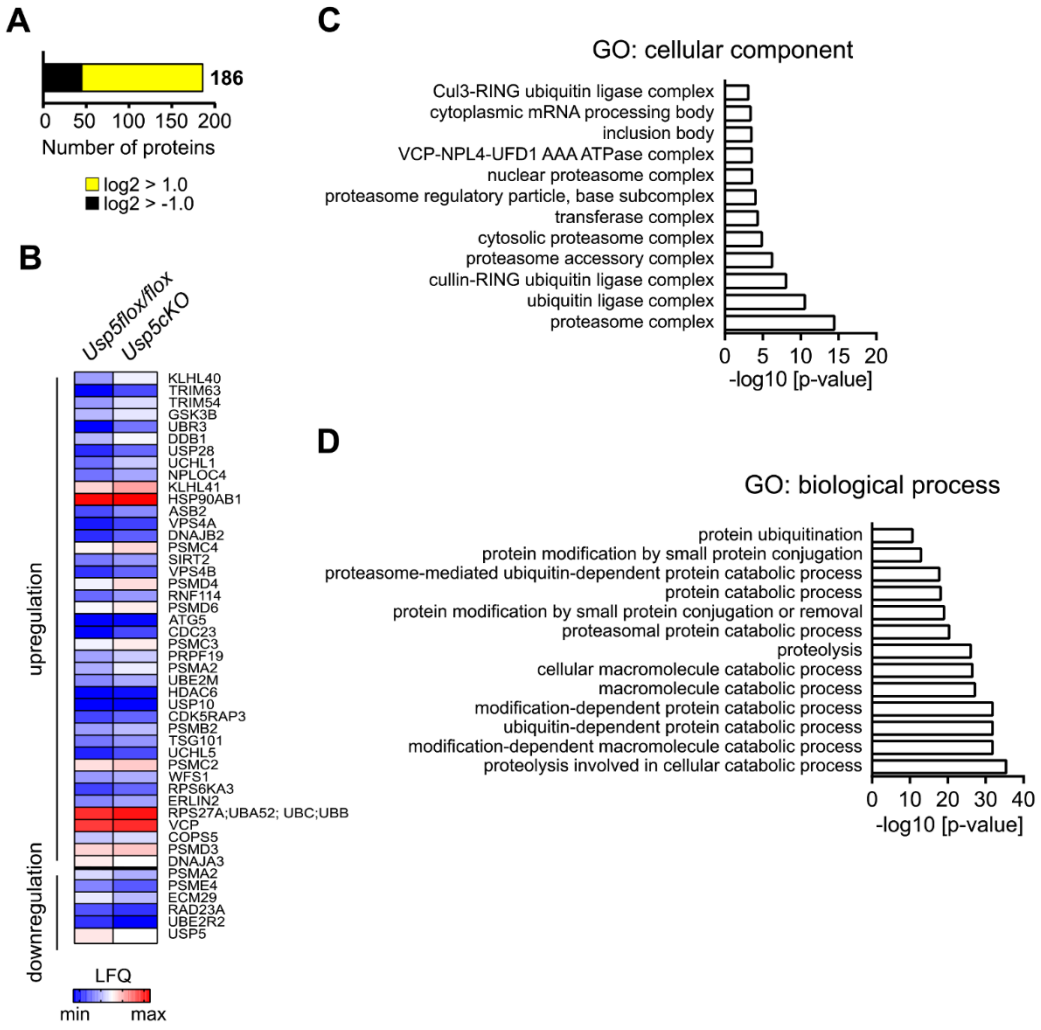

Figure 40 Whole proteome analysis of USP5-deficient cardiomyocytes.

A. Graph bar showing the total number of up- (yellow, $log_2 > 1.0$, $P < 0.05$) and down-regulated (black, $log_2 > -1.0$, $P < 0.05$) proteins in isolated cardiomyocytes from *Usp5 flox/flox* and *Usp5cKO* mice 15 days after the last tamoxifen administration. B. Heat map showing differences in LFQ-intensities of ubiquitin-related proteins. C, D. Box plots representing enriched GO terms of differentially expressed proteins based on the *-log10 P*-values. GO terms refer to cellular components (C) and biological processes (D).

Since whole proteome analysis identified dysregulation of several subunits of the 26S proteasome in response to inactivation of *Usp5* in cardiomyocytes, immunoblot analysis was performed to validate the changes. Indeed, immunoblot analysis revealed substantial changes in the expression of subunits mainly forming the accessory complex of the 19S proteasome, including PSMD12, PSMD11, PSMC3, and PSMC4 (Figure 41 A-C). The '–omics' data show that loss of USP5 in cardiomyocytes results in enhanced ubiquitin stress response and altered composition of mainly the 19S regulatory particle of the proteasome, both affecting proteolysis of proteins involved in catabolic processes.

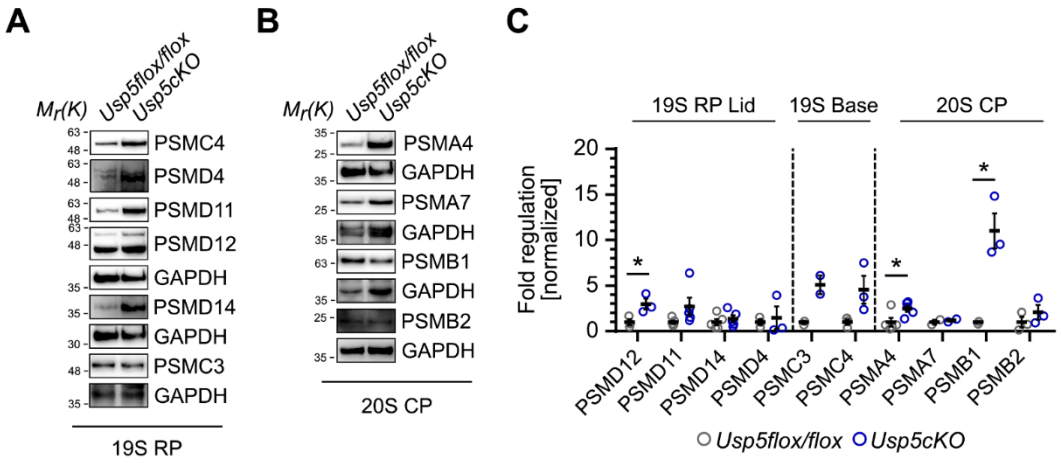

Figure 41 Altered proteasome composition in USP5-deficient cardiomyocytes.

A, B. Immunoblot analysis of indicated subunits of the 19S- and 20S proteasome in cardiomyocytes from *Usp5 flox/flox* and *Usp5cKO* mice 15 days after the last tamoxifen administration. C. Quantification of proteins levels relative to GAPDH protein levels. n = 3 for reach group. Two-tailed unpaired t-test with Welch's correlation or Wilcoxon-rank sum test. * $P < 0.05$.

Cardiac-restricted inactivation of USP5 causes DCM and early lethality

Since mature cardiomyocytes display a very limited self-renewal capacity, I explored potential consequences arising from altered ubiquitin pools, impaired UPS-dependent catabolic processes, altered proteasome composition, and accumulation of mainly ubiquitin-containing protein aggregates for cardiac function after inactivation of *Usp5* in cardiomyocytes. To this end, 100 mg kg^{-1} tamoxifen was administered for seven consecutive days to P56 male *Usp5cKO* and *Usp5 flox/flox* mice. Kaplan-Meier survival analysis showed that all *Usp5cKO* mice but none of the *Usp5 flox/flox* control littermates died within 28 days post-tamoxifen injection, with the first *Usp5cKO* mice dying 23 days after the last tamoxifen administration (Figure 42 A).

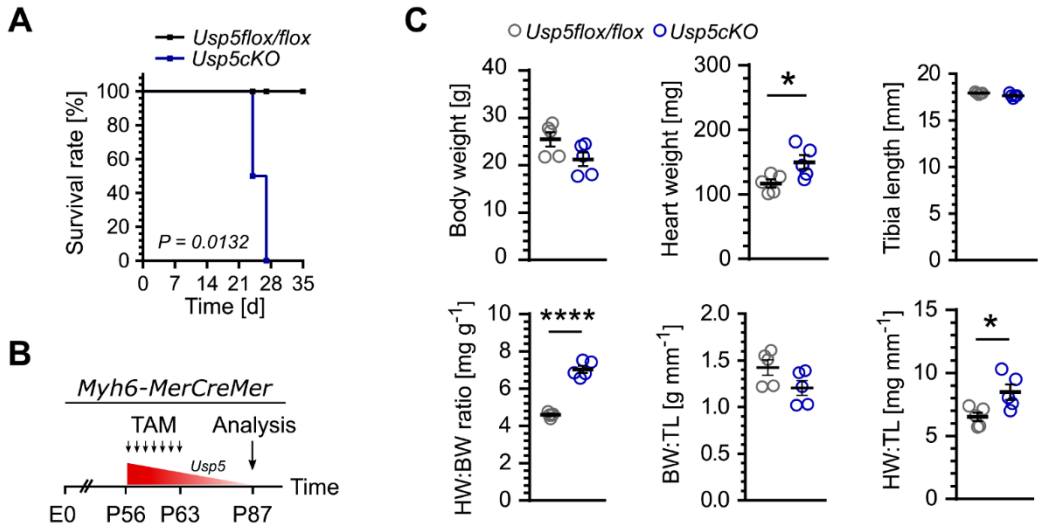

Figure 42 Increased lethality of *Usp5cKO* mice.

A. Kaplan-Meier survival analysis of *USp5cKO* mice in comparison to *Usp5 flox/flox* mice after tamoxifen administration. The *P*-value of the Log-rank (Mental-Cox) test is depicted in the graph. B. Timeline for analysis of cardiomyocyte-specific knockout of *Usp5*. *Usp5 flox/flox* and *Usp5cKO* mice were injected with 100 mg kg^{-1} tamoxifen for seven consecutive days at postnatal day (P) 56. Hearts and cardiomyocytes were isolated and analyzed 24-days after the last tamoxifen injection (= P87). C. Effects of cardiomyocyte-restricted loss of *Usp5* on body weight (BW), heart weight (HW), tibia length (TL), and heart weight to body weight (HW:BW), body weight to tibia length (BW:TL), or heart weight to tibia length ratios (HW:TL). n = 5 for each group. Two-tailed unpaired t-test with Welch's correlation. * $P < 0.05$; **** $P < 0.0001$.

Usp5cKO mice were subjected to a comprehensive phenotype analysis at P87 (25 days post-tamoxifen injection), which represents the median of the survival time (Figure 42 B). Long-term inactivation of *Usp5* in cardiomyocytes resulted in prominent weight loss, massive gain in heart weight, and consequently elevated heart weight to body weight (HW:BW) and heart weight to tibia length (HW:TL) ratios (Figure 42 C). Corresponding tibia lengths did not differ between the two groups, which indicate that changes in body weight and heart weight are not caused by growth problems of *Usp5cKO* mice (Figure 42 C).

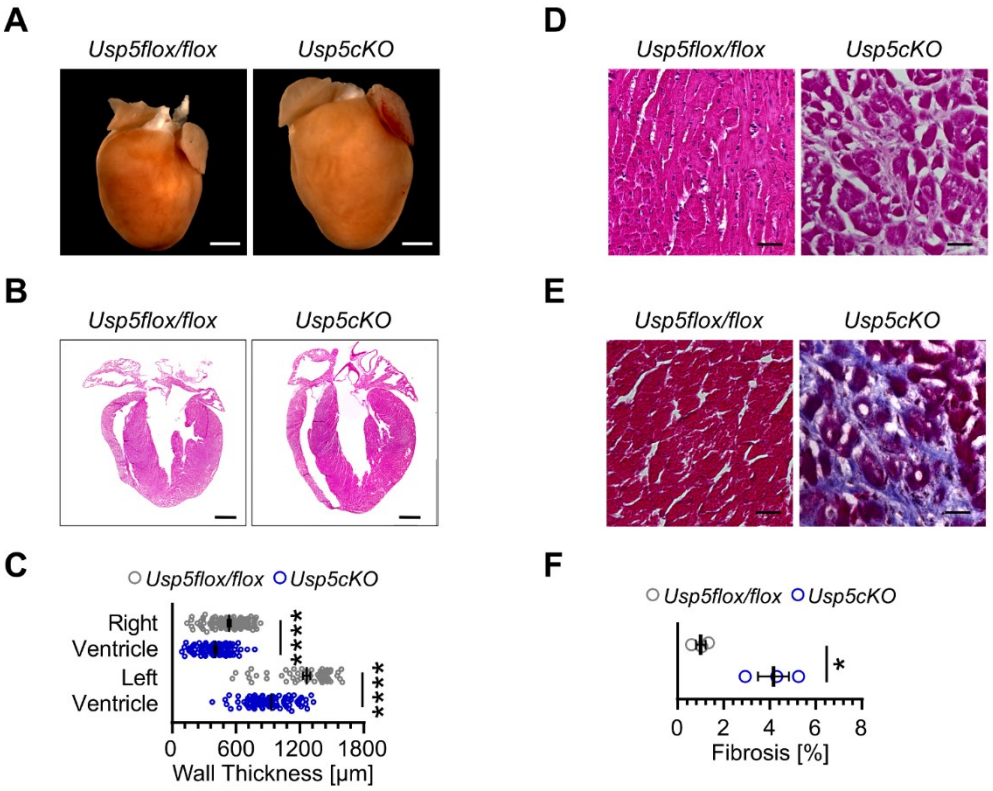

Figure 43 Loss of USP5 causes DCM.

A, B. Images of dissected hearts (A) and H&E stained cross sections (B) from *Usp5 flox/flox* and *Usp5cKO* mice 24 days after the last tamoxifen administration. n = 4 for each group. Scale bars, 1000 µm. C. Analysis of myocardial wall thickness between the two groups. n = 4 for each group. Two-tailed unpaired Wilcoxon-rank sum test. **** $P < 0.0001$. D, E. Images showing H&E stained (D) and Masson's trichrome stained (E) cross sections of the left ventricle from *Usp5 flox/flox* and *Usp5cKO* mice 24 days after the last tamoxifen administration. n = 4 for each group. Scale bars, 50 µm. Analysis of fibrotic collagen deposition in hearts from *Usp5 flox/flox* and *Usp5cKO* mice 24 days after the last tamoxifen administration. n = 4 for each group. Two-tailed unpaired t-test with Welch's correlation. * $P < 0.05$.

Consistent with the observed increase in heart weight, dissected hearts of *Usp5cKO* mice were larger in size. Macroscopic examination revealed immense enlargement of *Usp5cKO* ventricles and dilated atria with increased incidence of thrombus formation. H&E stained histological cross sections confirmed pathomorphological changes of *Usp5cKO* hearts in comparison to dissected hearts from *Usp5 flox/flox* control littermates (Figure 43 A, B), including substantial reduction of myocardial wall thickness in the left and right ventricle (Figure 43 C). H&E stained histological cross sections of *Usp5cKO* hearts uncovered changes in cardiomyocyte morphology and integrity (Figure 43 D), in addition to interstitial collagen deposition (Figure 43 E, F). Analysis by electron microscopy confirmed pathomorphological alterations in the majority of *Usp5cKO* cardiomyocytes, including disruption of sarcomere integrity (Figure 44 A, B), changes in the size and shape of nuclei and nucleoli (Figure 44 C), in addition to changes in the structure of intercalated discs (Figure 44 D).

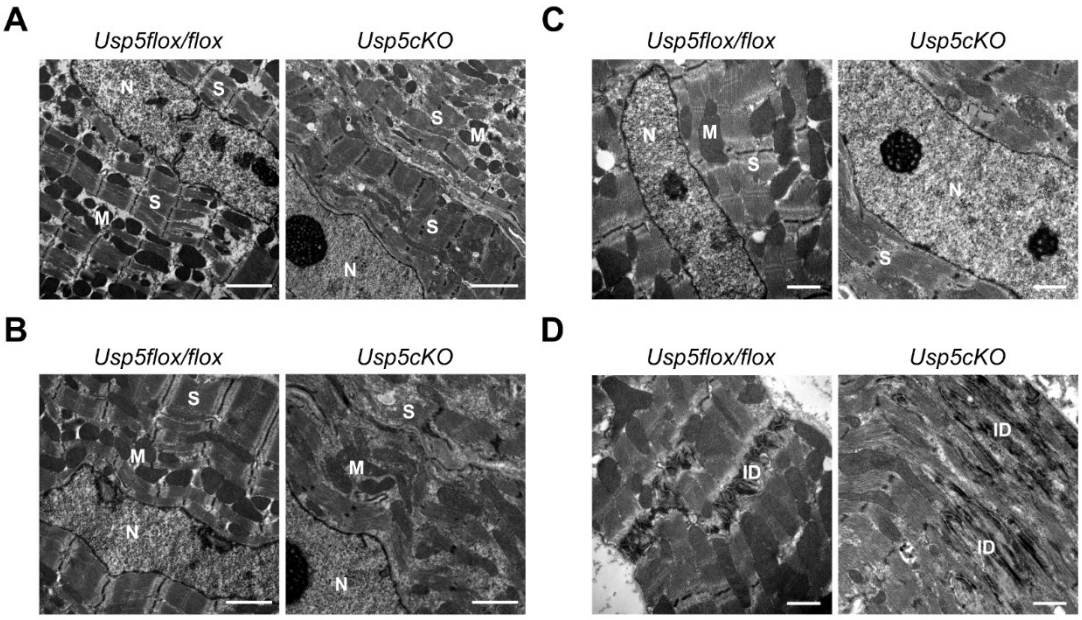

Figure 44 Pathomorphological alterations in the left ventricle of *Usp5cKO* mice.

A-D. Electron microscopy images showing sarcomeres (A, B), nucleus (C), and intercalated discs (D) in the left ventricle of *Usp5 flox/flox* and *Usp5cKO* mice 24 days after the last tamoxifen administration. n = 3 for each group. Scale bars, 2500 nm (A, B) and 1000 nm (C, D). ID, intercalated disks; M, mitochondria; N, nucleus; S, sarcomeres.

All listed pathomorphological changes are indicative of severely compromised cell-to-cell connection and cell-to-cell communication. Moreover, these findings are symptomatic for cardiac remodeling and progression of DCM, potentially contributing to the observed lethal phenotype. Since *Usp5cKO* mice did not show any classical symptoms of heart failure such as ascites or pulmonary edema, one might speculate that the sudden death of *Usp5cKO* mice within a narrow time window of 3-4 days post-tamoxifen inducible inactivation of *Usp5* causes acute contractile dysfunction or electric conductive defects due to severe disruption of intercalated discs.

Cardiac-restricted inactivation of USP5 causes accumulation of ubiquitin-enriched aggresomes

In addition to disease-related pathomorphological changes of cardiomyocytes from *Usp5cKO* mice, electron microscopy further identified electron-dense aggregates in regions with disrupted sarcomeres or otherwise damaged organelles (Figure 45 A, B).

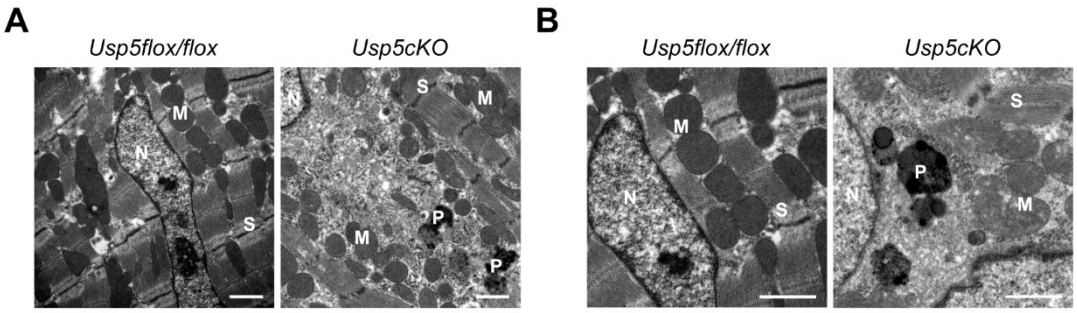

Figure 45 Perinuclear protein deposits in *Usp5cKO* mice.

A, B. Electron microscopy showing perinuclear protein-dense aggregates surrounded by cell debris in the left ventricle of *Usp5 flox/flox* and *Usp5cKO* mice 24-days after the last tamoxifen administration. n = 3 for each group. Scale bars, 1000 nm (A) and 2500 nm (B). M, mitochondria; N, nucleus; P, protein-dense aggregates; S, sarcomeres.

Since USP5 was actively recruited to aggregated proteins after MG132-induced inactivation of proteasome activity in cardiomyocytes (Figure 24 A), the questions arose whether such electron-dense aggregates may represent misfolded proteins that accumulated as a result of strongly impaired proteostasis in *Usp5cKO* cardiomyocytes.

Immunofluorescence staining using the PROTEOSTAT® aggregation assay in combination with a ubiquitin antibody corroborated enhanced load of mainly perinuclear aggresomes containing ubiquitin-enriched aggresomes in *Usp5cKO* cardiomyocytes (Figure 46 A-C), while the majority of aggresomes detected in cardiomyocytes from *Usp5 flox/flox* control littermates showed no co-localization with ubiquitin (Figure 46 A, C). Quantitative assessment of aggresome formation uncovered increase in the number of cardiomyocytes containing perinuclear aggresome in *Usp5cKO* mice compared to *Usp5 flox/flox* control littermates (Figure 46 D). Moreover, *Usp5cKO* cardiomyocytes contained significantly more aggresomes per view field (Figure 46 E). To summarize, immunohistological analysis of aggresome formation substantiates the hypothesis that accumulation of ubiquitin-enriched protein aggregates is linked to disturbed UPS-dependent proteolysis and dysregulated ubiquitin pools in *Usp5cKO* cardiomyocytes.

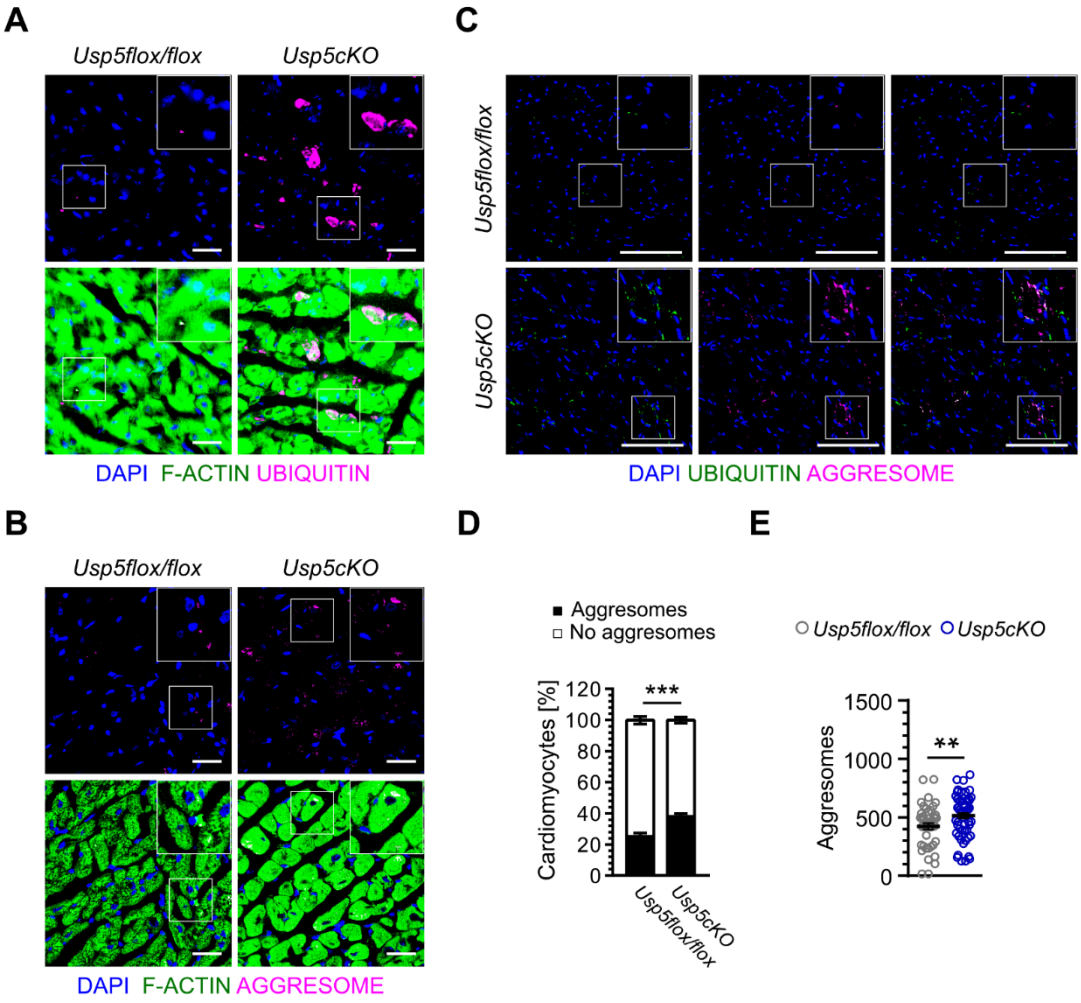

Figure 46 Accumulation of perinuclear ubiquitin-enriched aggresomes in hearts of *UspcKO* mice.

A. Immunofluorescence staining of F-actin (green), ubiquitin (magenta), and nuclei (DAPI, blue) in cross-sectioned hearts of *Usp5 flox/flox* and *Usp5cKO* mice 24-days after the last tamoxifen administration. n = 4 for each group. Scale bars, 50 µm. B. Immunofluorescence staining of F-actin (green), aggresomes (magenta), and nuclei (DAPI, blue) in cross-sectioned hearts of *Usp5 flox/flox* and *Usp5cKO* mice 24-days after the last tamoxifen administration. n = 4 for each group. Scale bars, 50 µm. C. Immunofluorescence staining of ubiquitin (green), aggresomes (magenta), and nuclei (DAPI, blue) in cross-sectioned hearts of *Usp5 flox/flox* and *Usp5cKO* mice 24-days after the last tamoxifen administration. n = 4 for each group. Scale bars, 50 µm. D, E. Quantification of cardiomyocytes containing aggresomes (D) and number of aggresomes counted per view field (E) in cross-sectioned hearts of *Usp5 flox/flox* and *Usp5cKO* mice. n = 4 for each group. Two-tailed unpaired Wilcoxon-rank sum test. ** $P < 0.0021$, *** $P < 0.0002$.

Impaired clearance of protein aggregates by selective autophagy contributes to persistent protein aggregation in USP5-deficient cardiomyocytes

So far, my data demonstrated that cardiac-specific loss of USP5 induced DCM due to altered ubiquitin pools, block of 20S proteasome activity, accompanied by altered proteasome composition, and formation of ubiquitin-enriched aggresomes. In contrast, inactivation of *Usp5* in MEFs caused formation of ubiquitin-enriched aggresomes despite the absence of major effects on ubiquitin pools or 20S proteasome activity, indicating that USP5 possesses a dual role for proteasomal and (selective) autophagy-mediated PQC. To test whether inactivation of *Usp5* in cardiomyocytes causes defects in selective clearance of protein aggregates, which may account for persistent aggresome formation and continuous impairment of cardiac homeostasis, expression of key components of selective autophagy were examined by immunoblot analysis (Figure 47 A-D). Immunoblot analysis uncovered elevated levels of Lys63-linkage specific ubiquitin in *Usp5cKO* cardiomyocytes (Figure 34 C, D), which suggests potential defects in the autophagic machinery in addition to impaired UPS-dependent proteolysis (Figure 47 C, D). In addition, immunoblot analysis of the early selective autophagy markers p62 and LC3 revealed elevated p62 levels in *Usp5cKO* cardiomyocytes, while the LC3-II/LC3-I ratio remained unchanged when compared to cardiomyocytes from *Usp5 flox/flox* control littermates (Figure 47 A-C). These data suggest arrest of autophagic flux in *Usp5cKO* cardiomyocytes. In addition, immunoblot analysis of late selective autophagy markers disclosed compromised autophagolysosome formation in *Usp5cKO* cardiomyocytes, since cortactin (CTTN) remained mainly in its acetylated state regardless of enhanced HDAC6 protein levels (Figure 47 D-F).

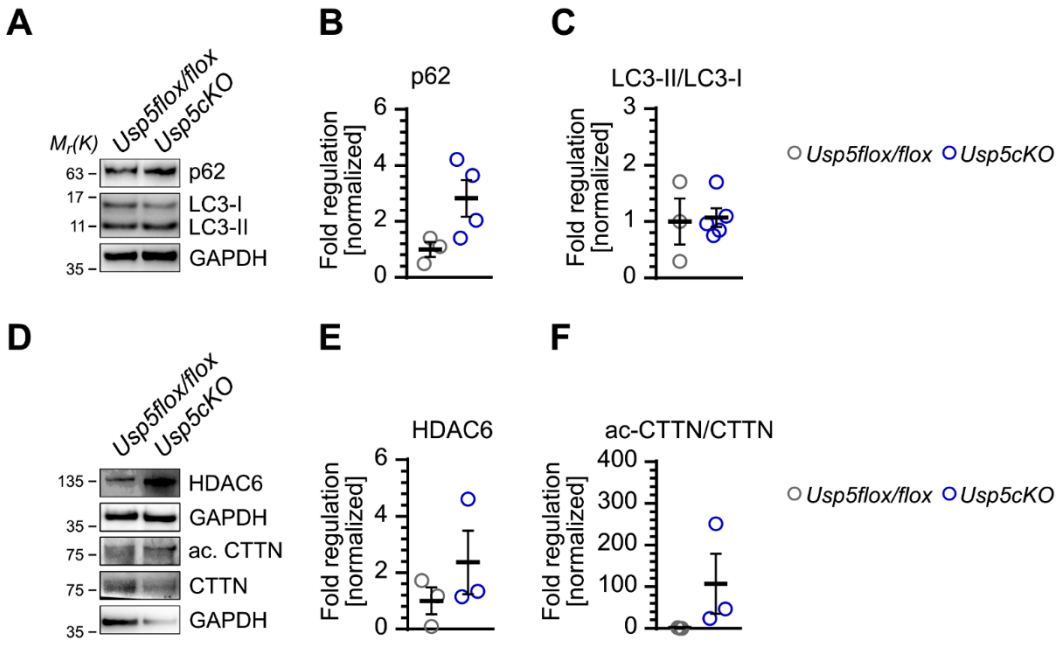

Figure 47 Impaired clearance of aggresomes by selective autophagy in USP5-deficient cardiomyocytes.

A. Immunoblot analysis of the early autophagy markers p62 and LC3 in isolated cardiomyocytes from *Usp5 flox/flox* and *Usp5cKO* mice 15 days after the last tamoxifen administration. B, C. Quantification of protein levels relative to GAPDH expression. n = 3 for *Usp5 flox/flox*, n = 4 for *Usp5cKO*. D. Immunoblot analysis of the late autophagy markers HDAC6 and CTTN in isolated cardiomyocytes from *Usp5 flox/flox* and *Usp5cKO* mice 15 days after the last tamoxifen administration. E, F. Quantification of protein levels relative to GAPDH expression. n = 3 for *Usp5flox/flox*, n = 4 for *Usp5cKO*.

Immunohistochemistry confirmed higher abundance of p62 and HDAC6 in *Usp5cKO* cardiomyocytes (Figure 48 A, B). However, aggresomes completely co-localized with p62 and HDAC6 (Figure 48 A, B), which indicated that recruitment and binding of p62 and HDAC6 to ubiquitin-enriched aggresomes during early steps of (selective) autophagy were not impaired. These results confirmed that defects in the selective clearance of ubiquitin-enriched protein aggregates cause persistent aggresome formation, which augments cytotoxic effects arising from disturbed UPS function.

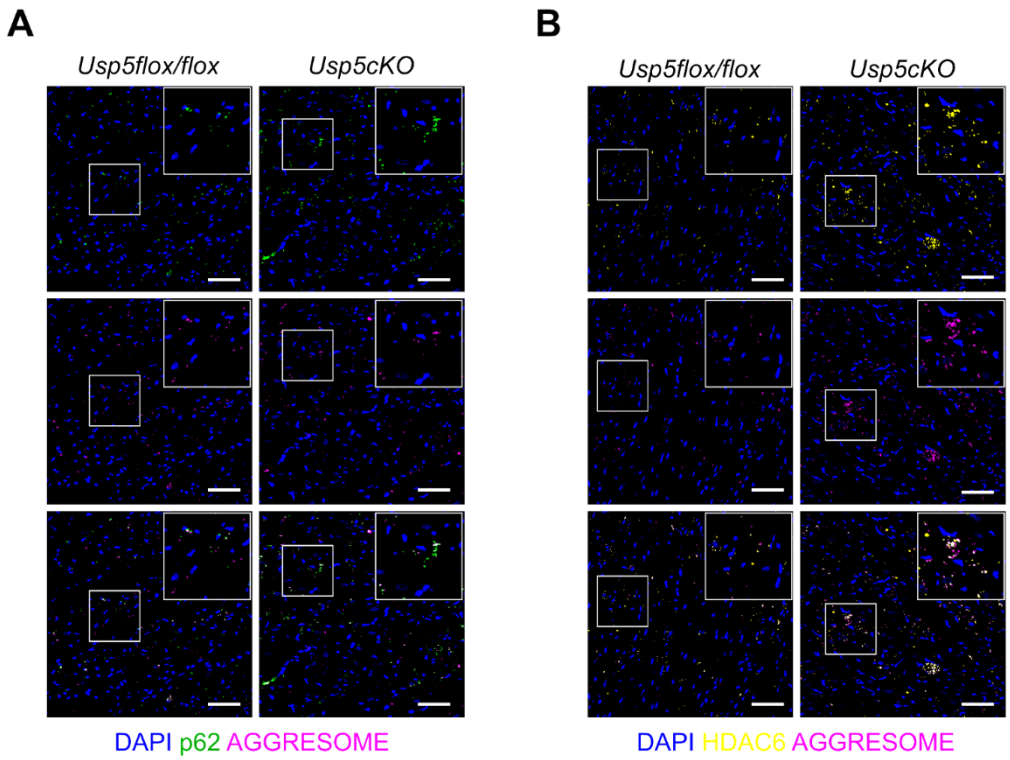

Figure 48 Selective autophagy markers co-localize with aggresomes in USP5-deficient cardiomyocytes.

A. Immunofluorescence staining of p62 (green), aggresomes (magenta) and nuclei (DAPI, blue) in cross-sectioned hearts of *Usp5 flox/flox* and *Usp5cKO* mice 24 days after the last tamoxifen administration. n = 4 for each group. Scale bars, 50 µm. B. Immunofluorescence staining of HDAC6 (yellow), aggresomes (magenta) and nuclei (DAPI, blue) in cross-sectioned hearts of *Usp5 flox/flox* and *Usp5cKO* mice 24 days after the last tamoxifen administration. n = 4 for each group. Scale bars, 50 µm.

As a consequence, elevated cytotoxic stress levels resulted in apoptotic cell death of *Usp5cKO* cardiomyocytes, as indicated by Caspase-3 activation and subsequent induction of PARP cleavage (Figure 49 A). Importantly, atypical protein aggregation caused by MG132-mediated impairment of UPS function was not sufficient to induce a similar degree of apoptotic cell death in cardiomyocytes from *Usp5 flox/flox* control littermates. Most likely, impairment of both branches of PQC in response to inactivation of *Usp5* is required to induce apoptosis of cardiomyocytes.

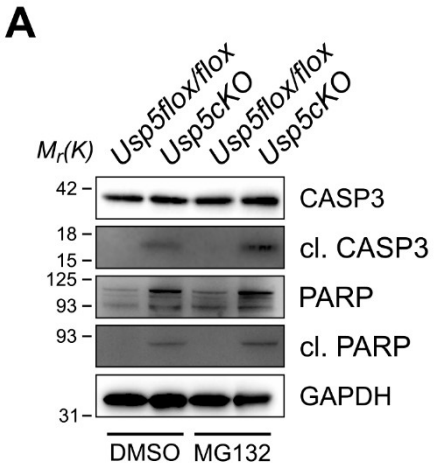

Figure 49 Enhanced apoptotic cell death of USP5-deficient cardiomyocytes.

A. Immunoblot analysis of Caspase-3, cleaved Caspase-3, PARP, and cleaved PARP in isolated cardiomyocytes of *Usp5 flox/flox* and *Usp5cKO* mice 15 days post-tamoxifen administration. n = 4 for each group.

USP5 is instrumental for cardiac development and survival

Since cardiomyocytes isolated at earlier developmental time points expressed both *Usp5* exon 15 isoforms (Figure 21 A), the next step was to investigate possible consequences arising from inactivation of *Usp5* both in embryonic and juvenile cardiomyocytes. To achieve inactivation of *Usp5* at embryonic stage, homozygous *Usp5 flox/flox* mice were crossbred with transgenic mice having the *cre*-recombinase gene driven by *Xenopus laevis light chain 2 (XMLC2)* promoter (Figure 12 A; Figure 50 A). Inactivation of *Usp5* in cardiac crescent cells at E7.5 was not compatible with life as no *XMLC2//Usp5 flox/flox* mice were born. Isolation of embryos at different time points uncovered that homozygous *XMLC2//Usp5 flox/flox* embryos die around E11.5 (Figure 50 A). Homozygous *XMLC2//Usp5 flox/flox* embryos were smaller in body size (Figure 50 B) and showed arrest of cardiac development (Figure 50 C), including reduced trabeculation and compaction (Figure 50 C-E), in addition to enlarged atria and substantially thinner left ventricular walls (Figure 50 D, F).

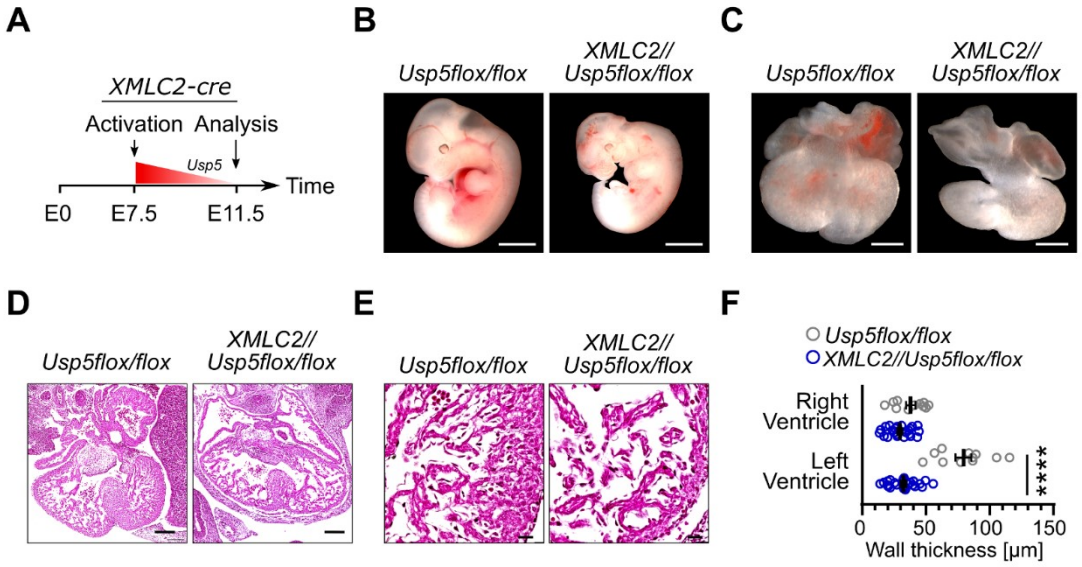

Figure 50 USP5 is essential for cardiac development and survival.

A. Timeline for analysis of cardiac-restricted inactivation of *Usp5* at embryonic stage. *Usp5 flox/flox* mice were crossbred with transgenic mice harboring the *XMLC2-cre* recombinase to drive *cre*-mediated recombination in cardiac crescent cells at E7.5. B, C. Images of *Usp5 flox/flox* and *XMLC2//Usp5 flox/flox* embryos (B) and hearts at E11.5 n = 4 for each group. Scale bars, 1000 µm (B) and 200 µm (C). D, E. H&E stained cross sections of *Usp5 flox/flox* and *XMLC2//Usp5 flox/flox* embryos as E11.5. n = 4 for each group. Scale bars, 50 mm (D) and 25 µm (E). F. Analysis of myocardial wall thickness between the two genotypes. n = 4 for each group. Two-tailed unpaired t-test with Welch's correlation. **** $P < 0.0001$.

In addition, inactivation of *Usp5* in cardiac- and skeletal muscle at juvenile stage was achieved by crossbreeding homozygous *Usp5 flox/flox* mice with transgenic mice having the *cre*-recombinase gene driven by muscle creatine kinase promoter (*MCK)* (Figure 12 A; Figure 51 A). In accordance with previous results, inactivation of *Usp5* by *MCK-cre* around E13.5 (Figure 51 A) resulted in 100 % lethality before P30 (Figure 51 B). Similar to *Usp5cKO* mice, homozygous *MCK//Usp5 flox/flox* died within a short time window of six days, starting at P21 (Figure 51 B). Notably, homozygous *MCK//Usp5 flox/flox* developed normally within the first three weeks after birth without showing any signs of incipient deterioration of their health status in comparison to *Usp5 flox/flox* littermate controls (Figure 51 C).

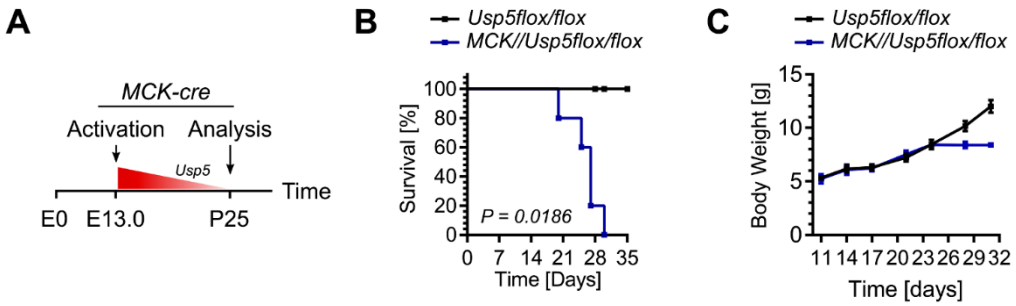

Figure 51 Cardiomyocyte-restricted deletion of USP5 at juvenile stage causes sudden death.

A. Timeline for analysis of cardiomyocyte-restricted inactivation of *Usp5* at juvenile stage. *Usp5flox/flox* mice were crossbred with a transgenic mouse strain by which a muscle creatine kinase promoter drives *cre-recombinase* expression *(MCK-cre)* in striated muscles. *Cre*-recombinase becomes activated around E13.5. Mice were analyzed at postnatal day P25. B. Kaplan-Meier survival curves of *Usp5 flox/flox* (n = 29) and *MCK//Usp5 flox/flox* (n = 13) mice. *P*-value is based on the Log-rank (Mental-Cox) test. C. Body weight curves of *Usp5 flox/flox* and *MCK//Usp5flox/flox* mice.

Usp5 flox/flox and *MCK//Usp5 flox/flox* mice were subjected to a comprehensive phenotype analysis at P25, which represents the median of survival (Figure 51 A, B). Homozygous *MCK//Usp5 flox/flox* mice showed dramatic weight loss accompanied by a decline in heart weight, which accounted for the elevated heart weight to body weight ratio (HW:BW). The observed effects were not caused by growth defects, since the corresponding tibia lengths did not differ between the two genotypes (Figure 52 A).

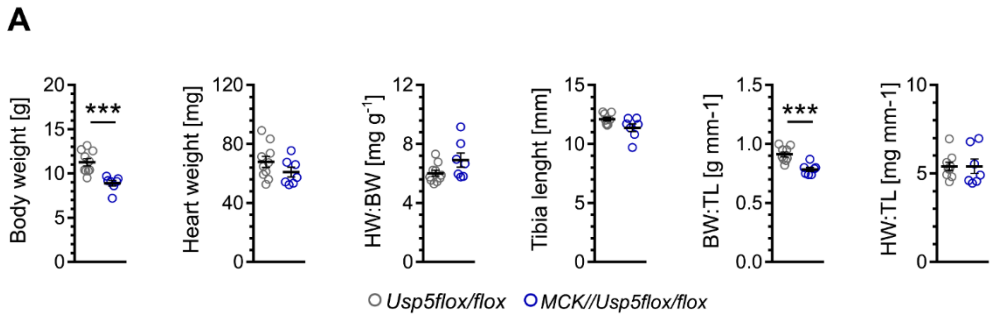

Figure 52 Effects of striated muscle-restricted knockout of USP5 on body weight, heart weight, and tibia length.

A. Effects of striated-muscle restricted inactivation of *Usp5* on body weight (BW), heart weight (HW), tibia length (TL), and ratios of heart weight to body weight (HW:BW), body weight to tibia length (BW:TL), and heart weight to tibia length (HW:TL). n = 10 for *Usp5 flox/flox*, n = 7 for *MCK//Usp5 flox/flox*. Unpaired t test with Welch's correction. *** $P < 0.0002$.

Similar to inactivation of *Usp5* in cardiac crescent cells and mature cardiomyocytes, inactivation of *Usp5* at juvenile stage resulted in progression of DCM as indicated by increased heart size despite reduction in heart weight (Figure 53 A). Histological analysis of H&E stained myocardial sections revealed massively enlarged atria, dilation of both ventricles, corresponding to tremendously thinner ventricular walls (Figure 53 B, C), severely impaired integrity of cardiomyocytes, and disruptive alterations in the formation of proper cell-to-cell contacts (Figure 53 D). In general, inactivation of *Usp5* during cardiac development caused a stronger DCM phenotype as observed in adult hearts, although the principle pathomorphological alterations seem to be identical. The data clearly illustrate that USP5 is instrumental for cardiac development and survival, as loss of USP5 correlates with rapid progression of DCM and a poor survival prognosis.

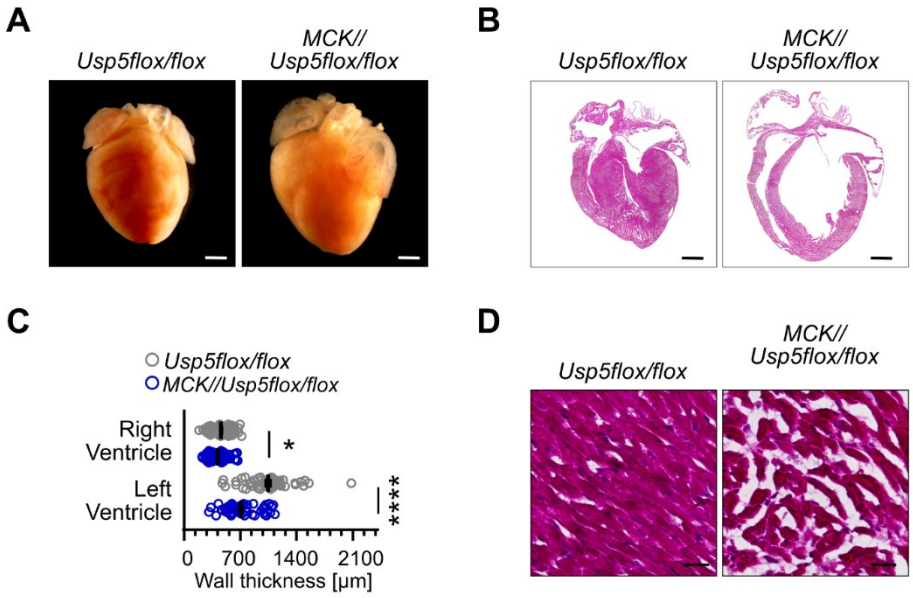

Figure 53 Cardiomyocyte-restricted deletion of USP5 at juvenile stage causes DCM.

A, B, D. Images of hearts (A) and H&E stained cross sections (B, D) of *Usp5 flox/flox* and *MCK//Usp5 flox/flox* mice at postnatal day (P) 25. n = 4 for each group. Scale bars, 1000 µm (A, B) and 50 µm (D). C. Analysis of myocardial wall thickness in *Usp5flox/flox* and *MCK//Usp5 flox/flox* mice at P25. n = 4 for each group. Two-tailed unpaired t-test with Welch's correlation or two-tailed unpaired t-test with Wilcoxon-rank sum test, respectively. * $P < 0.05$; **** $P < 0.0001$.

Cardiomyocytes from human DCM patients with late end-stage DCM display enhanced load of ubiquitin-containing aggresomes lacking USP5

To illustrate the importance of the present *in-vivo* findings, I wondered whether development of DCM in human individuals is linked to impairment of USP5-dependent processes. To directly address this aspect, left ventricular biopsies of explanted hearts from a cohort of randomly selected human patients with late-end stage DCM undergoing heart transplantation were analyzed. Left ventricular biopsies from non-failing individuals with preserved cardiac function and without any signs of myocardial damage or heart failure served as an appropriate control cohort. Main parameters, such as age and gender-to-female ratio, were nearly identical between the two groups, qualifying inclusion of all patients in the current study (Figure 54 A). Ultrastructural analysis by electron microscopy uncovered pathomorphological alterations in cardiomyocytes from end-stage DCM patients, including abnormally shaped nuclei and distortion of mitochondria and myofibrils (Figure 54 B). Most importantly, cardiomyocytes contained clusters of protein dense aggregates and phospholipids, which were mostly located in the proximity of nuclei. In addition, cardiomyocytes of DCM patients were further characterized by a roundish shape and increased volume of nuclei (Figure 54 C). In contrast, cardiomyocytes in the non-failing control cohort showed well-preserved sarcomere structures without deposition of phospholipids or protein aggregates (Figure 54 B). PROTEOSTAT® aggregation assay confirmed aberrant accumulation of misfolded proteins and formation of mainly perinuclear aggresomes in cardiomyocytes from late end-stage DCM patients, although a similar number of cardiomyocytes with perinuclear aggresomes were detected in non-failing individuals (Figure 54 C, D). Nevertheless, cardiomyocytes of late end-stage DCM patients contained more protein aggregates that were also larger in size (Figure 54 E, F).

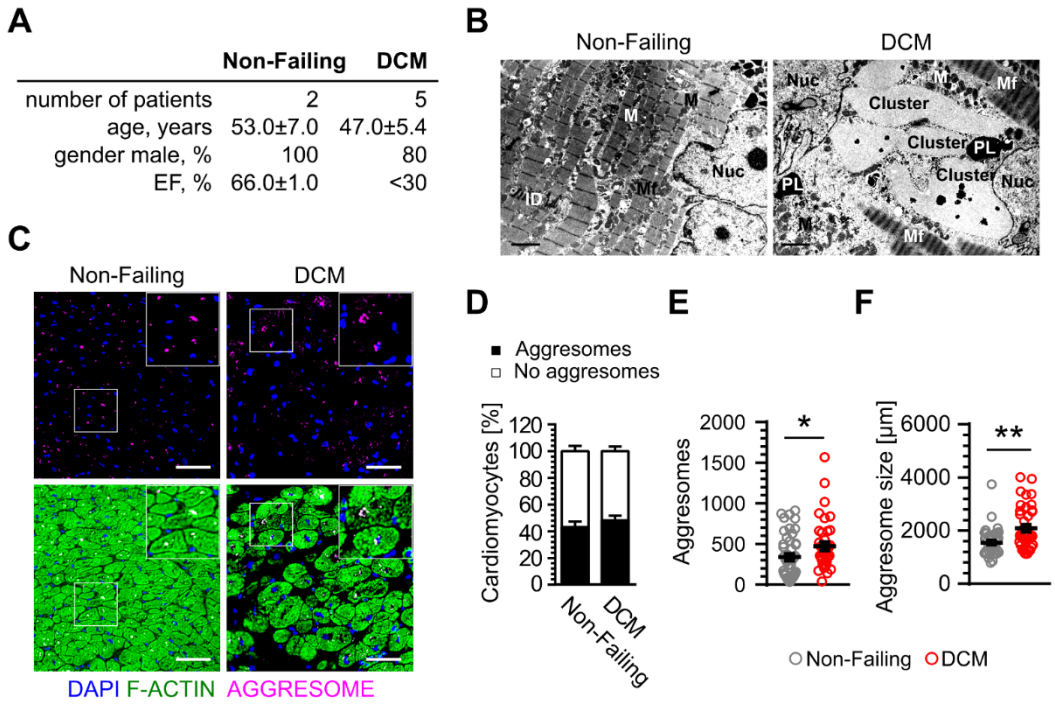

Figure 54 Randomly selected patients with late-end stage DCM show atypical accumulation of perinuclear protein aggregates.

A. Clinical characteristics of non-failing and late end-stage DCM patients analyzed in the study. B. Electron microscopy of hearts from non-failing (n = 2) and DCM individuals (n = 5). Perinuclear clusters in DCM individuals reflect protein aggregates and lipid droplets. ID, intercalated disks; M, mitochondria; Mf, myofibrils; Nuc, nucleus; PL, phospholipid droplets. C. Immunofluorescence staining of F-actin (green), aggresomes (magenta), and nuclei (DAPI, blue) in cross-sectioned hearts from non-failing (n = 2) and DCM individuals (n = 5). Scale bars, 50 µm. D. Quantitation of cardiomyocytes containing aggresomes in cross sections hearts from non-failing (n = 2) and DCM individuals (n = 5). E, F. Quantitation of the number of aggresomes counted per view field and average size of aggresomes in cross-sectioned hearts from non-failing (n = 2) and DCM individuals (n = 5). Two-tailed unpaired t-test with Wilcoxon-rank sum test. * $P < 0.05$, ** $P < 0.0021$.

Importantly, additional immunofluorescence staining revealed atypical deposition of large ubiquitin-containing debris in cardiomyocytes from late end-stage DCM patients, which co-localized with perinuclear aggresomes (Figure 55 A, B). Taken together, these data indicate that progression of DCM is linked to atypical accumulation of ubiquitin-conjugated protein aggregates in cardiomyocytes [135, 136].

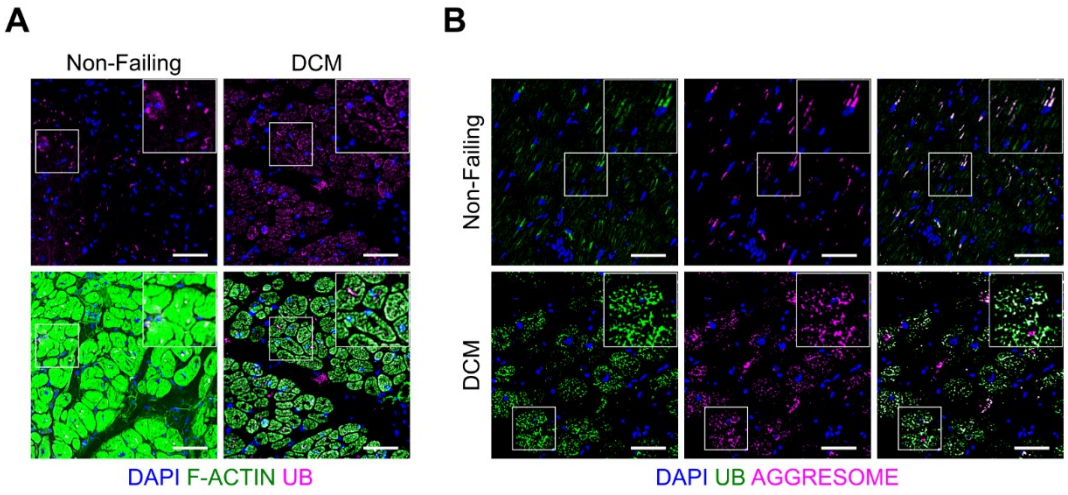

Figure 55 Accumulation of ubiquitin-containing aggresomes in cardiomyocytes from patients with late-end stage DCM.

A. Immunofluorescence staining of F-actin (green), ubiquitin (magenta), and nuclei (DAPI, blue) in cross-sectioned hearts from non-failing (n = 2) and DCM individuals (n = 5). Scale bars, 50 µm. B. Immunofluorescence staining of ubiquitin (green), aggresomes (magenta), and nuclei (DAPI, blue) in cross sectioned hearts from non-failing (n = 2) and DCM individuals (n = 5). Scale bars, 50 µm.

Since pathomorphological changes in cardiomyocytes from late end-stage DCM patients were similar to those observed in the present *in vivo* mouse model, immunoblot analysis in combination with immunohistochemistry was utilized to study the expression of USP5. Remarkably, USP5 protein levels were strongly reduced in myocardial cell lysates from late end-stage DCM patients in comparison to non-failing control patients (Figure 56 A, B). Consistently, immunofluorescence analysis revealed that cardiomyocytes from late end-stage DCM patients lack USP5 while cardiomyocytes from non-failing control patients showed high abundance in USP5 staining intensity (Figure 56 C). In line with these observations, ubiquitin-enriched aggresomes in cardiomyocytes from late end-stage DCM patients showed almost complete lack of USP5 labeling (Figure 56 D, E), while ubiquitin-enriched aggresomes in cardiomyocytes from non-failing control patients were mostly positive for USP5 (Figure 56 D, E).

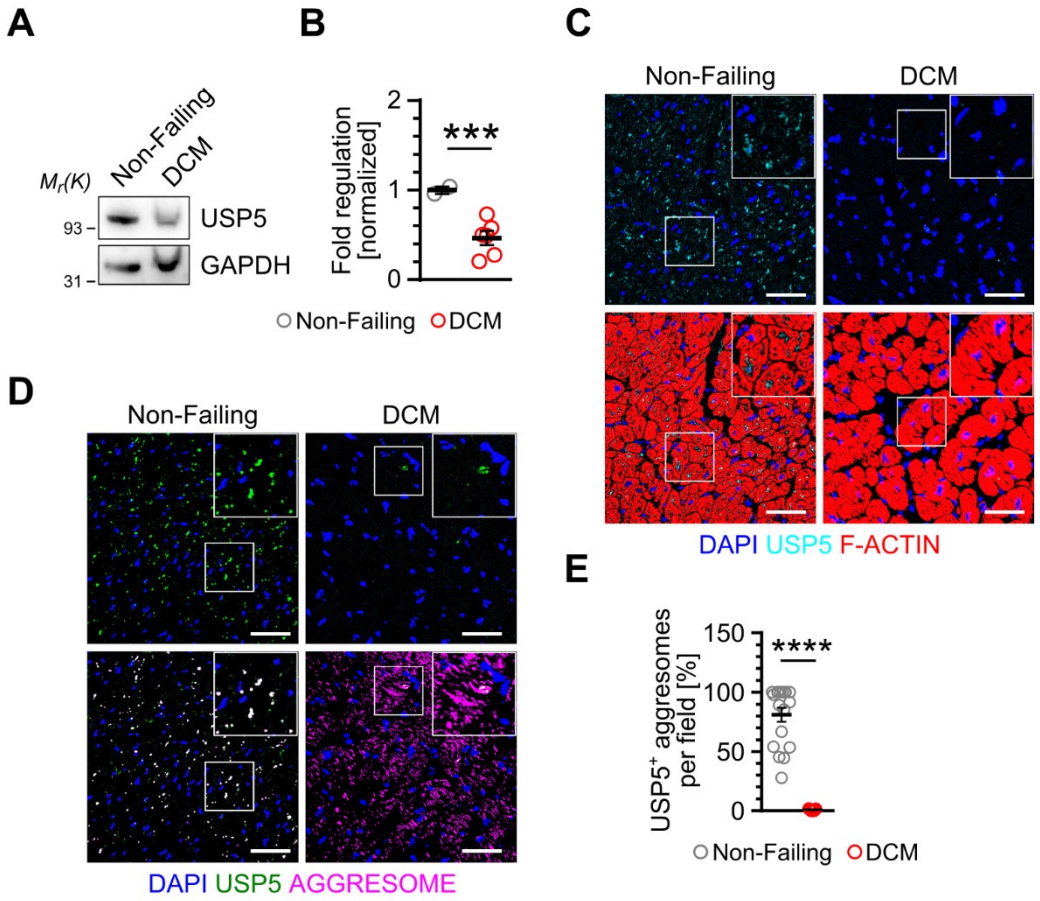

Figure 56 Lack of USP5 in cardiomyocytes from patients with late-end stage DCM.

A. Immunoblot analysis for USP5 in myocardial lysates from non-failing (n = 2) and late end-stage DCM individuals (n = 5). B. Quantification relative to GAPDH levels. Unpaired t-test with Welch's correlation. *** $P < 0.0002$. C. Immunofluorescence staining of USP5 (cyan), F-actin (red), and nuclei (DAPI, blue) in cross sectioned hearts from non-failing (n = 2) and late end-stage DCM individuals (n = 5). Scale bars, 50 µm. D. Immunofluorescence staining of USP5 (green), aggresomes (magenta), and nuclei (DAPI, blue) in cross sectioned hearts from non-failing (n = 2) and late end-stage DCM individuals (n = 5). Scale bars, 50 µm. E. Quantification of USP5-positive aggresomes in cardiomyocytes from non-failing (n = 2) and late end-stage DCM individuals (n = 5). Two-tailed unpaired t-test with Wilcoxon-rank sum test. **** $P < 0.0001$.

In summary, the data demonstrate a striking similarity between pathomorphological alterations in the heart from human late end-stage DCM patients and the DCM phenotype observed in the cardiomyocyte-restricted USP5 KO mouse model.

Overexpression of hsUSP5 in cardiomyocytes is compatible with normal cardiac proteostasis

The importance of USP5 for UPS-dependent catabolic processes and selective autophagy of protein aggregates in the murine heart and the downregulation of USP5 in human end-stage cardiomyocytes raised the possibility that the availability of USP5 is a rate-limiting step to prevent or resolve protein aggregates caused by impaired proteostasis. To get insights into this topic and to examine whether augmented expression of USP5 counteracts or prevents disease-related protein aggregation, the effects of different USP5 splice variants on ubiquitin turnover and PQC processes were analyzed first. Transfection of HEK293 cells with plasmids either encoding the human (hs) USP5 exon 15 long or short isoform in combination with immunoblot analysis to monitor ubiquitin levels demonstrated that the hsUSP5 exon 15 long isoform has more pronounced effects in reducing ubiquitin levels (Figure 57 A, B). I observed that hsUSP5 exon 15 long decreased the levels of polyubiquitin chains and polyubiquitinated proteins, while monoubiquitin levels, essential for de-novo ubiquitin conjugation and protein clearance, were elevated (Figure 57 B, C).

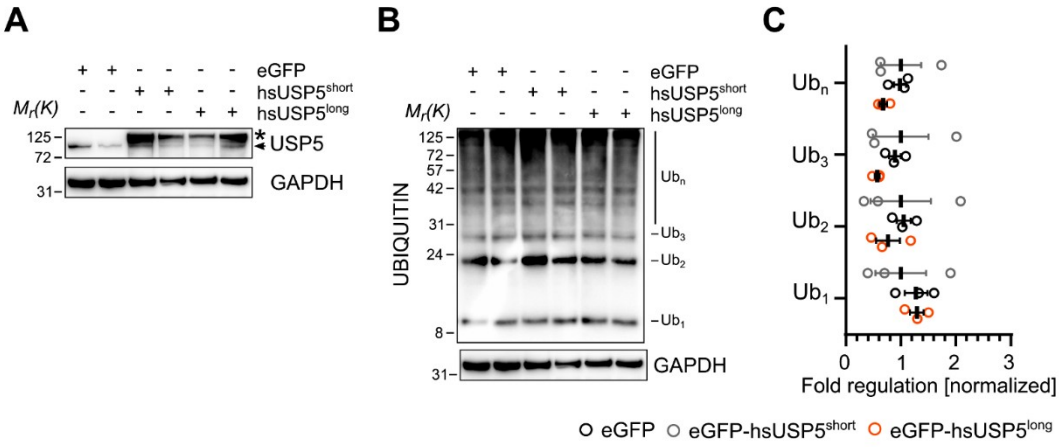

Figure 57 hsUSP5 exon 15 isoform specific differences in the ubiquitin pool.

A, B. Immunoblot analysis of hsUSP5 and ubiquitin levels in HEK293 cells transiently transfected with eGFP and GFP-tagged hsUSP5^{long} or hsUSP5^{short}, respectively. n = 3 for each group. Arrow head, endogenous USP5. *, eGFP-tagged hsUSP5. C. Quantification of ubiquitin chains relative to GAPDH levels. n = 3 for each group.

These *in-vitro* data suggest that the USP5 exon 15 long isoform has a more prominent role in maintaining ubiquitin homeostasis, which is particularly important in postmitotic cells, such as mature cardiomyocytes. To investigate whether moderate overexpression of hsUSP5 in cardiomyocytes interferes with cellular functions, another transgenic mouse strain was generated that harbors the FLAG-HA-tagged exon 15 long isoform of hsUSP5 in the Rosa26 genomic locus. Crossbreeding with transgenic mice expressing a *cre*-recombinase under the *XMLC2*-promoter resulted in conditional activation of hsUSP5 due to removal of the floxed stop cassette (Figure 58 A, B). To avoid side effects, which may arise from excessive overexpression, we kept transgenic mice constantly heterozygous. R26-FLAG-HA-hsUSP5long (hereafter called *hsUSP5 CO/+)* robustly expressed FLAG-HA-hsUSP5long during cardiac development and in mature cardiomyocytes (Figure 58 A, B). *hsUSP5 CO/+* mice were healthy and fertile, exert normal cardiac function, and did not show any significant changes in body weight, heart weight, or ratios of body weight to heart weight (BW:HW) or heart weight to tibia length (HW:TL) (Figure 58 C).

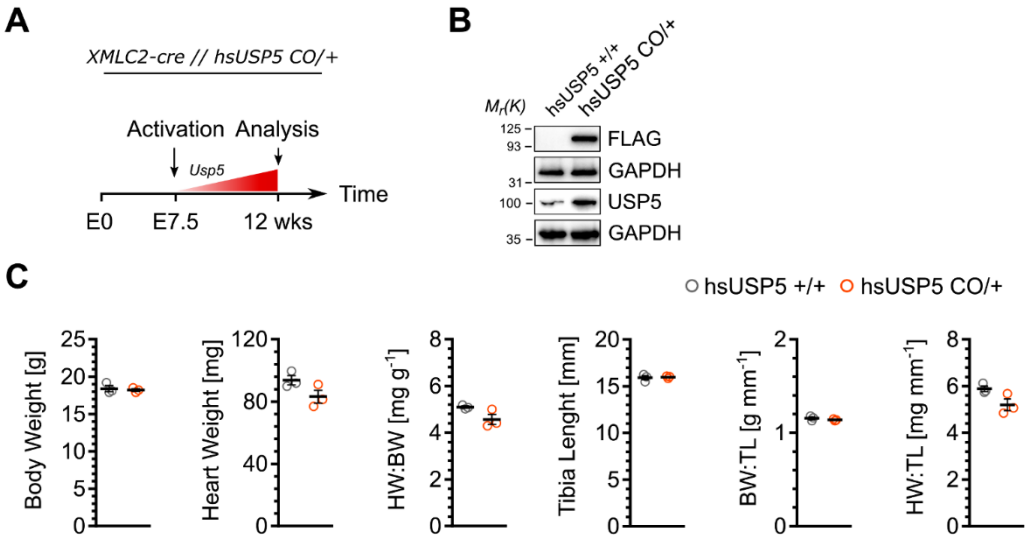

Figure 58 Effects of moderate overexpression of hsUSP5 in mature cardiomyocytes.

A. Timeline for analysis of cardiomyocyte-specific overexpression of hsUSP5. Heterozygous *hsUSP5 +/CO* mice were crossbred with a transgenic mouse strain harboring the *XMLC2-cre* recombinase to drive *cre*-mediated recombination in cardiac crescent cells around E7.5. B. Immunoblot analysis of USP5 expression in isolated cardiomyocytes from *hsUSP5* +/+ and *hsUSP5 CO*/+ mice using antibodies against the flag-tag (FLAG) or hsUSP5. C. Effects of cardiomyocyte-specific overexpression of hsUSP5 on body weight (BW), heart weight (HW), tibia length (TL), and ratios of heart to body weight (HW:BW), body weight to tibia length (BW:TL), and heart weight to tibia length (HW:TL). n = 3 for each group.

Immunoblot analysis revealed reduced ubiquitin levels, in low and high molecular weight range, in isolated cardiomyocytes of *hsUSP5 CO/+* mice, while monoubiquitin levels remained unchanged compared to *hsUSP5 +/+* control mice (Figure 59 A-C).

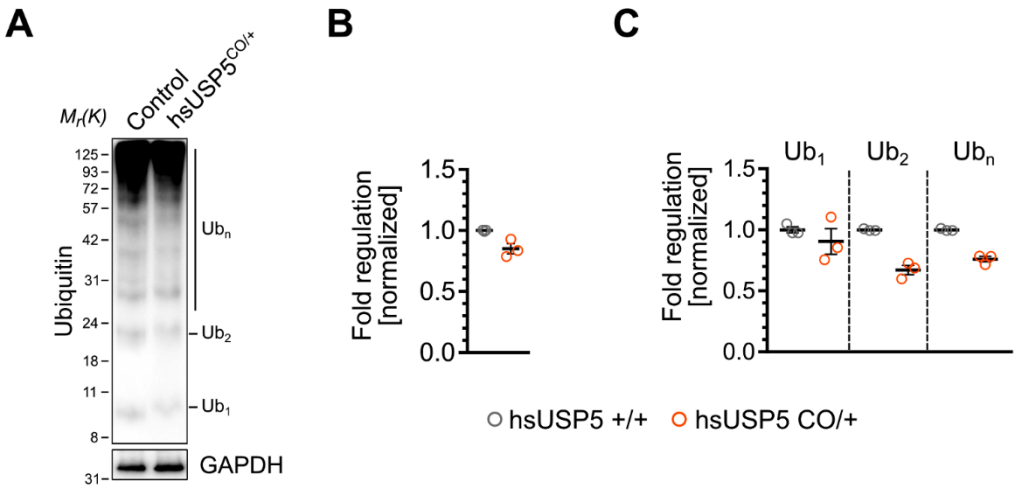

Figure 59 Moderate overexpression of hsUSP5 in cardiomyocytes reduces levels of ubiquitin.
A. Immunoblot analysis of ubiquitin levels in isolated cardiomyocytes from *hsUSP5 +/+* and *hsUSP5 CO/+* mice. n = 3 for each group. B, C. Quantification of ubiquitin levels (B) and ubiquitin chains (C) normalized to GAPDH. n = 3 for each group.

As loss of USP5 in cardiomyocytes caused arrest of autophagic flux, which resulted in defective clearance of ubiquitin-enriched protein aggregates, which was monitored by immunofluorescence staining of LC3. *hsUSP5 CO/+* cardiomyocytes showed reduced number of LC3-punctae compared to cardiomyocytes from *hsUSP5 +/+* control littermates, even in response to treatment with chloroquine (Figure 60 A, B). Chloroquine, a lysosomotropic agent, prevents both fusion of autophagosomes with lysosomes and lysosomal-dependent protein degradation by raising the lysosomal pH [137]. Together, these data demonstrate that moderate overexpression of hsUSP5 in cardiomyocytes is compatible with normal development and sustained cardiac function.

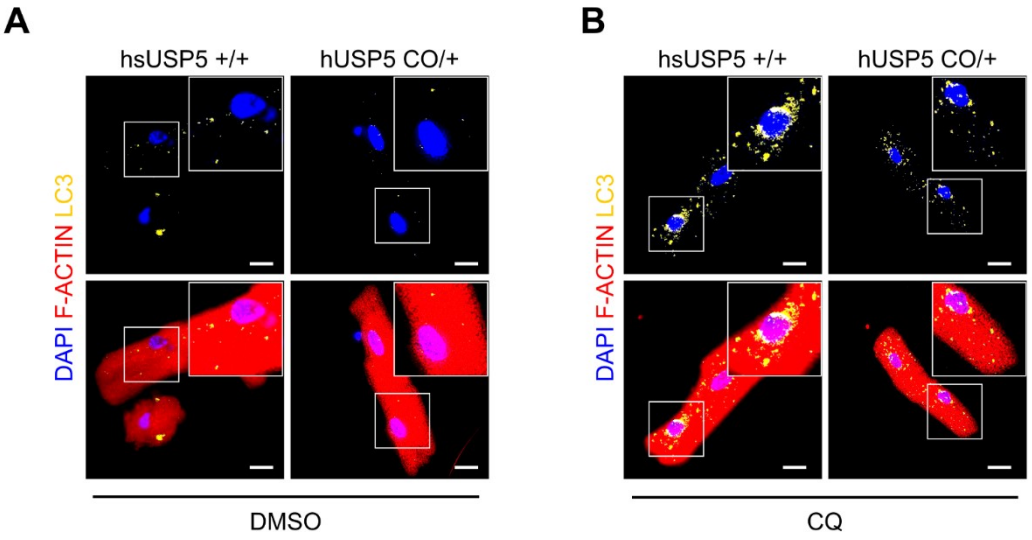

Figure 60 Moderate overexpression of hsUSP5 does not induce autophagy.

A, B. Immunofluorescence staining of F-actin (red), LC3 (yellow), and nuclei (DAPI, blue) in isolated cardiomyocytes from *hsUSP5* +/+ and *hsUSP5 CO*/+ mice without (A) or with (B) chloroquine treatment for 4 h. n = 2 for each group. Scale bars, 25 µm.

USP5 resolves protein aggregates induced by a disease-related mutation in titin

To address the question if cardiomyopathy-related protein aggregation phenotypes, mostly caused by mutations in structural proteins, can be reversed by moderate overexpression of hsUSP5, cardiomyocytes from *hsUSP5 CO*/+ and *hsUSP5* +/+ mice were infected with an adenovirus expressing either GFP-tagged wildtype titin or the GFP-tagged C31712R titin variant. 48 h post-infection, impact of elevated hsUSP5 protein levels on C31712R titin-induced protein aggregation was examined (Figure 61 A). The titin variant C31712R is one of the most frequently occurring mutations in the A-band region of titin, A150 (Fn3-119), known to cause protein destabilization and aggregation, which contributes to the development of HMERF (hereditary myopathy with early respiratory failure) [118, 138]. In addition to a muscle phenotype, studies show that HMERF-patients carrying the C31712R titin variant also show a cardiac-specific phenotype [139].

Transfection of cardiomyocytes with C31712R titin resulted in formation of large GFP-labeled titin aggregates in *hsUSP5* +/+ mice, which mainly formed in close proximity to nuclei or intercalated discs. In contrast, the number of GFP-labeled titin aggregates in *hsUSP5 CO*/+ transfected cardiomyocytes was substantially reduced in addition to significantly smaller titin aggregates (Figure 61 B-D).

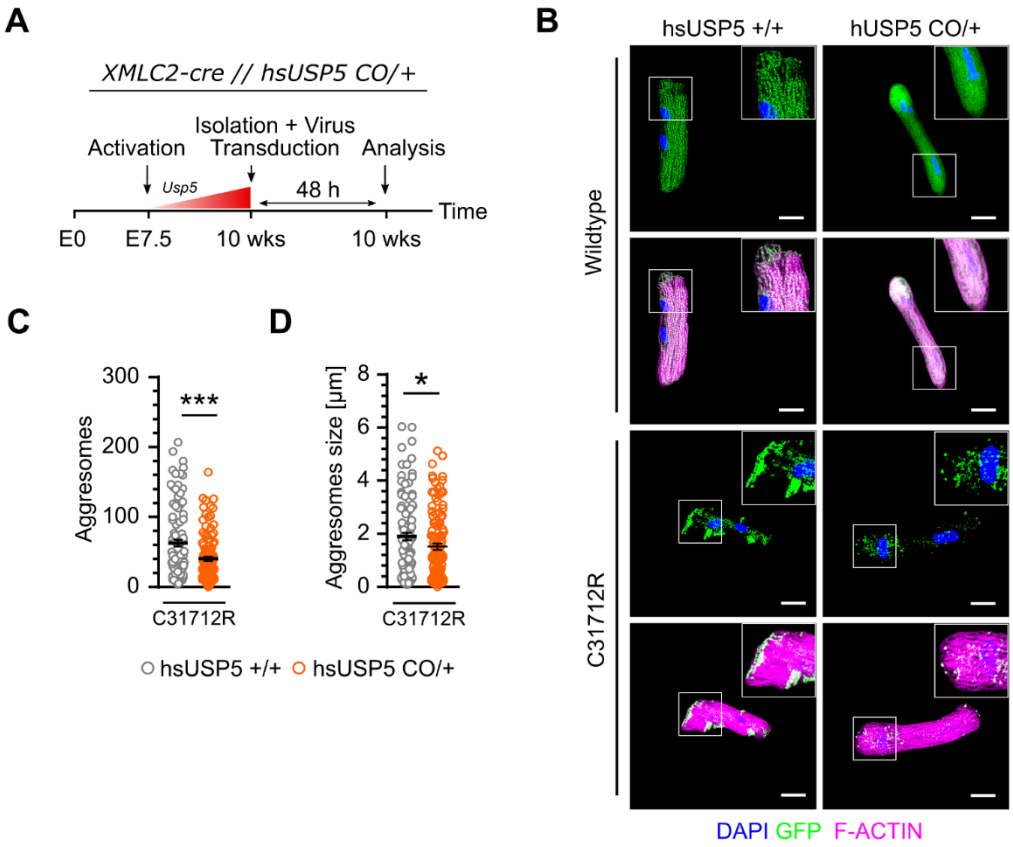

Figure 61 hsUSP5 clears protein aggregates caused by C31712R titin.

A. Timeline for analysis of cardiomyocyte-specific overexpression of hsUSP5 in respect to clearance of protein aggregates caused by the C31712R titin variant. B. Immunofluorescence staining of eGFP (green, representing titin), F-actin (magenta), and nuclei (DAPI, blue) in isolated cardiomyocytes from *hsUSP5* +/+ and *hsUSP5 CO*/+ mice 48 h after infection with an adenovirus encoding either GFP-tagged wildtype titin or GFP-tagged C31712R titin. n = 4 for each group. Scale bars, 25 µm. D, E. Quantification of the number (D) and average size of titin aggregates (E) in pooled isolated cardiomyocytes (n ≥ 140) from *hsUSP5* +/+ and *hsUSP5 CO*/+ mice. n = 4 mice per genotype. Two-tailed unpaired t-test with Wilcoxon-rank sum test. * $P < 0.05$; *** $P < 0.0002$.

To now elucidate the mechanism underlying the reduced presence of GFP-tagged C31712R titin aggregates in *hsUSP5 CO/+* cardiomyocytes, 20S proteasome activity in non-adenoviral and adenoviral infected cardiomyocytes was examined. At baseline, *hsUSP5 CO/+* cardiomyocytes showed an overall increase in 20S proteasome activity in comparison to isolated cardiomyocytes from *hsUSP5 +/+* mice, even though only trypsin-like peptidase activity reached statistical significance (Figure 62 A-C). Importantly, 20S proteasome activity measurement revealed substantially higher trypsin-and chymotrypsin-like peptidase activities in *hsUSP5 CO/+* cardiomyocytes expressing GFP-C31712R titin in comparison to *hsUSP5 +/+* cardiomyocytes (Figure 62 A-C). Moreover, 20S proteasome activity remained constant in cardiomyocytes of *hsUSP5 CO/+* mice infected with either GFP-tagged wildtype or GFP-C31712R titin. Overexpression of hsUSP5 further prevented decline of trypsin- and chymotrypsin-like peptidase activities in response to expression of aggregation-prone C31712R titin (Figure 62 A, C). These findings indicate that USP5 supports degradation of GFP-C31712R titin aggregates under conditions of increased proteostatic stress.

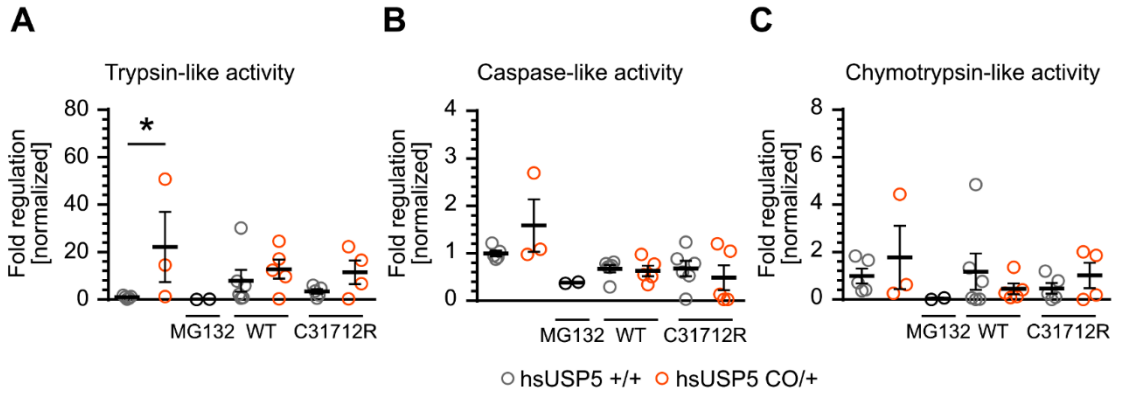

Figure 62 hsUSP5 clears protein aggregates caused by C31712R titin through sustained proteasome activity.

A-C. Quantification of 20S proteasome peptidase activities in isolated cardiomyocytes from *hsUSP5 +/+* and *hsUSP5 CO/+* mice 48 h after infection with an adenovirus encoding either GFP-tagged wildtype or GFP-tagged C31712R titin. n = 5 for each group. One-way ANOVA followed by Sidak's post-test. * $P < 0.05$.

Next, immunoblots were performed to investigate the impact of ameliorated hsUSP5 expression on clearance of GFP-C31712R titin aggregates by selective autophagy. At baseline, no changes in protein levels of the early autophagy markers p62 or LC3-II were observed, which indicated that overexpression of hsUSP5 in cardiomyocytes does not affect the autophagic flux (Figure 63 A-C). Consistent with these findings, p62 and LC3-II protein levels remained constant in *hsUSP5 CO/+* cardiomyocytes expressing GFP-C31712R titin, indicating that increased expression of USP5 in cardiomyocytes expressing mutant titin does not stimulate autophagy. In contrast, *hsUSP5 +/+* cardiomyocytes expressing GFP-C31712R titin showed higher protein levels of p62 with reduced levels of LC3-II, indicating severe impairment of autophagic flux in response to C31712R induced titin aggregation (Figure 63 A-C).

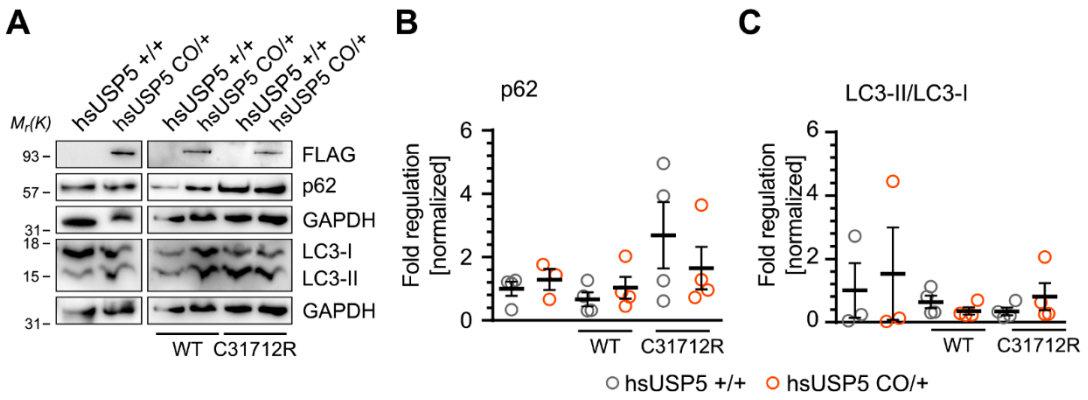

Figure 63 hsUSP5 clears protein aggregates caused by C31712R titin through sustained autophagic flux.

A. Immunoblot analysis of hsUSP5 (FLAG), p62, and LC3 in isolated cardiomyocytes from *hsUSP5 +/+* and *hsUSP5 CO/+* mice 48 h after infection with an adenovirus encoding either GFP-tagged wildtype or GFP-tagged C31712R titin. n = 5 for each group. B, C. Quantification of protein levels relative to GAPDH expression.

Collectively, these data confirm that suppression of proteasome activity in combination with impaired autophagic flux is associated with aberrant protein aggregation. Notably, the findings emphasize the importance of USP5 for appropriate proteasome activity and efficient autophagic flux, mainly in conditions of elevated cellular stress, which prevent the accumulation of harmful and toxic protein aggregates in the heart. I concluded that USP5 may represent a new target for the treatment of protein aggregation-related diseases in the heart.

DISCUSSION

The present study identified the ubiquitin-specific peptidase USP5 (Isopeptidase T, IsoT) as a critical component of cellular PQC in the myocardium. The data presented in this study demonstrate that conditional loss of USP5 in cardiomyocytes resulted in an imbalance of the cellular ubiquitin pools, caused by disturbed ubiquitin turnover, enhanced ubiquitin stress, and profoundly impaired UPS-dependent degradation of terminally misfolded proteins. Accumulation of such ubiquitin-ligated proteins to large, perinuclear located protein aggresomes, and defective clearance by selective autophagy resulted in remodeling of the heart, progression of DCM, and sudden death. Similarly, cardiomyocytes from human individuals with late end-stage DCM showed extensive accumulation of large ubiquitin-conjugated protein aggregates with substantially reduced USP5 protein levels in cardiomyocytes. Moreover, overexpression of USP5 in cardiomyocytes expressing the most common p.C31712R mutant variant of titin, known to cause protein destabilization and aggregation, abrogated excessive protein aggregate formation by sustaining UPS-dependent proteolysis. Importantly, all described effects were only observed in postmitotic cardiomyocytes expressing the non-spliced exon 15 long isoform of USP5. In contrast, conditional inactivation of the alternatively spliced variant of *Usp5*, USP5 exon 15 short, which is solely expressed in proliferating cells such as MEFs, resulted in moderately increased ubiquitin levels without inhibitory effects on 20S proteasome activity, although selective autophagy was impaired. In summary, the present study offers genetic evidence for the essential and rate-limiting function of USP5 for sustained proteostasis in the myocardium, both in mice and humans. Furthermore,

the data highlight the UPS-autophagy network to specifically rely on USP5-dependent ubiquitin homeostasis, which is indispensable for cardiomyocyte function.

Cellular functions rely on proper protein homeostasis, i.e. proteostasis, to maintain a healthy proteome [83, 91]. Gradual derailment of cellular PQC processes mainly caused by enhanced cellular stress or disease conditions, such as gene mutations or reduced efficiency of critical components of the proteostasis network during aging, impair acquisition of proper protein conformations, which results in the formation of terminally misfolded proteins [9, 13]. As misfolded proteins cannot be salvaged by molecular chaperones, they need to be removed by either of the two major protein degradation systems – ubiquitin-proteasome system (UPS) and lysosomal-dependent (selective) autophagy – to prevent accumulation of unutilized, terminally misfolded, mutated, or damaged proteins, which interfere with important cellular functions [2, 18]. Balanced proteostasis is important in organs containing large amounts of postmitotic cells, such as the brain and the heart. The high metabolic demand and mechanical stress, but also the nonregenerative capacity of neurons and mature cardiomyocytes make these cells particularly susceptible to disturbed PQC [2]. Accumulation of terminally misfolded proteins in neurons and cardiomyocytes causes an overload of the two proteolytic degradation machineries. Consequently, more and more proteins accumulate to form large protein aggregates exerting proteotoxicity [140]. Derailed proteostasis will drive multiple diseases, including neurodegenerative disorders or cardiac diseases, such as dilated cardiomyopathy (DCM) [85], although the exact molecular mechanisms have yet to be determined.

USP5 and cellular polyubiquitin turnover

Ubiquitination, the posttranslational modification of proteins with the 76 amino acid residue ubiquitin, controls tissue patterning and differentiation during maturation and development via various cellular processes. Ubiquitination is carried out by three enzymes – E1 ubiquitin-activating, E2 ubiquitin-transferring, and E3 ubiquitin-

ligating enzymes – which ensure conjugation of a ubiquitin molecule to a specific protein. The coordinated action of these three enzymes requires multiple protein modifications, ranging from conjugation of a single ubiquitin molecule or multiple monoubiquitin molecules to the attachment of one or more polyubiquitin chains to a lysine residue of the targeted protein substrate through an isopeptide bond [141]. Ubiquitination is a reversible process with specific enzymes – deubiquitinating enzymes (DUBs) – to ensure recycling of ubiquitin for its reuse. In this context, ubiquitination and recycling of ubiquitin are tightly controlled to determine protein levels and to guarantee fine-tuning of cellular processes. Although the human genome encodes approximately 100 active DUBs, the cell-specific function of most DUBs remains to be uncovered [142, 143].

Previous research on USP5 is limited to *in vivo* studies in yeast [56, 144], *Arabidopsis thaliana* [145], or *Drosophila melanogaster* [58], which disclosed the importance of USP5 for disassembly of free, unanchored ubiquitin chains to keep the proteasome free of inhibitory chains [56, 130, 134]. The *in vivo* mouse data presented in this study are fully compatible with this view but uncover functions of USP5 to be cell type- and USP5 isoform-specific. Disassembly of free, protein unattached polyubiquitin chains was impaired in mature cardiomyocytes lacking USP5 but not in USP5-deficient MEFs. Consistently, immunoblot analysis revealed severely disturbed ubiquitin pools, which resulted from accumulation of polyubiquitin chains and increased monoubiquitin levels in cardiomyocytes lacking USP5, while total ubiquitin levels or the composition of the ubiquitin pool were not different in USP5-deficient MEFs. Importantly, the observed effects in cardiomyocytes correlate to the expression of the exon 15 long isoform of USP5, which is solely expressed in organs containing large amounts of postmitotic cells. In contrast, USP5 undergoes alternative splicing in proliferating cells, such as MEFs, which results in expression of a shorter variant of *Usp5* [131]. This shorter isoform of USP5 lacks 23 amino acids at the carboxyl-terminus of exon 15, which does not encode any conserved or functional domain of USP5.

Moreover, the discrepancy in the requirement of USP5 for polyubiquitin turnover in MEFs and cardiomyocytes corresponds to general differences in the ubiquitin pool in proliferating, self-renewable cells, e.g. MEFs, versus postmitotic cells, such as cardiomyocytes. While the ubiquitin pool in MEFs is composed of ~ 65 % ubiquitin present as monoubiquitinated substrates, ~ 23 % ubiquitin monomers, and ~ 11 % polyubiquitin chains, the mouse brain contains only ~ 5 % polyubiquitin chains but three-fold more (~ 59 %) ubiquitin present as ubiquitin monomers, and 35 % as monoubiquitin on substrates [146]. These differences are even more pronounced in the human frontal cortex, which contains ~ 82 % free ubiquitin monomers but only ~ 4 % polyubiquitin chains [147]. These data suggest that postmitotic cells do not tolerate high polyubiquitin levels but need to sustain physiologically high levels of monoubiquitin. Increased levels of polyubiquitin chains might potentially impede proteasome function and interfere with ubiquitin-dependent signaling. In fact, impaired ubiquitin signaling or altered composition of ubiquitin pools render cells more susceptible to stress conditions [148, 149], which is particularly detrimental to postmitotic cells in the heart as well as in the brain. Since the limited self-renewal capacity hinders postmitotic cells to remove harmful and toxic cell fragments by cell division, cardiomyocytes and neurons must be more efficient than proliferating cells to eliminate terminally misfolded proteins by degradation. Hence, postmitotic cells require high levels of conjugation-competent ubiquitin monomers and low levels of polyubiquitin chains to guarantee proteolysis of terminally misfolded proteins. USP5 seems instrumental to achieve this efficiency.

Only few studies have attempted to determine shared and distinct features of the proteome and ubiquitinome in different cell lines, although cell-type specific clusters of protein expression are present in all cells [150]. The list of most abundant DUBs included components of the proteasome, the constitutive photomorphogenesis 9 (COP9) signalosome, and the translation initiation machinery. Importantly, USP5 was detected as one of the most abundant DUBs in HeLa, HEK, and Swiss3T3 cells with a copy number of $>4\times10^5$ copies, similar to copy numbers of the proteasomal DUBs PSMD14, UCHL5, and USP14, underlying its importance for maintaining ubiquitin

homeostasis [142]. Given the importance of ubiquitin to most aspects of eukaryotic cell function, it is of particularly important to gain more insights into cell-type specific differences in protein copy numbers and the demographics of the ubiquitin pool, especially under certain stress conditions.

Why loss of USP5 in proliferating MEFs had no impact on polyubiquitin turnover or ubiquitin homeostasis remains to be studied in more detail. Possibly, other DUBs involved in processing of protein-conjugated or unanchored polyubiquitin chains compensate for the loss of USP5 in MEFs. Different DUBs may target the same ubiquitin chain topology, thereby providing a cell-context dependent regulation of homeostatic ubiquitin pools. Since MEFs are proliferating cells, their ability to divide might allow MEFs to adapt to altered ubiquitin levels faster and more efficiently and therefore loss of USP5 had little or no impact on ubiquitin homeostasis. In this regard, more *in vivo* studies are needed to investigate the role of USP5 in other proliferating cells and to demonstrate whether the effects seen in MEFs can be recapitulated.

USP5 and processing of ubiquitin precursors

Cellular ubiquitin levels are tightly controlled by DUBs, which are indispensable for the generation of conjugation-competent ubiquitin [151]. DUBs fulfill this task by removing ubiquitin chains from posttranslationally modified proteins, by editing the length and/or type of ubiquitin chains on modified proteins, or by processing of ubiquitin precursors to generate ubiquitin [60]. In mammals, ubiquitin is synthesized by cytosolic ribosomes in four distinct, inactive precursor forms that must be properly processed by individual DUBs to generate active, conjugation-competent ubiquitin monomers. Each ubiquitin precursor is encoded by different genes [152, 153]: the ubiquitin-ribosomal precursors *UBA52* and *UBA80* (hereafter referred to as Ub-RPs) and the polyubiquitin precursors *UBB* and *UBC* (hereafter referred to as polyUbs). Ub-RPs are composed of a single ubiquitin that is fused to a ribosomal protein – L40 for *UBA52* and S27A for *UBA80* – at its carboxyl-terminus [154, 155]. In contrast,

polyUbs are translated as linear fusion proteins comprising multiple copies of ubiquitin – 3-4 ubiquitin's for *UBB* and 7-10 ubiquitin's for *UBC* – linked in a 'head-to-tail' manner, followed by a variable extension at the carboxyl-terminus [27, 156]. Early studies limited the number of DUBs involved in processing of ubiquitin precursors to three, while referring to USP5 as the only DUB that aids processing of polyUbs [55]. Nowadays, five DUBs – UCHL3, USP9X, USP7, USP5, and Otulin – are characterized to be active towards ubiquitin precursors, but only USP5 and Otulin show high reactivity towards polyUbs [25]. The data presented in this study show that the inactivation of *Usp5* in cardiomyocytes results in profoundly increased mRNA levels of polyUbs but not Ub-RPs, which argues for compensatory mechanisms by upregulating transcription of polyUbs to replenish the pool of free, unconjugated ubiquitin with ubiquitin monomers. Although Otulin is also involved in processing of polyUbs, the "-omics" data showed that loss of USP5 in cardiomyocytes does not affect mRNA or protein expression of Otulin. Therefore, Otulin cannot compensate for the loss of USP5 in cardiomyocytes, showing that USP5 is essential for processing of polyUbs. Otulin, unlike USP5, cleaves randomly anchored and unanchored linear ubiquitin chains and is thus an important regulator of signaling cascades controlled by the ubiquitin-ligase linear-ubiquitin-assembly complex (LUBAC), such as immune homeostasis, responses to infection, and NFκB signaling [157-159]. Constitutive loss of Otulin in mice is similar to USP5 early embryonic lethal (E12.5-E14), which indicates both DUBs to be crucial for developmental processes.

Transcription of polyUbs is known to be highly induced in response to certain stress conditions, such as oxidative or proteotoxic stress [26, 160]. The data presented in this study are fully consistent with this view, since enhanced proteotoxic stress in cardiomyocytes, induced by MG132 treatment, resulted in profound upregulation of polyUbs, but not Ub-RPs. Remarkably, wildtype cardiomyocytes treated with MG132 showed a similar increase in mRNA levels of polyUbs compared to cardiomyocytes lacking USP5, indicating that inactivation of *Usp5* in postmitotic cells resulted in elevated proteotoxic stress.

USP5 and PQC processes: function at the 26S proteasome

The function of the proteasome is critical for proteostasis as it impacts the regulation of cellular processes in all organs, including the heart [161]. UPS-dependent proteolysis of terminally misfolded, mutated, oxidized, or otherwise damaged proteins is carried out as a multi-step process that involves binding of (poly-) ubiquitinated proteins, deubiquitination, ATP-dependent unfolding, and translocation into the 20S CP of the proteasome for degradation [162]. The lysine residue at which ubiquitin is attached to, either at the protein or within a polyubiquitin chain, not only determines the functional property of the modified protein, it also imparts the specific outcome on the fate of the protein substrate [146]. Lys48-, Lys29-, and Lys11-linkage specific ubiquitin chains specifically target proteins for proteasomal degradation, while Lys63-linkage specific polyubiquitin chains are essential for selective autophagy-mediated PQC processes [18, 163]. Deubiquitination of proteins targeted for degradation by the 26S proteasome is carried out by three DUBs: Rpn11/POH1/PSMD14, UCH37/UCHL5, and USP14 [36, 63, 164-167]. However, other studies report the association of several other ubiquitin-specific peptidases (USPs), including USP5, with the proteasome in human cells, the rat cortex, and rat skeletal muscle [168-170]. The findings in the present study are fully consistent with these reports, showing that USP5 forms a complex with PSMD14 that is essential for deubiquitination of proteins prior to proteasomal degradation. In addition, the BioID approach uncovered that USP5 also associates with other components of the 26S proteasome, which needs to be further investigated in more detail. However, a close interaction between USP5 and PSMD14 clearly makes sense, since USP5 selectively cleaves PSMD14-released free, unanchored polyubiquitin chains at the proteasome to replenish the pool of free monoubiquitin, which – as I discussed earlier – is especially important in postmitotic cells. On the other hand, disassembly of PSMD14-released polyubiquitin chains by USP5 guarantees rapid elimination of such polyubiquitin chains and therefore keeps the 26S proteasome free of inhibitory polyubiquitin chains, which suppress all three peptidase activities of the 20S proteasome in addition to accumulation of ubiquitin-enriched proteins [56, 144, 161]. Therefore, recruitment of accessory factors such as

USP5 enables the 26S proteasome to cope with cell-type specific proteolytic demands [171]. The results in this study show that inactivation of *Usp5* elevates ubiquitin levels, including accumulation of Lys48-linkage specific polyubiquitin chains, accompanied by severely impaired 20S enzymatic peptidase activities. Importantly, alteration of UPS-dependent processes, resulting either from decreased 20S proteasome activity, altered composition of the 26S proteasome, or failure in deubiquitination of proteins is described to promote the progression of DCM [172-175]. However, this scenario was only observed in cardiomyocytes, while inactivation of *Usp5* in MEFs had no impact on ubiquitin levels or the proteolytic capability of the 20S proteasome. This raised the question if proliferative cells other than MEFs might be also tolerant to inactivation of *Usp5*, or if MEFs alone compensate the loss of USP5 by upregulation of other DUBs, involved in processing of ubiquitin precursors and maintaining homeostatic ubiquitin pools.

USP5 and PQC processes: function in (selective) autophagy

Autophagy is an evolutionarily conserved process that plays an important role for cellular homeostasis under normal physiological conditions, ensuring basal turnover of long-lived proteins and organelles [176]. Autophagy becomes potently induced in response to cellular stress or nutrient deprivation to degrade damaged organelles, oxidized lipids, or intracellular pathogens. In addition, selective autophagy serves as a compensatory catabolic pathway in PQC whenever the 26S proteasome or other UPS-dependent processes are impaired or severely disturbed to relieve cells from cytotoxic effects of protein aggregates for which no other cellular pathway can compensate [177, 178].

Before toxic protein aggregates are processed for autophagic clearance, they need to be transported by microtubule-dependent dynein motors to be concentrated at the microtubule-organizing center (MTOC) to form perinuclear inclusion bodies, called aggresomes [133, 179]. The deacetylase HDAC6 plays a crucial role during selective

autophagy by regulating the transport, concentration, and autophagic clearance of aggresomes by lysosomal digestion [71, 129, 132]. HDAC6 contains a C-terminal BUZ ubiquitin binding domain that allows binding to Lys63-linked ubiquitin chains on protein aggregates, which are released by the non-canonical deubiquitinating activity of PSMD14. Binding to Lys63-linkage specific ubiquitin chains results in the retrograde transport of protein aggregates towards the MTOC [71], where HDAC6 dissociates from the protein aggregates. Since HDAC6 no longer binds Lys63-linked ubiquitin chains, it deacetylates its target cortactin, which induces remodeling of the actinomyosin network and retrograde transport of autophagosomes and lysosomes to the MTOC to promote de-aggregation, formation of autolysosomes, and autophagic degradation of newly formed aggresomes [129, 180, 181]. The data presented in this study indicates that USP5 plays an additional role for the clearance of aggregated proteins and aggresomes by selective autophagy. Although inhibition of all three enzymatic peptidase activities of the 20S proteasome due to accumulation misfolded proteins and Lys48-linkage specific ubiquitin chains is the major defect of PQC in cardiomyocytes in response to inactivation of *Usp5*, I noticed impairment of the autophagic machinery in cardiomyocytes lacking USP5. Adverse effects included increased levels of Lys63-linkage specific ubiquitin chains and proteins, formation of p62-containing aggresomes, and sequestration of proteins from proteolysis by the 26S proteasome. Impairment of clearance of protein aggregates by selective autophagy and accumulation of p62- containing aggresomes is caused by defects in the activation of HDAC6 to deacetylate its target protein cortactin. Potentially, USP5 controls the catalytic activity of HDAC6 or the switch of HDAC6-dependent binding to Lys63-linkage specific ubiquitin chains and deacetylation of cortactin to promote the retrograde transport and de-aggregation of aggresomes. As an alternative, increase in Lys63-linkage specific ubiquitin chains and impairment of the UPS blocks the activity of PSMD14 and thus permits activation of HDAC6. Prolonged aggregation in USP5-deficient cardiomyocytes, caused by severe impairment of both protein degradation pathways, resulted in progressive cell death, as demonstrated by caspase-3 cleavage and PARP activation, which was not observed in MG132-treated cardiomyocytes from control littermates.

Interestingly, early steps in autophagy-mediated clearance of aggresomes, i.e. binding of the cargo and autophagosome formation, were not disturbed, as indicated by co-localization of ubiquitin-conjugated aggresomes with HDAC6 and the autophagy receptor p62. Similar to HDAC6, p62 contains a ubiquitin domain that allows binding to Lys48- and Lys63-linkage specific polyubiquitin chains on protein aggregates and aggresomes. In addition, p62 possesses a zinc-finger binding domain that facilitates direct binding to the microtubule-associated protein 1A/1B-light chain 3 (LC3) that promotes autophagosome formation [182, 183]. Therefore, p62 acts as an important adaptor molecule for selective autophagy of protein aggregates and aggresomes as it binds Lys63-linkage specific polyubiquitin chains on the protein cargo and mediates the interaction of protein aggregates and aggresomes with the autophagic machinery through binding to LC3 [184, 185]. Moreover, p62 acts as a proteotoxic stress sensor that mediates crosstalk between the UPS and selective autophagy. Indeed, a crosstalk between the both protein degradation systems is supported by several studies showing that activation of autophagy, e.g. in the heart, occurs in response to severely impaired UPS-dependent catabolic processes [186, 187]. The present study shows that elevated levels of proteotoxic stress in USP5-deficient cardiomyocytes resulted in impaired autophagic flux, as indicated by elevated p62 protein levels with faulty conversion of LC3-I to generate the active, lipidated form LC3-II [188, 189]. These effects might also be caused by impaired activation of HDAC6 and subsequently defects in the fusion of autophagosome with lysosomes. Hence, USP5 signaling in cardiomyocytes is necessary for continuous autophagic flux and lysosomal degradation of aggresomes along with the adapter molecule p62, but does not affect early steps during selective autophagy, such as protein cargo recognition or the interaction of the cargo with the autophagic phagophore machinery. These finding indicate that impaired selective autophagy of aggresomes, in addition to already impaired function of the UPS, further exacerbates defects in PQC processes with deleterious consequences respective to cardiac proteostasis. Accumulation of p62 in response to inhibition of autophagy impairs the proteasomal flux and delays degradation of polyubiquitinated proteins by the UPS, which is mainly caused by excessive interaction between p62 and Lys48-linkage specific polyubiquitin chains on misfolded proteins [190, 191]. This in turn

results in elevated levels of short-lived proteins, accumulation of proteins prone for aggregation, and formation of 62-containing aggresomes with delirious consequences [192]. Defects in clearance of protein aggregates are linked to heart failure [193], aging, and the development of certain cardiovascular diseases, including DCM [194].

USP5 and disease-related protein aggregation

Proper function of newly synthesized proteins relies on maturation, correct folding into a native 3D state, appropriate transport, posttranslational modification, and breakdown by degradation. All these steps are controlled by several distinct components of the proteostasis network. To function properly, cells highly depend on balanced proteostasis that is mediated by crosstalk between the different PQC processes [83]. Gradual derailment of proteostasis due to defective PQC, primarily affecting the UPS and selective autophagy, results in continuous accumulation of ubiquitin-conjugated protein aggregates. Presence of ubiquitin-conjugated protein aggregates is an invariant feature of neurodegenerative diseases, such as Alzheimer's disease (AD), Parkinson's disease (PD), Huntington's disease (HD), or amyotrophic lateral sclerosis (ALS) [92, 195]. Importantly, reports show derailed proteostasis to drive the progression and development of several cardiac diseases, including cardiac hypertrophy (HCM), dilated cardiomyopathy (DCM), and atrial fibrillation (AF), although the exact molecular mechanisms remain to be uncovered [3, 85]. Derailed proteostasis constitutes a prominent trigger for cardiomyocyte dysfunction and impaired cardiac function. Impaired cardiac function, in turn, results from alterations in cardiac performance, loss of cardiomyocytes, cardiac remodeling, and activation of systemic or neurohumoral inflammatory pathways [20]. As discussed in the previous sections, inactivation of *Usp5* in cardiomyocytes at various stages of development resulted in perinuclear deposition of ubiquitin-enriched protein aggregates, formation of large aggresomes, and profound DCM. Progressive impairment of the two main protein degradation systems – the UPS and autophagy – is one of the leading causes for the development of DCM [175, 196]. Persistent formation of protein aggregates

and perinuclear aggresomes in response to inactivation of *Usp5* in cardiomyocytes was sufficient to initiate remodeling processes in the heart, including apoptosis, loss of cardiomyocytes, oxidative stress, and activation of fibroblasts along with deposition of collagen (fibrosis). Fibrosis is a known compensatory mechanism of the heart to maintain cardiac mass in response to loss of cardiomyocytes. Overall, derailment of cardiac proteostasis in combination with remodeling of the myocardium leads to aberrant architecture and increased stiffness, ultimately resulting in development of DCM and sudden death. Sudden cardiac death accounts for up to 50 % of all deaths and is mostly caused by ventricular tachycardia or ventricular fibrillation and less often by bradyarrhythmia or asystole. However, the cause of death in the USP5 transgenic mice might either be caused by mechanical or electrical problems, which needs to be investigated.

Furthermore, the findings in this study revealed dramatically reduced USP5 protein levels and enhanced load of ubiquitin-enriched aggresomes in cardiomyocytes from randomly selected human patients with late end-stage DCM. Previous research to measure the protein levels of USP5 in DCM patients have been inconclusive, reporting a ~ 2.3-fold reduction in the expression of USP5 by referring to a molecular weight of ~ 25 kDa of USP5 that did not match the calculated molecular weight of ~96 kDa observed in this study [197]. However, in agreement to the molecular data obtained from USP5-deficient cardiomyocytes and cardiomyocytes from human end-stage DCM patients, Kostin *et al.* reported elevated mRNA levels of ubiquitin and UCHL1 in combination with polyubiquitinated proteins in myocardial samples from human DCM patients compared to cardiac samples from a control cohort. The present study demonstrates almost complete lack of USP5 in ubiquitin-enriched aggresomes in cardiomyocytes from human late end-stage DCM patients. In contrast, cardiomyocytes from non-failing, control individuals showed presence of USP5-enriched but ubiquitin-negative aggresomes. The findings that aggresomes in DCM patients were conjugated with ubiquitin indicate that these aggresomes were marked for degradation but that downregulation of USP5 caused failure of PQC, resulting in disturbed cardiac proteostasis and clinical manifestation of DCM. In conclusion, the

data in this study demonstrate a striking similarity between the DCM phenotype observed in a human cohort with late end-stage DCM and present animal models of USP5-deficient mice, as characterized by substantially reduced USP5 protein levels and accumulation of USP5-lacking but ubiquitin-conjugated aggresomes in cardiomyocytes. Translating these data to pathological relevant cardiac disorders demonstrates that USP5 is indispensable for normal cardiac development, cardiac function, and survival.

USP5 as a potential drug to target PQC to maintain cardiac proteostasis

Research has started to uncover the molecular mechanisms driving disease-causing derailment of proteostasis, as mainly characterized by atypical protein aggregation compromising cellular functions, especially in the brain and the heart. None of these so called 'proteinopathies' are currently curable. Therefore, approaches to enhance PQC in disease condition might improve intracellular or extracellular proteostasis pathways, involved in protein folding, trafficking and degradation to prevent or reverse detrimental effects of aberrant protein aggregation. Moreover, enhancing PQC processes might enhance the interaction between the destabilized disease-associated, aggregation-prone protein with components of the proteostasis network [10, 198, 199]. Enhancing the activity of UPS-dependent processes, e.g. by increasing the pool of free ubiquitin pool [200] or overexpression of certain E3 ubiquitin ligating enzymes [201, 202], substantially reduces proteotoxicity induced by protein aggregates. As an alternative approach, enhancing the proteolytic activity of the 20S proteasome by small-molecule compounds exerted beneficial effects on neurodegenerative diseases [149, 203]. However, most of these studies were performed *in vitro* and their effectiveness *in vivo* needs to be uncovered. Enhancement of (selective) autophagy to promote clearance of protein aggregates in neurodegenerative diseases, such as Huntington's disease (HD), yielded promising results in many cell- and mouse models, by reducing the number of disease-related

aggregates, and attenuating disease progression as well as life span of the tested transgenic mice [204-206]. Since autophagy also enhances the clearance of many infectious agents in addition to its protective effects for apoptosis, its activation might improve treatment of various diseases. A combination of molecules that stimulate proteasome activity with activators of autophagy would maximize the therapeutic efficiency. Boosting of the proteostasis network represents an attractive new strategy to prevent and possibly treat proteinopathies [85], including cardiomyopathies. In this respect, the requirement of highly efficient PQC processes in the heart is particularly evident in human individuals carrying mutations in genes encoding sarcomere, cytoskeletal, and nuclear envelope proteins [86, 207].

The present study highlights USP5 as a molecule with substantial therapeutic potential for the treatment of cardiac disorders, such as DCM and potentially other proteinopathies, e.g. neurodegenerative diseases, by enhancing PQC processes. Enhanced expression of USP5 in cardiomyocytes did not cause any noticeable adverse effects on the cardiovascular system, arguing for the safety of USP5 overexpression and activation. Importantly, enhanced expression of USP5 in conditions favoring aggregation of disease-related, mutated proteins stimulated the crosstalk between the UPS and selective autophagy, thereby enhancing the proteolytic capacity of the 20S proteasome and potentially autophagic flux. In particular, increased 20S proteasome activity and consistent levels of selective autophagy prevented or reversed aberrant aggresome formation in cardiomyocytes induced by the most common missense C31712R mutation in the sarcomere protein titin. Mutant C31712R titin, which is known to cause protein destabilization is also linked to the development of hereditary myopathy with early respiratory failure (HMERF) [81, 175]. HMERF is characterized by aberrant protein aggregation and the presence of rimmed vacuoles enriched with ubiquitin, p62, and LC3 [138]. Furthermore, the clinical manifestation of human patients carrying such a C31712R variant is closely associated with a cardiac-specific phenotype [139]. Ongoing research will reveal whether forced or induced expression of USP5 might prevent or reverse cardiomyopathy-associated protein aggregation in animal models and human individuals.

Proposed model for the regulation of cardiac PQC by USP5

The molecular data presented in this study show that USP5 plays an important role for two important PQC processes, which also represent the most important cellular protein degradation pathways – the UPS and selective autophagy. First, USP5 forms a complex with the 19S proteasomal DUB PSMD14, which ensures disassembly and processing of free, unanchored ubiquitin chains to generate ubiquitin monomers and to guarantee proteolysis of misfolded proteins by the 26S proteasome. Processing of PSMD14-released free, unanchored ubiquitin chains prevents such ubiquitin chains from competitively overloading or inhibiting the 26S proteasome. In addition to its canonical role, PSMD14 is important for lysosomal degradation of protein aggregates, which due to their stoichiometry cannot be degraded by the 26S proteasome. By providing Lys63-linkage specific ubiquitin chains, PSMD14 activates the autophagic adaptor HDAC6, which builds a complex with USP5. However, further studies are needed to investigate how USP5 regulates HDAC6 and how the complexes between USP5 and HDAC6 is controlled and activated. It is conceivable that USP5 regulates the switch between the two catalytic activities of HDAC6 – tubulin binding and deacetylation of cortactin – and its ubiquitin-binding property to ensure binding, transport, and temporarily concentration of protein aggregates as aggresomes before initiating lysosomal degradation.

In summary, the study shows that loss of USP5 in cardiomyocytes disrupts PQC processes by interfering with polyubiquitin turnover. As a consequence, accumulation of Lys48- and Lys63-linkage specific polyubiquitin chains competitively inhibit 20S proteasome activity, which prevents PSMD14-mediated deubiquitination of proteins destined for proteasomal degradation. This in turn favors accumulation of ubiquitin-conjugated proteins and causes formation of large ubiquitin-enriched aggresomes that competitively interfere with binding of ubiquitinated proteins at the 20S proteasome. In addition, impaired clearance of aggresomes by selective autophagy further disturbs ubiquitin homeostasis, which enhances cellular stress-dependent cardiac remodeling, development of DCM, and sudden cardiac death. Overexpression of USP5 prevents

formation of ubiquitin-enriched protein aggregates in conditions of disease-related protein aggregation by promoting a crosstalk between UPS-dependent proteolysis and selective autophagy and thus reverses one of many forms of DCM caused by proteotoxicity (Figure 64). I consider this as a ground-breaking new finding, which opens numerous perspectives for the treatment of DCM and other disorders associated with protein aggregation, e.g. neurodegenerative diseases. Furthermore, research on DUBs regulating polyubiquitin turnover were mostly performed in cell culture and yeast. The present study is the first to demonstrate a cell type- and isoform- specific function of a DUB that exhibits a crucial role in polyubiquitin turnover, which is essential for proteostasis in postmitotic cells.

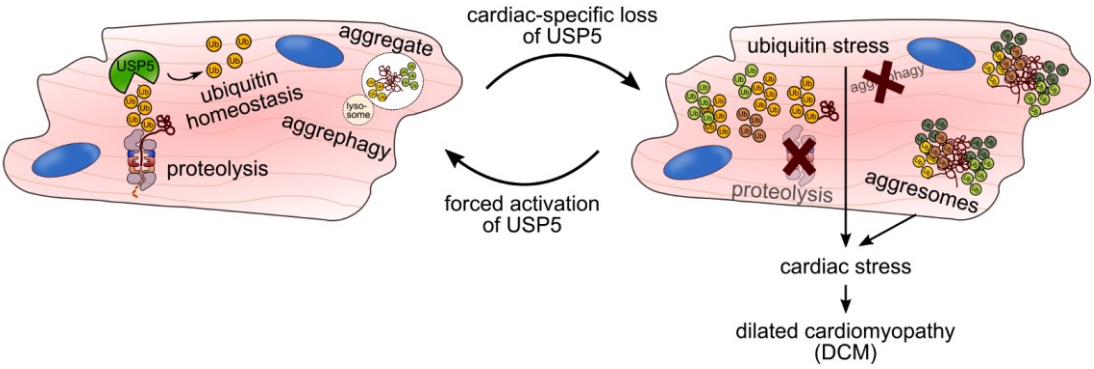

Figure 64 USP5 is crucial to maintain cardiac PQC.

FUTURE DIRECTIONS

The study described in this thesis lays an important foundation for future studies of the function of DUBs in the myocardium. Primarily, it defines the ubiquitin-specific peptidase USP5 as a DUB regulating PQC processes in the myocardium, which is essential for sustained proteostasis and cardiac function. USP5 contributes to homeostatic ubiquitin pools, polyubiquitin turnover, and persistent proteasome activity in cardiomyocytes. In this context, the data demonstrate the importance of USP5 as a critical DUB residing at the proteasome for disassembly of free, protein unattached polyubiquitin chains, released by PSMD14-mediated deubiquitination, to be particularly relevant in cardiomyocytes. However, the study also shows other DUBs belonging to the USP family to potentially contribute to proteasomal PQC by building a complex with PSMD14, which functions need to be addressed.

Although the present study is the first to characterize the *in vivo* function of USP5 using transgenic mouse models, more questions seem to be raised than answered from such an initial effort. First, more *in vivo* models are needed to uncover the cell-type specific role of USP5 in more detail. Second, such an approach would help to further elucidate why alternative spliced variants of USP5 behave differently in maintaining ubiquitin homeostasis, polyubiquitin turnover, and PQC, or if the observed effects are restricted to MEFs and cardiomyocytes. Third, *in vivo* models will also help to address the question whether all proteinopathies will benefit from USP5 overexpression, or whether only certain protein aggregation-related diseases are sensitive to increased expression of USP5. Unraveling the effects of increased USP5

protein levels in other cardiomyopathies will help to get more insights into the mechanism by which USP5 reverses or prevents protein aggregation and if the beneficial effects are also based on augmented proteasome activity, as already seen in the titin model used in this study. Furthermore, sqRT-PCR analysis of brain tissue samples revealed expression of both USP5 exon 15 isoforms, which suggest that neurons may also escape from alternative splicing as already demonstrated for postmitotic cardiomyocytes. In addition, neurons rely on low levels of polyubiquitin chains, similar to the observed results in cardiomyocytes. While protein aggregation is one of the prominent features of neurodegenerative diseases, very little is known about how neurons handle toxic protein aggregates in response to altered ubiquitin homeostasis. Although the brain represents only 2 % of the body weight, it receives 15 % of the cardiac output and consumes approximately 20 % of the total body oxygen, mostly by neurons [208]. Therefore, neurons, similar to oxygen demanding cardiomyocytes, must have evolved mechanisms to deal with protein oxidation and elevated stress conditions. We are just beginning to understand how neurons handle misfolded proteins and how alterations in the ubiquitin pool and PQC processes contribute to development and progression of various neurodegenerative disorders. In this context, it might be very useful to investigate possible consequences arising from a neuron-specific loss of USP5, particularly in terms of altered ubiquitin levels, impaired proteasome activity, and protein aggregation. Such a conditional knockout approach of USP5 in neurons might help answering the question, if other postmitotic cells rely on USP5-dependent ubiquitin homeostasis and proteostasis, or whether compensating USPs or DUBs may exit in neurons similar to MEFs. However, it is possible that loss or altered activity of USP5 may play a significant role in the development of neurodegenerative diseases. Enhancing proteasome activity may aid in degradation of misfolded proteins in the brain. However, no therapeutical agent has been shown to improve proteasome function in the cell. Taking this into account, future studies could investigate to what extend – similar to the results presented in this study – overexpression of USP5 minimizes, reverses, or prevents protein aggregation in the brain and if USP5 also provides opportunities for the development of therapies for the treatment of neurodegenerative disorders.

BIBLIOGRAPHY

1. Patterson, C., et al., *The bitter end: the ubiquitin-proteasome system and cardiac dysfunction.* Circulation, 2007. **115**(11): p. 1456-63.
2. McLendon, P.M. and J. Robbins, *Proteotoxicity and cardiac dysfunction.* Circ Res, 2015. **116**(11): p. 1863-82.
3. Brundel, B.J., et al., *Induction of heat shock response protects the heart against atrial fibrillation.* Circ Res, 2006. **99**(12): p. 1394-402.
4. Zhang, H., et al., *ROS regulation of microdomain Ca(2+) signalling at the dyads.* Cardiovasc Res, 2013. **98**(2): p. 248-58.
5. Rujano, M.A., et al., *Polarised asymmetric inheritance of accumulated protein damage in higher eukaryotes.* PLoS Biol, 2006. **4**(12): p. e417.
6. Willis, M.S. and C. Patterson, *Proteotoxicity and cardiac dysfunction.* N Engl J Med, 2013. **368**(18): p. 1755.
7. Sala, A.J., L.C. Bott, and R.I. Morimoto, *Shaping proteostasis at the cellular, tissue, and organismal level.* J Cell Biol, 2017. **216**(5): p. 1231-1241.
8. Klaips, C.L., G.G. Jayaraj, and F.U. Hartl, *Pathways of cellular proteostasis in aging and disease.* J Cell Biol, 2018. **217**(1): p. 51-63.
9. Kim, Y.E., et al., *Molecular chaperone functions in protein folding and proteostasis.* Annu Rev Biochem, 2013. **82**: p. 323-55.
10. Balch, W.E., et al., *Adapting proteostasis for disease intervention.* Science, 2008. **319**(5865): p. 916-9.
11. Balchin, D., M. Hayer-Hartl, and F.U. Hartl, *In vivo aspects of protein folding and quality control.* Science, 2016. **353**(6294): p. aac4354.
12. Hartl, F.U., *Molecular chaperones in cellular protein folding.* Nature, 1996. **381**(6583): p. 571-9.
13. Hartl, F.U., A. Bracher, and M. Hayer-Hartl, *Molecular chaperones in protein folding and proteostasis.* Nature, 2011. **475**(7356): p. 324-32.
14. Finley, D., *Recognition and processing of ubiquitin-protein conjugates by the proteasome.* Annu Rev Biochem, 2009. **78**: p. 477-513.

15. Maron, B.J., et al., *Contemporary definitions and classification of the cardiomyopathies: an American Heart Association Scientific Statement from the Council on Clinical Cardiology, Heart Failure and Transplantation Committee; Quality of Care and Outcomes Research and Functional Genomics and Translational Biology Interdisciplinary Working Groups; and Council on Epidemiology and Prevention.* Circulation, 2006. **113**(14): p. 1807-16.

16. Willis, M.S. and C. Patterson, *Proteotoxicity and cardiac dysfunction--Alzheimer's disease of the heart?* N Engl J Med, 2013. **368**(5): p. 455-64.

17. He, C. and D.J. Klionsky, *Regulation mechanisms and signaling pathways of autophagy.* Annu Rev Genet, 2009. **43**: p. 67-93.

18. Kwon, Y.T. and A. Ciechanover, *The Ubiquitin Code in the Ubiquitin-Proteasome System and Autophagy.* Trends Biochem Sci, 2017. **42**(11): p. 873-886.

19. Hein, S., et al., *The role of the cytoskeleton in heart failure.* Cardiovasc Res, 2000. **45**(2): p. 273-8.

20. Henning, R.H. and B. Brundel, *Proteostasis in cardiac health and disease.* Nat Rev Cardiol, 2017. **14**(11): p. 637-653.

21. Knoll, R., B. Buyandelger, and M. Lab, *The sarcomeric Z-disc and Z-discopathies.* J Biomed Biotechnol, 2011. **2011**: p. 569628.

22. Lange, S., E. Ehler, and M. Gautel, *From A to Z and back? Multicompartment proteins in the sarcomere.* Trends Cell Biol, 2006. **16**(1): p. 11-8.

23. Lehmann, L.H., et al., *Histone deacetylase signaling in cardioprotection.* Cell Mol Life Sci, 2014. **71**(9): p. 1673-90.

24. Zhang, D., et al., *Activation of histone deacetylase-6 induces contractile dysfunction through derailment of alpha-tubulin proteostasis in experimental and human atrial fibrillation.* Circulation, 2014. **129**(3): p. 346-58.

25. Grou, C.P., et al., *The de novo synthesis of ubiquitin: identification of deubiquitinases acting on ubiquitin precursors.* Sci Rep, 2015. **5**: p. 12836.

26. Bond, U. and M.J. Schlesinger, *The chicken ubiquitin gene contains a heat shock promoter and expresses an unstable mRNA in heat-shocked cells.* Mol Cell Biol, 1986. **6**(12): p. 4602-10.

27. Ozkaynak, E., D. Finley, and A. Varshavsky, *The yeast ubiquitin gene: head-to-tail repeats encoding a polyubiquitin precursor protein.* Nature, 1984. **312**(5995): p. 663-6.

28. Ciechanover, A., *The unravelling of the ubiquitin system.* Nat Rev Mol Cell Biol, 2015. **16**(5): p. 322-4.

29. Komander, D. and M. Rape, *The ubiquitin code.* Annu Rev Biochem, 2012. **81**: p. 203-29.

30. Kulathu, Y. and D. Komander, *Atypical ubiquitylation - the unexplored world of polyubiquitin beyond Lys48 and Lys63 linkages.* Nat Rev Mol Cell Biol, 2012. **13**(8): p. 508-23.

31. Livneh, I., et al., *Monoubiquitination joins polyubiquitination as an esteemed proteasomal targeting signal.* Bioessays, 2017. **39**(6).

32. Yau, R. and M. Rape, *The increasing complexity of the ubiquitin code.* Nat Cell Biol, 2016. **18**(6): p. 579-86.

33. Coux, O., K. Tanaka, and A.L. Goldberg, *Structure and functions of the 20S and 26S proteasomes.* Annu Rev Biochem, 1996. **65**: p. 801-47.

34. Hedhli, N. and C. Depre, *Proteasome inhibitors and cardiac cell growth.* Cardiovasc Res, 2010. **85**(2): p. 321-9.

35. Kisselev, A.F. and A.L. Goldberg, *Monitoring activity and inhibition of 26S proteasomes with fluorogenic peptide substrates.* Methods Enzymol, 2005. **398**: p. 364-78.

36. Yao, T. and R.E. Cohen, *A cryptic protease couples deubiquitination and degradation by the proteasome.* Nature, 2002. **419**(6905): p. 403-7.

37. Lander, G.C., et al., *Complete subunit architecture of the proteasome regulatory particle.* Nature, 2012. **482**(7384): p. 186-91.

38. Baumeister, W., et al., *The proteasome: paradigm of a self-compartmentalizing protease.* Cell, 1998. **92**(3): p. 367-80.

39. Stadtmueller, B.M. and C.P. Hill, *Proteasome activators.* Mol Cell, 2011. **41**(1): p. 8-19.

40. Bousquet-Dubouch, M.P., et al., *Proteomics to study the diversity and dynamics of proteasome complexes: from fundamentals to the clinic.* Expert Rev Proteomics, 2011. **8**(4): p. 459-81.

41. Livnat-Levanon, N., et al., *Reversible 26S proteasome disassembly upon mitochondrial stress.* Cell Rep, 2014. **7**(5): p. 1371-1380.

42. Hanna, J., et al., *A ubiquitin stress response induces altered proteasome composition.* Cell, 2007. **129**(4): p. 747-759.

43. Baraibar, M.A. and B. Friguet, *Changes of the proteasomal system during the aging process.* Prog Mol Biol Transl Sci, 2012. **109**: p. 249-75.

44. Goldberg, A.L., *Protein degradation and protection against misfolded or damaged proteins.* Nature, 2003. **426**(6968): p. 895-9.

45. Schmidt, M. and D. Finley, *Regulation of proteasome activity in health and disease.* Biochim Biophys Acta, 2014. **1843**(1): p. 13-25.

46. Tai, H.C. and E.M. Schuman, *Ubiquitin, the proteasome and protein degradation in neuronal function and dysfunction.* Nat Rev Neurosci, 2008. **9**(11): p. 826-38.

47. Dahlmann, B., *Role of proteasomes in disease.* BMC Biochem, 2007. **8 Suppl 1**: p. S3.

48. Vilchez, D., I. Saez, and A. Dillin, *The role of protein clearance mechanisms in organismal ageing and age-related diseases.* Nat Commun, 2014. **5**: p. 5659.

49. Suraweera, A., et al., *Failure of amino acid homeostasis causes cell death following proteasome inhibition.* Mol Cell, 2012. **48**(2): p. 242-53.

50. Dikic, I., *Proteasomal and Autophagic Degradation Systems.* Annu Rev Biochem, 2017. **86**: p. 193-224.

51. Zaffagnini, G. and S. Martens, *Mechanisms of Selective Autophagy.* J Mol Biol, 2016. **428**(9 Pt A): p. 1714-24.

52. Leznicki, P. and Y. Kulathu, *Mechanisms of regulation and diversification of deubiquitylating enzyme function.* J Cell Sci, 2017. **130**(12): p. 1997-2006.

53. Abdul Rehman, S.A., et al., *MINDY-1 Is a Member of an Evolutionarily Conserved and Structurally Distinct New Family of Deubiquitinating Enzymes.* Mol Cell, 2016. **63**(1): p. 146-55.

54. Ristic, G., W.L. Tsou, and S.V. Todi, *An optimal ubiquitin-proteasome pathway in the nervous system: the role of deubiquitinating enzymes.* Front Mol Neurosci, 2014. **7**: p. 72.

55. Falquet, L., et al., *A human de-ubiquitinating enzyme with both isopeptidase and peptidase activities in vitro.* FEBS Lett, 1995. **359**(1): p. 73-7.

56. Hadari, T., et al., *A ubiquitin C-terminal isopeptidase that acts on polyubiquitin chains. Role in protein degradation.* J Biol Chem, 1992. **267**(2): p. 719-27.

57. Reyes-Turcu, F.E., et al., *The ubiquitin binding domain ZnF UBP recognizes the C-terminal diglycine motif of unanchored ubiquitin.* Cell, 2006. **124**(6): p. 1197-208.

58. Wang, C.H., G.C. Chen, and C.T. Chien, *The deubiquitinase Leon/USP5 regulates ubiquitin homeostasis during Drosophila development.* Biochem Biophys Res Commun, 2014. **452**(3): p. 369-75.

59. Finley, D., X. Chen, and K.J. Walters, *Gates, Channels, and Switches: Elements of the Proteasome Machine.* Trends Biochem Sci, 2016. **41**(1): p. 77-93.

60. Komander, D., M.J. Clague, and S. Urbe, *Breaking the chains: structure and function of the deubiquitinases.* Nat Rev Mol Cell Biol, 2009. **10**(8): p. 550-63.

61. Lam, Y.A., et al., *Editing of ubiquitin conjugates by an isopeptidase in the 26S proteasome.* Nature, 1997. **385**(6618): p. 737-40.

62. Livneh, I., et al., *The life cycle of the 26S proteasome: from birth, through regulation and function, and onto its death.* Cell Res, 2016. **26**(8): p. 869-85.

63. Verma, R., et al., *Role of Rpn11 metalloprotease in deubiquitination and degradation by the 26S proteasome.* Science, 2002. **298**(5593): p. 611-5.

64. Bashore, C., et al., *Ubp6 deubiquitinase controls conformational dynamics and substrate degradation of the 26S proteasome.* Nat Struct Mol Biol, 2015. **22**(9): p. 712-9.

65. Lee, B.H., et al., *USP14 deubiquitinates proteasome-bound substrates that are ubiquitinated at multiple sites.* Nature, 2016. **532**(7599): p. 398-401.

66. Song, L. and M. Rape, *Reverse the curse--the role of deubiquitination in cell cycle control.* Curr Opin Cell Biol, 2008. **20**(2): p. 156-63.

67. Daniel, J.A. and P.A. Grant, *Multi-tasking on chromatin with the SAGA coactivator complexes.* Mutat Res, 2007. **618**(1-2): p. 135-48.

68. Komada, M., *Controlling receptor downregulation by ubiquitination and deubiquitination.* Curr Drug Discov Technol, 2008. **5**(1): p. 78-84.

69. Rytkonen, A. and D.W. Holden, *Bacterial interference of ubiquitination and deubiquitination.* Cell Host Microbe, 2007. **1**(1): p. 13-22.

70. Schmidt, M., et al., *Proteasome-associated proteins: regulation of a proteolytic machine.* Biol Chem, 2005. **386**(8): p. 725-37.

71. Iwata, A., et al., *HDAC6 and microtubules are required for autophagic degradation of aggregated huntingtin.* J Biol Chem, 2005. **280**(48): p. 40282-92.

72. Ravikumar, B., et al., *Inhibition of mTOR induces autophagy and reduces toxicity of polyglutamine expansions in fly and mouse models of Huntington disease.* Nat Genet, 2004. **36**(6): p. 585-95.

73. Shimomura, H., et al., *Autophagic degeneration as a possible mechanism of myocardial cell death in dilated cardiomyopathy.* Jpn Circ J, 2001. **65**(11): p. 965-8.

74. Saijo, M., et al., *Cardiomyopathy with prominent autophagic degeneration, accompanied by an elevated plasma brain natriuretic peptide level despite the lack of overt heart failure.* Intern Med, 2004. **43**(8): p. 700-3.

75. Gomes, L.R., C.F.M. Menck, and G.S. Leandro, *Autophagy Roles in the Modulation of DNA Repair Pathways.* Int J Mol Sci, 2017. **18**(11).

76. Lim, J. and Z. Yue, *Neuronal aggregates: formation, clearance, and spreading.* Dev Cell, 2015. **32**(4): p. 491-501.

77. Olzmann, J.A., et al., *Parkin-mediated K63-linked polyubiquitination targets misfolded DJ-1 to aggresomes via binding to HDAC6.* J Cell Biol, 2007. **178**(6): p. 1025-38.

78. Liang, V., et al., *Altered proteostasis in aging and heat shock response in C. elegans revealed by analysis of the global and de novo synthesized proteome.* Cell Mol Life Sci, 2014. **71**(17): p. 3339-61.

79. Ben-Zvi, A., E.A. Miller, and R.I. Morimoto, *Collapse of proteostasis represents an early molecular event in Caenorhabditis elegans aging.* Proc Natl Acad Sci U S A, 2009. **106**(35): p. 14914-9.

80. Walther, D.M., et al., *Widespread Proteome Remodeling and Aggregation in Aging C. elegans.* Cell, 2015. **161**(4): p. 919-32.

81. Chakravarti, B., et al., *Proteomic profiling of aging in the mouse heart: Altered expression of mitochondrial proteins.* Arch Biochem Biophys, 2008. **474**(1): p. 22-31.

82. Chakravarti, B., et al., *Proteome profiling of aging in mouse models: differential expression of proteins involved in metabolism, transport, and stress response in kidney.* Proteomics, 2009. **9**(3): p. 580-97.

83. Labbadia, J. and R.I. Morimoto, *The biology of proteostasis in aging and disease.* Annu Rev Biochem, 2015. **84**: p. 435-64.

84. Yerbury, J.J., et al., *Walking the tightrope: proteostasis and neurodegenerative disease.* J Neurochem, 2016. **137**(4): p. 489-505.

85. Wiersma, M., R.H. Henning, and B.J. Brundel, *Derailed Proteostasis as a Determinant of Cardiac Aging.* Can J Cardiol, 2016. **32**(9): p. 1166 e11-20.

86. Weintraub, R.G., C. Semsarian, and P. Macdonald, *Dilated cardiomyopathy.* Lancet, 2017. **390**(10092): p. 400-414.

87. Olzscha, H., et al., *Amyloid-like aggregates sequester numerous metastable proteins with essential cellular functions.* Cell, 2011. **144**(1): p. 67-78.

88. Maron, B.J. and M.S. Maron, *Hypertrophic cardiomyopathy.* Lancet, 2013. **381**(9862): p. 242-55.

89. Morley, J.F. and R.I. Morimoto, *Regulation of longevity in Caenorhabditis elegans by heat shock factor and molecular chaperones.* Mol Biol Cell, 2004. **15**(2): p. 657-64.

90. Pattison, J.S. and J. Robbins, *Protein misfolding and cardiac disease: establishing cause and effect.* Autophagy, 2008. **4**(6): p. 821-3.

91. Ross, C.A. and M.A. Poirier, *Opinion: What is the role of protein aggregation in neurodegeneration?* Nat Rev Mol Cell Biol, 2005. **6**(11): p. 891-8.

92. Ross, C.A. and M.A. Poirier, *Protein aggregation and neurodegenerative disease.* Nat Med, 2004. **10 Suppl**: p. S10-7.

93. Sanbe, A., et al., *Desmin-related cardiomyopathy in transgenic mice: a cardiac amyloidosis.* Proc Natl Acad Sci U S A, 2004. **101**(27): p. 10132-6.

94. Elliott, P., et al., *Classification of the cardiomyopathies: a position statement from the European Society Of Cardiology Working Group on Myocardial and Pericardial Diseases.* Eur Heart J, 2008. **29**(2): p. 270-6.

95. Corrado, D., C. Basso, and D.P. Judge, *Arrhythmogenic Cardiomyopathy.* Circ Res, 2017. **121**(7): p. 784-802.

96. Sisakian, H., *Cardiomyopathies: Evolution of pathogenesis concepts and potential for new therapies.* World J Cardiol, 2014. **6**(6): p. 478-94.

97. Rammos, A., et al., *Restrictive Cardiomyopathies: The Importance of Noninvasive Cardiac Imaging Modalities in Diagnosis and Treatment-A Systematic Review.* Radiol Res Pract, 2017. **2017**: p. 2874902.

98. Elliott, P. and W.J. McKenna, *Hypertrophic cardiomyopathy.* Lancet, 2004. **363**(9424): p. 1881-91.

99. Girolami, F., et al., *Clinical Features and Outcome of Hypertrophic Cardiomyopathy Associated With Triple Sarcomere Protein Gene Mutations.* Journal of the American College of Cardiology, 2010. **55**(14): p. 1444-1453.

100. Marian, A.J. and E. Braunwald, *Hypertrophic Cardiomyopathy: Genetics, Pathogenesis, Clinical Manifestations, Diagnosis, and Therapy.* Circ Res, 2017. **121**(7): p. 749-770.

101. Lombardi, R., et al., *[Myocardial interstitial fibrosis and diastolic dysfunction in hypertrophic cardiomyopathy].* Ital Heart J Suppl, 2003. **4**(8): p. 645-50.

102. Herman, D.S., et al., *Truncations of titin causing dilated cardiomyopathy.* N Engl J Med, 2012. **366**(7): p. 619-28.

103. Gerull, B., et al., *Mutations of TTN, encoding the giant muscle filament titin, cause familial dilated cardiomyopathy.* Nat Genet, 2002. **30**(2): p. 201-4.

104. Taylor, M.R., et al., *Prevalence of desmin mutations in dilated cardiomyopathy.* Circulation, 2007. **115**(10): p. 1244-51.

105. McNally, E.M., J.R. Golbus, and M.J. Puckelwartz, *Genetic mutations and mechanisms in dilated cardiomyopathy.* J Clin Invest, 2013. **123**(1): p. 19-26.

106. Araco, M., et al., *Genetic bases of dilated cardiomyopathy.* J Cardiovasc Med (Hagerstown), 2017. **18**(3): p. 123-130.

107. Pinto, Y.M., et al., *Proposal for a revised definition of dilated cardiomyopathy, hypokinetic non-dilated cardiomyopathy, and its implications for clinical practice: a position statement of the ESC working group on myocardial and pericardial diseases.* Eur Heart J, 2016. **37**(23): p. 1850-8.

108. Dec, G.W. and V. Fuster, *Idiopathic dilated cardiomyopathy.* N Engl J Med, 1994. **331**(23): p. 1564-75.

109. Manolio, T.A., et al., *Prevalence and etiology of idiopathic dilated cardiomyopathy (summary of a National Heart, Lung, and Blood Institute workshop.* Am J Cardiol, 1992. **69**(17): p. 1458-66.

110. Rodriguez, C.I., et al., *High-efficiency deleter mice show that FLPe is an alternative to Cre-loxP.* Nat Genet, 2000. **25**(2): p. 139-40.

111. Breckenridge, R., et al., *Pan-myocardial expression of Cre recombinase throughout mouse development.* Genesis, 2007. **45**(3): p. 135-44.

112. Bruning, J.C., et al., *A muscle-specific insulin receptor knockout exhibits features of the metabolic syndrome of NIDDM without altering glucose tolerance.* Mol Cell, 1998. **2**(5): p. 559-69.

113. Sohal, D.S., et al., *Temporally regulated and tissue-specific gene manipulations in the adult and embryonic heart using a tamoxifen-inducible Cre protein.* Circ Res, 2001. **89**(1): p. 20-5.

114. Vooijs, M., J. Jonkers, and A. Berns, *A highly efficient ligand-regulated Cre recombinase mouse line shows that LoxP recombination is position dependent.* EMBO Rep, 2001. **2**(4): p. 292-7.

115. Srinivas, S., et al., *Cre reporter strains produced by targeted insertion of EYFP and ECFP into the ROSA26 locus.* BMC Dev Biol, 2001. **1**: p. 4.

116. O'Connell, T.D., M.C. Rodrigo, and P.C. Simpson, *Isolation and culture of adult mouse cardiac myocytes.* Methods Mol Biol, 2007. **357**: p. 271-96.

117. Jozefczuk, J., K. Drews, and J. Adjaye, *Preparation of mouse embryonic fibroblast cells suitable for culturing human embryonic and induced pluripotent stem cells.* J Vis Exp, 2012(64).

118. Hedberg, C., et al., *Hereditary myopathy with early respiratory failure is associated with misfolding of the titin fibronectin III 119 subdomain.* Neuromuscul Disord, 2014. **24**(5): p. 373-9.

119. Pfeffer, G., et al., *A new disease allele for the p.C30071R mutation in titin causing hereditary myopathy with early respiratory failure.* Neuromuscul Disord, 2014. **24**(3): p. 241-4.

120. Potsch, M.S., et al., *The anabolic catabolic transforming agent (ACTA) espindolol increases muscle mass and decreases fat mass in old rats.* J Cachexia Sarcopenia Muscle, 2014. **5**(2): p. 149-58.

121. Boettger, T., et al., *Acquisition of the contractile phenotype by murine arterial smooth muscle cells depends on the Mir143/145 gene cluster.* J Clin Invest, 2009. **119**(9): p. 2634-47.

122. Shevchenko, A., et al., *In-gel digestion for mass spectrometric characterization of proteins and proteomes.* Nat Protoc, 2006. **1**(6): p. 2856-60.

123. Rappsilber, J., M. Mann, and Y. Ishihama, *Protocol for micro-purification, enrichment, pre-fractionation and storage of peptides for proteomics using StageTips.* Nat Protoc, 2007. **2**(8): p. 1896-906.

124. Cox, J. and M. Mann, *MaxQuant enables high peptide identification rates, individualized p.p.b.-range mass accuracies and proteome-wide protein quantification.* Nat Biotechnol, 2008. **26**(12): p. 1367-72.

125. Cox, J., et al., *Andromeda: a peptide search engine integrated into the MaxQuant environment.* J Proteome Res, 2011. **10**(4): p. 1794-805.

126. Shen, D., et al., *Novel cell- and tissue-based assays for detecting misfolded and aggregated protein accumulation within aggresomes and inclusion bodies.* Cell Biochem Biophys, 2011. **60**(3): p. 173-85.

127. Roux, K.J., D.I. Kim, and B. Burke, *BioID: a screen for protein-protein interactions.* Curr Protoc Protein Sci, 2013. **74**: p. Unit 19 23.

128. Schindelin, J., et al., *Fiji: an open-source platform for biological-image analysis.* Nat Methods, 2012. **9**(7): p. 676-82.

129. Lee, J.Y., et al., *HDAC6 controls autophagosome maturation essential for ubiquitin-selective quality-control autophagy.* EMBO J, 2010. **29**(5): p. 969-80.

130. Wilkinson, K.D., et al., *Metabolism of the polyubiquitin degradation signal: structure, mechanism, and role of isopeptidase T.* Biochemistry, 1995. **34**(44): p. 14535-46.

131. Izaguirre, D.I., et al., *PTBP1-dependent regulation of USP5 alternative RNA splicing plays a role in glioblastoma tumorigenesis.* Mol Carcinog, 2012. **51**(11): p. 895-906.

132. Kawaguchi, Y., et al., *The deacetylase HDAC6 regulates aggresome formation and cell viability in response to misfolded protein stress.* Cell, 2003. **115**(6): p. 727-38.

133. Yao, T.P., *The role of ubiquitin in autophagy-dependent protein aggregate processing.* Genes Cancer, 2010. **1**(7): p. 779-786.

134. Stein, R.L., Z. Chen, and F. Melandri, *Kinetic studies of isopeptidase T: modulation of peptidase activity by ubiquitin.* Biochemistry, 1995. **34**(39): p. 12616-23.

135. Gianni, D., et al., *Protein aggregates and novel presenilin gene variants in idiopathic dilated cardiomyopathy.* Circulation, 2010. **121**(10): p. 1216-26.

136. Weekes, J., et al., *Hyperubiquitination of proteins in dilated cardiomyopathy.* Proteomics, 2003. **3**(2): p. 208-16.

137. Shintani, T. and D.J. Klionsky, *Autophagy in health and disease: a double-edged sword.* Science, 2004. **306**(5698): p. 990-5.

138. Palmio, J., et al., *Hereditary myopathy with early respiratory failure: occurrence in various populations.* J Neurol Neurosurg Psychiatry, 2014. **85**(3): p. 345-53.

139. Steele, H.E., et al., *Cardiac involvement in hereditary myopathy with early respiratory failure: A cohort study.* Neurology, 2016. **87**(10): p. 1031-5.

140. Chiti, F. and C.M. Dobson, *Protein Misfolding, Amyloid Formation, and Human Disease: A Summary of Progress Over the Last Decade.* Annu Rev Biochem, 2017. **86**: p. 27-68.

141. Ristic, G., et al., *USP5 Is Dispensable for Monoubiquitin Maintenance in Drosophila.* J Biol Chem, 2016. **291**(17): p. 9161-72.

142. Clague, M.J., C. Heride, and S. Urbe, *The demographics of the ubiquitin system.* Trends Cell Biol, 2015. **25**(7): p. 417-26.

143. Nijman, S.M., et al., *A genomic and functional inventory of deubiquitinating enzymes.* Cell, 2005. **123**(5): p. 773-86.

144. Amerik, A., et al., *In vivo disassembly of free polyubiquitin chains by yeast Ubp14 modulates rates of protein degradation by the proteasome.* EMBO J, 1997. **16**(16): p. 4826-38.

145. Doelling, J.H., et al., *The ubiquitin-specific protease UBP14 is essential for early embryo development in Arabidopsis thaliana.* Plant J, 2001. **27**(5): p. 393-405.

146. Pickart, C.M., *Ubiquitin in chains.* Trends Biochem Sci, 2000. **25**(11): p. 544-8.

147. Kaiser, S.E., et al., *Protein standard absolute quantification (PSAQ) method for the measurement of cellular ubiquitin pools.* Nat Methods, 2011. **8**(8): p. 691-6.

148. Hoeller, D. and I. Dikic, *Targeting the ubiquitin system in cancer therapy.* Nature, 2009. **458**(7237): p. 438-44.

149. Lee, B.H., et al., *Enhancement of proteasome activity by a small-molecule inhibitor of USP14.* Nature, 2010. **467**(7312): p. 179-84.

150. Geiger, T., et al., *Comparative proteomic analysis of eleven common cell lines reveals ubiquitous but varying expression of most proteins.* Mol Cell Proteomics, 2012. **11**(3): p. M111 014050.

151. Amerik, A.Y. and M. Hochstrasser, *Mechanism and function of deubiquitinating enzymes.* Biochim Biophys Acta, 2004. **1695**(1-3): p. 189-207.

152. Lund, P.K., et al., *Nucleotide sequence analysis of a cDNA encoding human ubiquitin reveals that ubiquitin is synthesized as a precursor.* J Biol Chem, 1985. **260**(12): p. 7609-13.

153. Wiborg, O., et al., *The human ubiquitin multigene family: some genes contain multiple directly repeated ubiquitin coding sequences.* EMBO J, 1985. **4**(3): p. 755-9.

154. Baker, R.T. and P.G. Board, *The human ubiquitin-52 amino acid fusion protein gene shares several structural features with mammalian ribosomal protein genes.* Nucleic Acids Res, 1991. **19**(5): p. 1035-40.

155. Redman, K.L. and M. Rechsteiner, *Identification of the long ubiquitin extension as ribosomal protein S27a.* Nature, 1989. **338**(6214): p. 438-40.

156. Finley, D., E. Ozkaynak, and A. Varshavsky, *The yeast polyubiquitin gene is essential for resistance to high temperatures, starvation, and other stresses.* Cell, 1987. **48**(6): p. 1035-46.

157. Damgaard, R.B., et al., *The Deubiquitinase OTULIN Is an Essential Negative Regulator of Inflammation and Autoimmunity.* Cell, 2016. **166**(5): p. 1215-1230 e20.

158. Keusekotten, K., et al., *OTULIN antagonizes LUBAC signaling by specifically hydrolyzing Met1-linked polyubiquitin.* Cell, 2013. **153**(6): p. 1312-26.

159. Rivkin, E., et al., *The linear ubiquitin-specific deubiquitinase gumby regulates angiogenesis.* Nature, 2013. **498**(7454): p. 318-24.

160. Fornace, A.J., Jr., et al., *Ubiquitin mRNA is a major stress-induced transcript in mammalian cells.* Nucleic Acids Res, 1989. **17**(3): p. 1215-30.

161. Day, S.M., *The ubiquitin proteasome system in human cardiomyopathies and heart failure.* Am J Physiol Heart Circ Physiol, 2013. **304**(10): p. H1283-93.

162. Collins, G.A. and A.L. Goldberg, *The Logic of the 26S Proteasome.* Cell, 2017. **169**(5): p. 792-806.

163. Swatek, K.N. and D. Komander, *Ubiquitin modifications.* Cell Res, 2016. **26**(4): p. 399-422.

164. Borodovsky, A., et al., *A novel active site-directed probe specific for deubiquitylating enzymes reveals proteasome association of USP14.* EMBO J, 2001. **20**(18): p. 5187-96.

165. Hanna, J., et al., *Deubiquitinating enzyme Ubp6 functions noncatalytically to delay proteasomal degradation.* Cell, 2006. **127**(1): p. 99-111.

166. Koulich, E., X. Li, and G.N. DeMartino, *Relative structural and functional roles of multiple deubiquitylating proteins associated with mammalian 26S proteasome.* Mol Biol Cell, 2008. **19**(3): p. 1072-82.

167. Stone, M., et al., *Uch2/Uch37 is the major deubiquitinating enzyme associated with the 26S proteasome in fission yeast.* J Mol Biol, 2004. **344**(3): p. 697-706.

168. Besche, H.C., et al., *Isolation of mammalian 26S proteasomes and p97/VCP complexes using the ubiquitin-like domain from HHR23B reveals novel proteasome-associated proteins.* Biochemistry, 2009. **48**(11): p. 2538-49.

169. Scanlon, T.C., et al., *Isolation of human proteasomes and putative proteasome-interacting proteins using a novel affinity chromatography method.* Exp Cell Res, 2009. **315**(2): p. 176-89.

170. Tai, H.C., et al., *Characterization of the Brain 26S Proteasome and its Interacting Proteins.* Front Mol Neurosci, 2010. **3**.

171. Gomes, A.V., et al., *The murine cardiac 26S proteasome: an organelle awaiting exploration.* Ann N Y Acad Sci, 2005. **1047**: p. 197-207.

172. Liu, J., et al., *Aberrant protein aggregation is essential for a mutant desmin to impair the proteolytic function of the ubiquitin-proteasome system in cardiomyocytes.* J Mol Cell Cardiol, 2006. **40**(4): p. 451-4.

173. Predmore, J.M., et al., *Ubiquitin proteasome dysfunction in human hypertrophic and dilated cardiomyopathies.* Circulation, 2010. **121**(8): p. 997-1004.

174. Schlossarek, S. and L. Carrier, *The ubiquitin-proteasome system in cardiomyopathies.* Curr Opin Cardiol, 2011. **26**(3): p. 190-5.

175. Tannous, P., et al., *Intracellular protein aggregation is a proximal trigger of cardiomyocyte autophagy.* Circulation, 2008. **117**(24): p. 3070-8.

176. Orogo, A.M. and A.B. Gustafsson, *Therapeutic targeting of autophagy: potential and concerns in treating cardiovascular disease.* Circ Res, 2015. **116**(3): p. 489-503.

177. Holmberg, C.I., et al., *Inefficient degradation of truncated polyglutamine proteins by the proteasome.* EMBO J, 2004. **23**(21): p. 4307-18.

178. Tran, P.B. and R.J. Miller, *Aggregates in neurodegenerative disease: crowds and power?* Trends Neurosci, 1999. **22**(5): p. 194-7.

179. Kopito, R.R., *Aggresomes, inclusion bodies and protein aggregation.* Trends Cell Biol, 2000. **10**(12): p. 524-30.

180. Hao, R., et al., *Proteasomes activate aggresome disassembly and clearance by producing unanchored ubiquitin chains.* Mol Cell, 2013. **51**(6): p. 819-28.

181. Hyttinen, J.M., et al., *Clearance of misfolded and aggregated proteins by aggrephagy and implications for aggregation diseases.* Ageing Res Rev, 2014. **18**: p. 16-28.

182. Su, H. and X. Wang, *p62 Stages an interplay between the ubiquitin-proteasome system and autophagy in the heart of defense against proteotoxic stress.* Trends Cardiovasc Med, 2011. **21**(8): p. 224-8.

183. Wang, X., J.S. Pattison, and H. Su, *Posttranslational modification and quality control.* Circ Res, 2013. **112**(2): p. 367-81.

184. Evans, T.D., et al., *Target acquired: Selective autophagy in cardiometabolic disease.* Sci Signal, 2017. **10**(468).

185. Lamark, T. and T. Johansen, *Aggrephagy: selective disposal of protein aggregates by macroautophagy.* Int J Cell Biol, 2012. **2012**: p. 736905.

186. Lamark, T. and T. Johansen, *Autophagy: links with the proteasome.* Curr Opin Cell Biol, 2010. **22**(2): p. 192-8.

187. Zheng, Q., et al., *Proteasome malfunction activates macroautophagy in the heart.* Am J Cardiovasc Dis, 2011. **1**(3): p. 214-26.

188. Kishi-Itakura, C., et al., *Ultrastructural analysis of autophagosome organization using mammalian autophagy-deficient cells.* J Cell Sci, 2014. **127**(Pt 18): p. 4089-102.

189. Pankiv, S., et al., *p62/SQSTM1 binds directly to Atg8/LC3 to facilitate degradation of ubiquitinated protein aggregates by autophagy.* J Biol Chem, 2007. **282**(33): p. 24131-45.

190. Matsumoto, G., et al., *Serine 403 phosphorylation of p62/SQSTM1 regulates selective autophagic clearance of ubiquitinated proteins.* Mol Cell, 2011. **44**(2): p. 279-89.

191. Munch, D., et al., *Autophagy deficiency leads to accumulation of ubiquitinated proteins, ER stress, and cell death in Arabidopsis.* Autophagy, 2014. **10**(9): p. 1579-87.

192. Korolchuk, V.I., et al., *Autophagy inhibition compromises degradation of ubiquitin-proteasome pathway substrates.* Mol Cell, 2009. **33**(4): p. 517-27.

193. Nakai, A., et al., *The role of autophagy in cardiomyocytes in the basal state and in response to hemodynamic stress.* Nat Med, 2007. **13**(5): p. 619-24.

194. Cuervo, A.M., *Autophagy and aging: keeping that old broom working.* Trends Genet, 2008. **24**(12): p. 604-12.

195. Kumar, V., et al., *Protein aggregation and neurodegenerative diseases: From theory to therapy.* Eur J Med Chem, 2016. **124**: p. 1105-1120.

196. Powell, S.R., et al., *The ubiquitin-proteasome system and cardiovascular disease.* Prog Mol Biol Transl Sci, 2012. **109**: p. 295-346.

197. Kostin, S., et al., *Myocytes die by multiple mechanisms in failing human hearts.* Circ Res, 2003. **92**(7): p. 715-24.

198. Mu, T.W., et al., *Chemical and biological approaches synergize to ameliorate protein-folding diseases.* Cell, 2008. **134**(5): p. 769-81.

199. Powers, E.T., et al., *Biological and chemical approaches to diseases of proteostasis deficiency.* Annu Rev Biochem, 2009. **78**: p. 959-91.

200. Lee, F.K., et al., *The role of ubiquitin linkages on alpha-synuclein induced-toxicity in a Drosophila model of Parkinson's disease.* J Neurochem, 2009. **110**(1): p. 208-19.

201. Al-Ramahi, I., et al., *CHIP protects from the neurotoxicity of expanded and wild-type ataxin-1 and promotes their ubiquitination and degradation.* J Biol Chem, 2006. **281**(36): p. 26714-24.

202. Tsai, Y.C., et al., *Parkin facilitates the elimination of expanded polyglutamine proteins and leads to preservation of proteasome function.* J Biol Chem, 2003. **278**(24): p. 22044-55.

203. Dantuma, N.P. and L.C. Bott, *The ubiquitin-proteasome system in neurodegenerative diseases: precipitating factor, yet part of the solution.* Front Mol Neurosci, 2014. **7**: p. 70.

204. Ravikumar, B., R. Duden, and D.C. Rubinsztein, *Aggregate-prone proteins with polyglutamine and polyalanine expansions are degraded by autophagy.* Hum Mol Genet, 2002. **11**(9): p. 1107-17.

205. Rose, C., et al., *Rilmenidine attenuates toxicity of polyglutamine expansions in a mouse model of Huntington's disease.* Hum Mol Genet, 2010. **19**(11): p. 2144-53.

206. Zheng, S., et al., *Deletion of the huntingtin polyglutamine stretch enhances neuronal autophagy and longevity in mice.* PLoS Genet, 2010. **6**(2): p. e1000838.

207. Carrier, L., et al., *Organization and sequence of human cardiac myosin binding protein C gene (MYBPC3) and identification of mutations predicted to produce truncated proteins in familial hypertrophic cardiomyopathy.* Circ Res, 1997. **80**(3): p. 427-34.

208. Magistretti, P.J. and L. Pellerin, *Cellular mechanisms of brain energy metabolism. Relevance to functional brain imaging and to neurodegenerative disorders.* Ann N Y Acad Sci, 1996. **777**: p. 380-7.

LIST OF ABREVIATIONS

μm	Micrometer
3D	Three-dimensional
4-OHT	4-Hydroxy-tamoxifen
aa	Amino acids
ACTC1	Actin, alpha, cardiac muscle 1
Ad	Adenovirus
AD	Alzheimer's disease
AF	Atrial fibrillation
ALS	Amyotrophic lateral sclerosis
ARVC	Arrhythmogenic right ventricular cardiomyopathy
ATP	Adenosine 5'-triphosphate
BirA*	Mutated Biotin ligase
bp	Base pairs
bpA	Bovine growth hormone polyadenylation site
BSA	Bovine serum albumin
BW	Body weight
C57bl/6	C57 black 6 mice
cDNA	Complementary deoxyribonucleic acid
CMV	Cytomegalovirus
CO2	Carbon dioxide
CP	Core particle
DAPI	4',6-diamidino-2-phenylindole
DCM	Dilated cardiomyopathy
ddH_2O	Double distilled water
DES	Desmin
DMEM	Dulbecco Modified Eagle Medium
DMSO	Dimethyl sulfoxide
DNA	Deoxyribonucleic acid
dNTPs	Nucleoside triphosphate
DTA	Subunit of the diphtheria toxin gene
DTT	1,4-Dithiothreit
DUBs	Deubiquitinating enzymes
E	Exon
E11.5	Embryonic day 11.5
EDTA	Ethylenediaminetetraacetic acid

EF	Ejection fraction
eGFP	Enhanced green fluorescent protein
EGTA	Ethylene glycol-bis (β-aminoethyl ether)-N,N,N',N'-tetraacetic acid
EM	Electron microscopy
ER	Endoplasmic reticulum
ES cell	Embryonic stem cell
EtOH	Ethanol
FC	Fold change
FCS	Fetal calf serum
FLPe	FLP protein
For	Forward
FRT	FLPe recognition target site
GAPDH	Glyceraldehyde 3-phosphate dehydrogenase
GO	Gene Ontology
H&E	Hematoxylin & eosin
HCM	Hypertrophic cardiomyopathy
HD	Huntington's disease
HDAC6	Histone deacetylating enzyme 6
HEK293	Human embryonic kidney cells 293
Hs	Human
Hsc70	Heat shock complex 70
HW	Heart weight
i.p.	Intraperitoneally
IB	Immunoblot
iCre	Inducible Cre
ID	Intercalated disk
IgG	Immunoglobulin G
IP	Immunoprecipitation
JAMMs	JAB1/MPN/MOV34 family
kDa	Kilo Dalton
kg	Kilogram
LAMP-2A	Lysosome-associated membrane protein 2
LC-MS/MS	Liquid chromatography–mass spectrometry
Lys	Lysine
M1	Methionine
MCK	Muscle creatine kinase
MCS	Multiple cloning site
MEFs	Mouse embryonic fibroblasts
Mf	Myofibrils
mg	Milligrams
min	Minutes
MINDYs	Motif interacting with Ubiquitin-containing DUB family
MJDs	Machado-Josephin domain proteases
MTOC	Microtubule-organizing center
MYBPC3	Myosin-binding protein C
Myh6-MCM	Myosin heavy chain 6-MerCreMer
Myh7	Myosin heavy chain 7

NaCl	Sodium chloride
Nbr1	Neighbor of BRCA1 gene 1 protein
Neo	Neomycin
NF	
nm	Nanometers
Optn	Optineurin
ORF	Open reading frame
OTUs	Ovarian tumor proteases
P78	Postnatal day 78
PBS	Phosphate-buffered saline
PCR	Polymerase chain reaction
PD	Parkinson's disease
PFA	Paraformaldehyde
PFU	Plaque forming units
PMSF	Phenylmethylsulfonyl fluoride
PN	Proteostasis network
PQC	Protein quality control
qRT-PCR	Quantitative reverse transcription PCR
RCM	Restrictive cardiomyopathy
Rev	Reverse
RFU	Relative fluorescence units
RNA	Ribonucleic acid
RP	Regulatory particle
RPM	Revolutions per minute
RT	Room temperature
RT-PCR	Reverse transcription PCR
S	Second
SDS	Sodium dodecyl sulfate
sqRT-PCR	Semi-quantitative reverse transcription PCR
SQSTM1	Sequestosome-1
SR	Sarcoplasmic reticulum
TAE	Tris-acetate-EDTA
TBS	Tris-buffered saline
TBS-T	Tris-buffered saline / Tween-20
TE	Tris-EDTA
TEMED	Tetramethylethylenediamine
TL	Tibia length
TNNC1	Troponin C, type 1
TNNT2	Cardiac muscle troponin T
tpA	Transcriptional polyA stop sequence
TPM1	Tropomyosin alpha-1 chain
Ttn	Titin
Ub	Ubiquitin
UBA	Ubiquitin-binding associated
Uba52	Ubiquitin A-52 residue ribosomal protein fusion product 1
Uba80/Rps27a	40S ribosomal protein S27a
Ubb	Ubiquitin B gene

Ubc	Ubiquitin C gene
UCH	Ubiquitin carboxyl-terminal hydrolase domain
UCHs	Ubiquitin carboxyl -terminal hydrolases
UPS	Ubiquitin proteasome system
USPs	Ubiquitin specific peptidase family
USP5	Ubiquitin specific peptidase 5
Usp5cKO	Usp5 cardiac conditional knockout
Usp5iKO	Usp5 inducible knockout
UV	Ultraviolet
WT	Wildtype
XMLC2	Xenopus laevis light chain 2
ZnF-UBP	Zinc-finger ubiquitin binding domain
α-MHC	α-Myosin heavy chain

LIST OF FIGURES

LIST OF TABLES